Emplacement of the Santa Rita Flat pluton and kinematic analysis of cross cutting shear zones, eastern California

John A. Vines

Thesis submitted to the faculty of the Virginia Polytechnic Institute and State University
in partial fulfullment of the requirements for the degree of

MASTER OF SCIENCE
IN
GEOLOGY

Dr. Richard D. Law, Chair
Dr. Allen Glazner
Dr. James Spotila
Dr. Krishna Sinha

December 14, 1999
Blacksburg, Virginia

Keywords:
White-Inyo Range, Pluton Emplacement, Shear Zones, Transpression, Kinematic Analysis, Deformation Mechanisms

Emplacement of the Santa Rita Flat pluton and kinematic analysis of cross cutting shear zones, eastern California

John A. Vines

Abstract

This study documents the deformation history of the Santa Rita Flat pluton, eastern California, from the time of emplacement to post-emplacement transpressional shearing, and consists of manuscripts that make up three chapters. The first chapter addresses the emplacement of the Santa Rita Flat pluton using anisotropy of magnetic susceptibility (AMS). The second chapter describes the kinematic analysis of cross-cutting shear zones within the western margin of the pluton. The third chapter is an informal paper on the U/Pb dating of two sheared felsic dikes from the pluton.

AMS of the Santa Rita Flat pluton indicates that the paramagnetic and ferromagnetic minerals define a foliation which is arched into an antiformal structure in the central to southern parts of the pluton. The northern part of the pluton displays an east-west striking magnetic foliation which lacks a fold-like geometry. Previously published field mapping and petrologic surveys of the pluton and surrounding wall rocks indicate that the southern margin and northern part of the Santa Rita Flat pluton represents the roof and core of the pluton, respectively.

Integration of our analysis of the internal structure of the pluton with previously published work on the regional structure of the surrounding metasedimentary wall rocks, suggests that the pluton may have initially been intruded as a sill-like or “saddle reef” structure along a stratigraphically controlled mechanical discontinuity in the hinge zone of an enveloping regional-scale synform. Subsequent vertical inflation of this sill resulted in local upward doming of the overlying pluton roof and formation of the antiformal structure now observed at the current erosion level in the central-southern part of the pluton and overlying locally preserved roof rocks. No corresponding fold structure is indicated by AMS analysis in the northern part of the pluton, which is exposed at a deeper level, and represents a section closer to the pluton core.

Emplacement of the Santa Rita Flat pluton at 164 Ma overlaps in time with regional deformation at ~185 - ~148 Ma (Middle – Late Jurassic) recognized in the southern Inyo

Mountains. Northwest trending folds are pervasive along the western flank of the Inyo and White Mountains, and may have accommodated strains at the lateral tips of thrust faults which crop out in the southern Inyo Mountains. We speculate that space for initial emplacement of the Santa Rita Flat pluton may have been produced by layer-parallel slip and hinge-zone dilation, accompanied by axis-parallel slip during formation of a regional scale thrust-related synform.

The Santa Rita shear system (SRSS) is composed of a series of discrete NW-SE striking steeply dipping shear zones that cut and plastically deform granitic rocks of the Santa Rita Flat pluton. The shear zones exhibit a domainal distribution of gently and steeply plunging stretching lineations, and are located at planar mechanical discontinuities between the granite and a series of felsic/mafic dikes which intrude the pluton. Mylonitized dikes within the shear zones contain syntectonic mineral assemblages not observed in dikes outside the shear zones, indicating that the dikes were intruded prior to shear zone development. Correlation with geometrically similar shear zones in the Sierra Nevada batholith to the west, suggests that the SRSS probably nucleated from a regional stress field in Cretaceous times (~90-78 Ma).

Strain is heterogeneous within the shear zones, with local development of protomylonite, mylonite, ultramylonite and phyllonite. Strain heterogeneity within the granite is attributed to fluid infiltration and chemical reaction and alteration of feldspar to fine-grained mica. These deformation-induced mineral changes would have resulted in progressive mechanical weakening over time of rocks within the SRSS. The phyllonites occur predominantly within steeply lineated shear zones and contain mylonitized foliation-parallel quartz veins. The pattern of c-axis preferred orientation in these quartz veins indicates that deformation within the shear zones occurred under plane strain conditions. Locally, quartz veins also cut the foliation planes, reflecting high pore fluid pressures during evolution of the SRSS. These cross-cutting quartz veins are also plastically deformed, and their c-axis patterns indicate weak constrictional strains. The orientation of the shear zones, together with their strain paths, are used to develop a transpressional kinematic model for development of the SRSS within a progressively rotating stress field.

Acknowledgements

First, I would like to thank the Geological Sciences Department at Virginia Tech for accepting me into the graduate program. Specifically, Dr. Krishna Sinha and Dr. Richard Law were very hospitable and showed keen interest in my geologic interests. I hope I have not disappointed Rick, Krishna, and the Virginia Tech Geology Department.

Rick has inspired me during my stay at Virginia Tech, and I am sure he will continue to do so as I begin a Ph.D. under him in the fall of 2000. His experience in structural geology and solving geological problems has helped me answer some of my own research.

Dr. Allen Glazner has been very generous in sparing me some of his time and posing questions on California geology. Jim Spotila and John Hole are thanked for discussions regarding fundamental processes that occur in active fault systems. Dr. Donald Rimstidt is thanked for editorial comments towards my thesis, and for substituting for one of my committee members during my oral defense. Jean-Luc Bouchez and Michel de Saint Blanquat allowed me to use their AMS facilities in Toulouse, France and are thanked for reviewing the AMS chapter. Dr. Mario Karfakis in Mining Engineering allowed me to use his rock drill for coring.

This research would never have been thought of without discussion from Sven Morgan. His encouragement during this research has helped me incredibly. I wish to thank Peter Welch for allowing me to bother him with petrography questions and for taking the time to debate other esoteric questions. Jay Thomas helped me through countless and painstaking hours on dating two felsic dikes from the Santa Rita shear system. Brian Coffey, Bill Seaton, and Jason Pope gave me valuable computer assistance. Joel Maynard helped with some of the figure illustrations.

Linda Bland, Connie Lowe, Ellen Mathena, Mary McMurray, and Carolyn Williams have been very patient and extremely friendly with any questions I have had. Their assistance has made my life a little easier within the department.

Scott Hetzler's friendliness, 'tacos', and home brew helped me through my two field seasons in California. Thanks also Scott for going on the hike from hell with me. Cecil Patrick cooked some of the best meals I have had during my two field seasons in California. He also was a very good friend, and would always make time for a talk.

My best friend and wife, Erin Vines, has been the true inspiration in my life. I have gained so much from her during the last seven years. Hopefully, we will have a lifetime of inspiration and growth together.

Finanicial support was provided by the Geological Society of America, Sigma Xi, National Science Foundation, University of California White Mountain Research Station, and Heath Robinson-Roy J. Holden Geoscience Endowed Scholarships.

Table of Contents

CHAPTER 1

Emplacement of the Santa Rita Flat pluton as a pluton-scale saddle reef structure

ABSTRACT

An anisotropy of magnetic susceptibility (AMS) survey has been made of the Middle-Late Jurassic Santa Rita Flat pluton, exposed in the Inyo Range of eastern California. Results from this survey have been integrated with previously published field mapping and petrologic surveys of the pluton and surrounding wall rocks. Regional mapping indicates that the pluton is situated close to the core of a southward-plunging synformal structure in the surrounding and underlying metasedimentary wall rocks. However, paradoxically, layering in locally preserved metasedimentary rocks above the pluton defines a southward-plunging antiformal structure. At the map scale the pluton appears to be homogeneous, but detailed petrologic analysis indicates a cryptic zonation within the pluton. AMS analysis has revealed that magnetic foliation within the pluton defines a southward plunging antiformal structure, and the accompanying lineation plunges at 10-40° subparallel to the axis of this antiform. Microstructural analysis indicates that this foliation and lineation are of magmatic origin, solid-state deformation microstructures only being recorded in later shear zones which cut the pluton.

Integration of our analysis of the internal structure of the pluton, with previously published work on the regional structure of the surrounding metasedimentary wall rocks, suggests that the pluton was initially intruded as a sill-like or "saddle reef" structure along a stratigraphically controlled mechanical discontinuity in the hinge zone of an enveloping regional-scale synform. Subsequent vertical inflation of this sill resulted in local upward doming of the overlying pluton roof and formation of the antiformal structure now observed at the current erosion level in the central-southern part of the pluton and overlying locally preserved roof rocks. No corresponding fold structure is indicated by AMS analysis in the northern part of the pluton, which is exposed at a deeper level, and represents a section closer to the pluton core.

Emplacement of the Santa Rita Flat pluton at 164 Ma overlaps in time with regional deformation at ~185 - ~148 Ma (Middle – Late Jurassic) recognized in the southern Inyo Mountains. Northwest trending km-scale folds are pervasive along the western flank of

the Inyo and White Mountains, and may have accommodated strains at the lateral tips of thrust faults which crop out in the southern Inyo Mountains. We speculate that space for initial emplacement of the Santa Rita Flat pluton may have been produced by layer-parallel slip and hinge-zone dilation, accompanied by axis-parallel slip during formation of a regional scale thrust-related synform.

INTRODUCTION

The orientation of fabrics within a pluton may be controlled by a wide range of factors including: 1) mechanical anisotropies in the wall rocks which may control the geometry of initial pluton emplacement, 2) the presence of local feeder conduits and their intersection with the main pluton (e.g. point source or linear), 3) magma flow within the evolving pluton, 4) deformation of previously solidified or partially solidified magma batches by forcible emplacement of younger magma pulses, and 5) overprinting by externally applied tectonic strains and associated shear zones (Bouchez and Gleizes, 1995; Tobisch and Cruden, 1995; Aranguren et. al., 1997; Saint Blanquat and Tikoff, 1997; Saint Blanquat et. al., in review). Shear zones and tensional fracture feeder zones are primarily governed by tectonically induced mechanisms (Bouchez and Gleizes, 1995; Tobisch and Cruden, 1995; Saint Blanquat and Tikoff, 1997;). Thus, fabrics from plutons that are emplaced along either shear zones or tensional fracture feeder zones are likely controlled by tectonic induced processes. Wall rocks surrounding a pluton may be strained by tectonically and/or magma-induced pressures (Hutton, 1988; Paterson, 1991; Law et. al., 1992; Paterson and Fowler, 1993; Clemens, 1998; Cruden, 1998; Morgan et. al., 1998a). Fabrics from plutons that are neither emplaced along shear zones or tensional fracture feeder zones will likely by controlled by local wall rock geometries that may reflect either tectonically-induced or forcible emplacement-induced mechanisms. Wherever possible, studies of pluton emplacement should not be based on a single data set, such as fabric variation, but should incorporate as many data sets (e.g. petrology, wall rock studies, geophysical surveys) as possible in order to more accurately determine the three dimensional structure and zonation of the pluton, and to distinguish between tectonically-induced and magma-induced processes.

Numerous studies over the last 15-20 years indicate that anisotropy of magnetic susceptibility (AMS) is a powerful tool for rapidly and efficiently determining the internal fabric of a pluton, both in terms of fabric elements such as foliation and particularly lineation (which is commonly difficult/impossible to measure in the field), and also in terms of the degree of fabric anisotropy (see recent review by Bouchez,

1997). Microstructural correlation with such AMS analyses allows us to determine the flow/deformation mechanism (e.g. magmatic flow, high, medium or low temperature solid state deformation) responsible for formation of the observed fabric elements, and such integrated geometric and process-oriented studies are now commonly regarded as being essential for reconstructing pluton emplacement histories.

AMS data, such as magnetic anisotropy, magnetic foliation and lineation, are traditionally presented in map form. However, as with all map data, care must be taken to avoid over-interpreting such data which is usually only collected from a two dimensional erosion surface. For example, AMS measurements collected from the present erosional surface of a pluton may not represent the same structural level throughout the entire pluton. This problem becomes acute in the case of tilted plutons. Outcrop- and map-scale features, such as roof pendants, can help to determine the structural level that AMS measurements were taken from within a pluton. However, more detailed petrologic study may provide more reliable information on exposed structural level within a pluton. Paterson and Fowler (1993) have emphasized that plutons are rarely emplaced by a single mechanism, and that the dominant emplacement mechanism may vary with structural position. Determining the structural level at which a pluton is exposed may help to constrain whether tectonic- or magma-induced processes controlled the orientation of fabrics observed.

The Santa Rita Flat pluton, located in the northern Inyo Mountains of eastern California, is an ideal candidate for comparing petrologic data with AMS parameters. Metz (1978) conducted a detailed petrologic study of the pluton, based on samples collected on a 1 km grid spacing, in order to determine the thermal history, structural level of exposure, and original shape of the pluton. To more fully reconstruct the emplacement history of the pluton, a detailed AMS study was carried out and integrated with the petrologic work of Metz (1978).

GEOLOGIC BACKGROUND

The Santa Rita Flat pluton has been dated at 164 Ma (U-Pb zircon age) by Chen (1977) and is one of many Middle-Late Jurassic plutons in the White-Inyo Range (Fig. 1) that intruded metasedimentary rocks ranging in age from Neoproterozoic through late Paleozoic (Nelson, 1962; Bateman et al., 1963; Ross, 1967; Bateman, 1992). Although the Santa Rita Flat pluton lies within the Inyo Range, the pluton is considered part of the Sierra Nevada Batholith, and has been correlated with the Tinemaha granodiorite that lies in the eastern portion of the Sierra (Fig. 1) (Ross, 1962, 1969). The pluton is composed

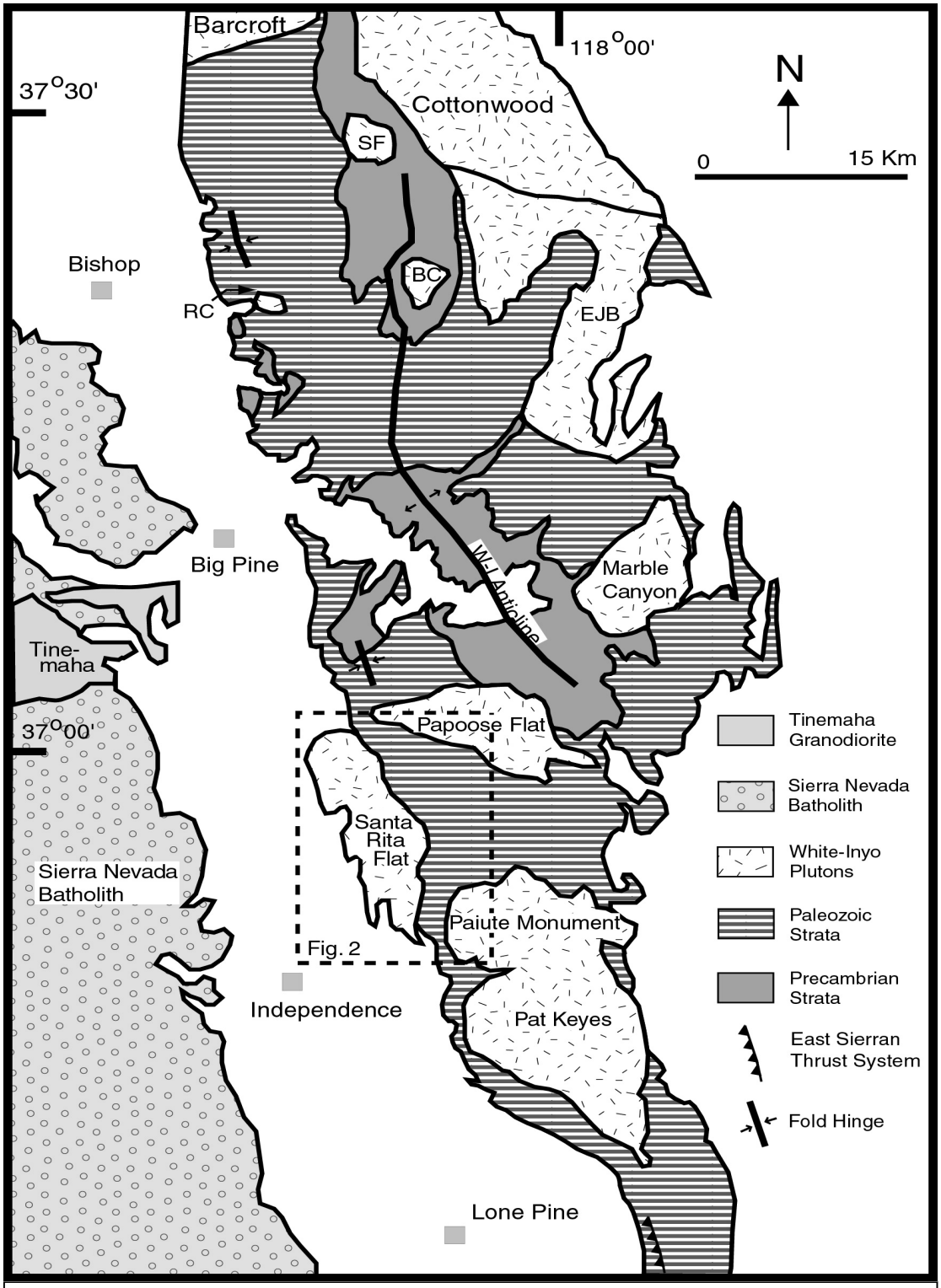

Figure 1: Simplified regional geologic map of White-Inyo Range (compiled from maps of Ross, 1962, 1965; Bateman, 1965; Nelson, 1966a, 1966b; ; McKee and Nelson, 1967; Nelson, 1971; Krauskopf, 1971; Crowder and Sheridan, 1972; Dunne et al., 1978; Hanson, 1986; Ernst and Hall, 1987). Note: SF=Sage Hen Flat pluton; BC=Birch Creek pluton; EJB=Eureka Valley-Joshua Flat-Beek Creek composite pluton; RC=Redding Canyon pluton; W-I=White Inyo anticline.

of granite with megacrysts of hornblende and K-feldspar, and is exposed over an area measuring approximately 6 by 17.5 km (Ross, 1965; Metz, 1978). One of the most impressive features of the Santa Rita Flat pluton is its homogeneous nature and lack of macroscopic foliation.

The western and northern margins of the pluton are covered by alluvium and Quaternary basaltic lava flows, respectively. The eastern and southern margins of the pluton rest against folded Pennsylvanian metasediments (Fig. 2). Near the southern margin, km-scale roof pendants and shallowly dipping wall rocks that rest above the pluton indicate an exposure level at the local position of the pluton roof. Stratigraphic layers in the wall rocks young towards the pluton, and the effects of contact metamorphism extend for a distance of 2 km out from the pluton margin (Ross, 1969). The contact aureole is characterized by an albite-epidote hornfels facies mineral assemblage in the outer part of the aureole, which abruptly changes to an upper hornblende hornfels facies assemblage close to the pluton margin. Ross (1969) interpreted emplacement of the Santa Rita Flat pluton to be by both passive and forceful mechanisms, but was unable to determine the relative importance of each mechanism. However, unlike the Cretaceous age Papoose Flat and Birch Creek plutons exposed in the White-Inyo mountains to the north (Fig. 1), which were forcibly emplaced and are surrounded by highly strained wall rocks (Nelson and Sylvester, 1971; Sylvester et al., 1978; Law et al., 1992; Morgan et al., 1998a; Saint Blanquat et al., in review), the metasedimentary rocks surrounding the Santa Rita Flat pluton do not contain a syn-plutonic schistosity and, although folded, have not been penetratively deformed. This suggests a dominantly passive emplacement mechanism.

PETROLOGY

Initial petrologic descriptions of the Santa Rita Flat pluton were made by Ross (1965, 1969) in reports accompanying the USGS quadrangle maps for this area. Follow-up work by Metz (1978) focussed on attempting to identify cryptic zonation within this macroscopically homogeneous pluton, and incorporated field and petrographic data, whole rock chemical analyses, X-ray diffraction data, and microprobe analyses. Metz (1978) sampled the pluton on a 1 km grid spacing (Fig. 3). Hand samples were analyzed

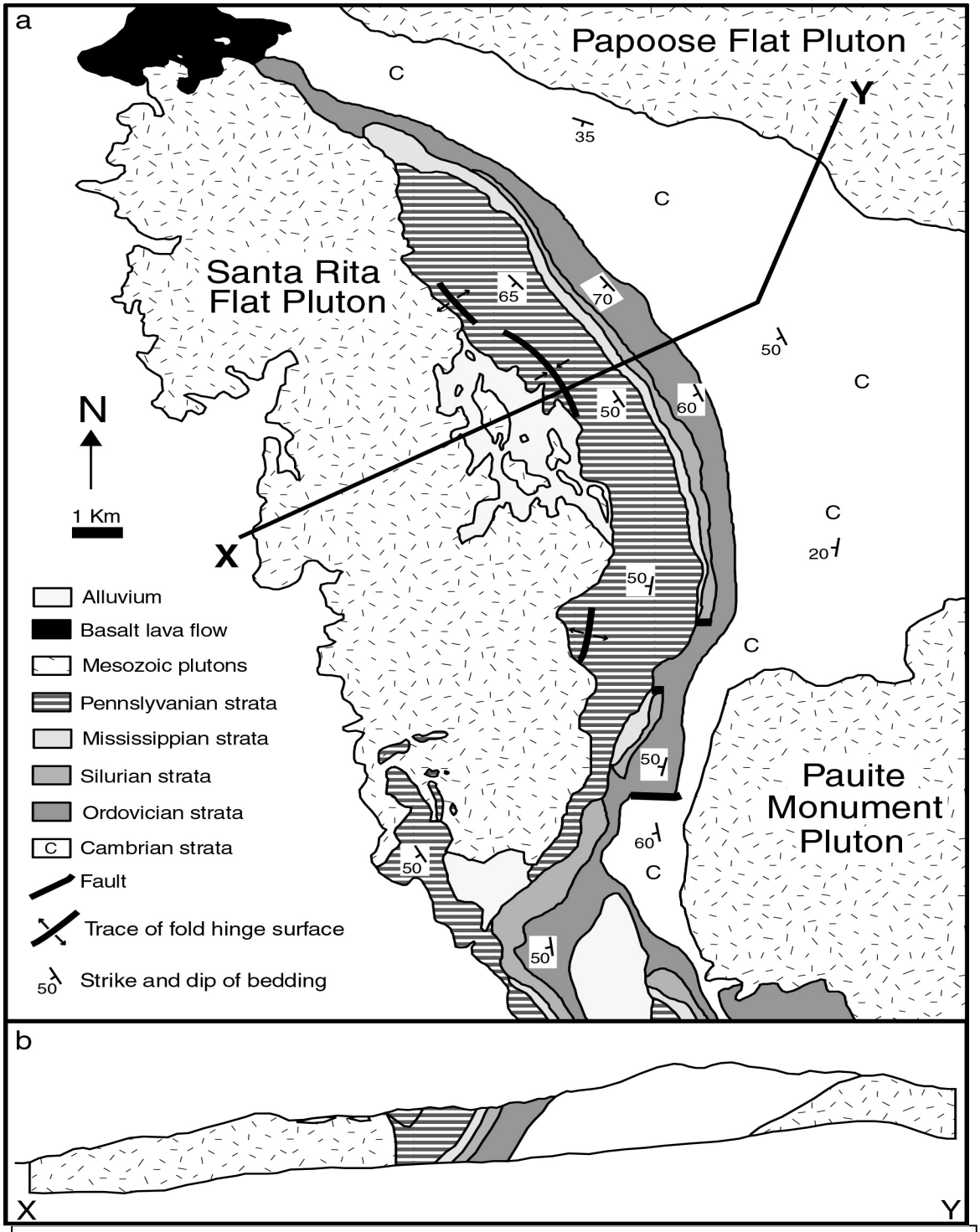

Figure 2: Simplified geologic map (a) and cross section (b) of the Independence Quadrangle (modified from Ross, 1965). Location indicated in Figure 1. Line of cross-section (XY) shown in Figure 15 is indicated.

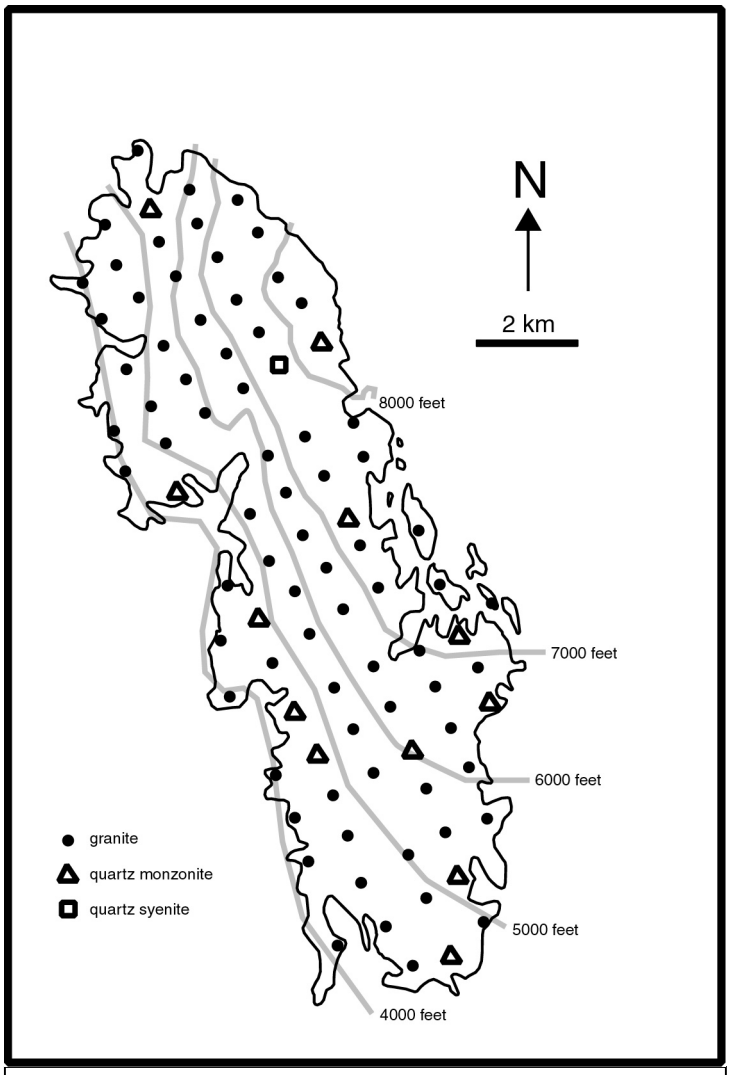

Figure 3: Map indicating rock types from Metz's (1978) sample locations. Erosion surface is indicated by 1000′ topographic contours across the Santa Rita Flat pluton. Note: northern portion of pluton is exposed at higher topographic level than southern portion.

for specific gravity; modal mineral compositions, microtextures and relationships between the different mineral phases were investigated using standard thin section techniques. The following petrologic description summarizes the work of Metz (1978).

Compositionally the Santa Rita Flat pluton falls within the granite field as defined by LeMaitre (1989). Primary minerals include plagioclase feldspar (Or_{1-3}, Ab_{56-60}, An_{38-41}), K-feldspar, quartz, hornblende and biotite; accessory minerals include magnetite, titanite, pyroxene, zircon, allanite, apatite and copper minerals. Plagioclase, K-feldspar and quartz make up 85% of the rock, while biotite and hornblende comprise approximately 11%. Textural relationships indicate that epidote, chlorite, muscovite and hematite are only present as alteration minerals. Unaltered and unzoned plagioclase grains, and euhedral hornblende crystals, are more prominent at the margins of the pluton and decrease in abundance northwards towards the interior of the pluton which is exposed at higher topographic elevations. The plagioclase crystals exhibit synneusis twinning and display no evidence for solid-state deformation. Locally, K-feldspar and hornblende form up to 3 cm long megacrysts that impart a porphyritic texture to the rock, although no discernible preferred orientation of these phenocrysts was observed in thin section. The modal composition of these porphyritic rocks falls within the quartz monzonite field. K-feldspar was observed to be more prominent and coarser grained towards the interior of the pluton.

The margins of the Santa Rita Flat pluton are dominantly more mafic (higher plagioclase and hornblende content) than the pluton interior, and are characterized by higher densities. Specific gravity is lower in the northern section of the pluton, which is though to represent an erosional level closer to the pluton interior. However, variation in specific gravity may also be related to changes in the proportion of oxide minerals. Magnetite is the principal oxide mineral within the pluton and occurs both as inclusions and as grain clusters surrounding hornblende (Fig. 4). No genetic association between magnetite and biotite was observed. Pluton-scale domainal variations in the ratio of hornblende to biotite abundance is summarized in Figure 5. Hornblende becomes more abundant, and biotite less abundant, traced southward from the interior of the pluton towards the pluton roof. Therefore, the increase of hornblende towards the southern margin of the pluton, and the close association of magnetite with hornblende grains,

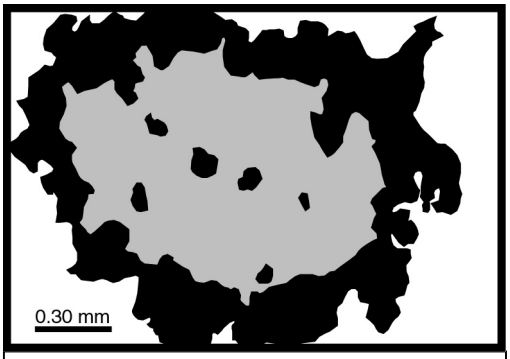

Figure 4: Sketch of amphibole surrounded by magnetite grains (adapted from Metz, 1978). Note: some magnetite grains also occur as inclusions within amphibole.

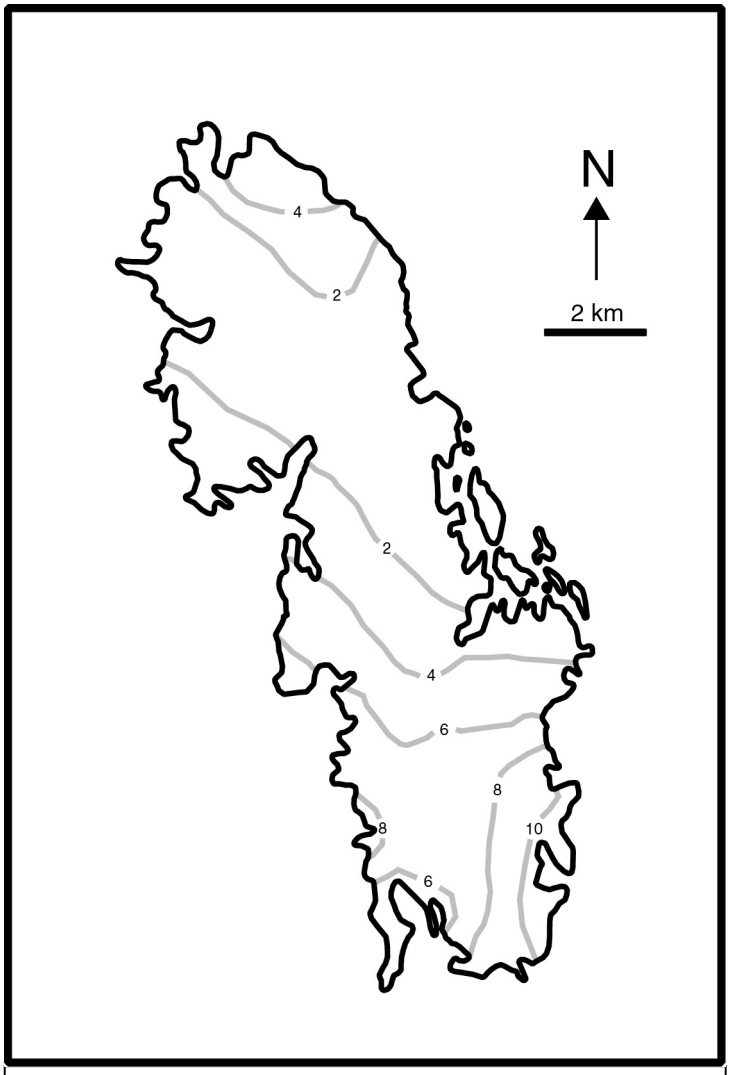

Figure 5: Hornblende/biotite ratio map of the Santa Rita Flat pluton (adapted from Metz, 1978).

should correlate with an increase in magnetite content towards the pluton margin. Fe_2O_3 concentrations from bulk chemical analyses do gradually increase towards the southern portion of the pluton, and correlate with an increase of both hornblende and magnetite towards the southern part of the pluton. Electron microprobe analyses of the magnetite grains indicate that they are dominantly composed of Fe, and have small amounts of Al, Si, K, Ti, Mn, Mg, and Cr.

The thermal history of the pluton interior has been investigated by Metz (1978) using X-ray diffraction based analyses of the structural state of the K-feldspar grains. The structural state of K-feldspar is a measure of the degree of Al-Si ordering within the SiO_4 tetrahedra (Ribbe, 1975). Random substitution of Al within the tetrahedral sites (referred to as disordered or low structural state) occurs at high temperatures, whereas Al that is preferentially ordered in selective tetrahedral sites occurs at low temperature. Generally, the more ordered feldspars are located in the northern part of the pluton, while less ordered feldspars were observed around the southern margin of the pluton. Thus, K-feldspar located around the southern margin of the pluton crystallized under high temperatures and at fast crystallization rates, close to pluton roof. In contrast, K-feldspar in the northern part of the pluton crystallized in the pluton interior at lower temperatures and probably lower crystallization rates. The fact that higher crystallization temperatures are indicated close to the pluton roof, rather than in the pluton interior, suggests that formation of the pluton may have involved injection of several magma batches at progressively lower temperatures. This is in agreement with the observation that the more mafic phases are concentrated towards the pluton roof and side walls.

ANISOTROPY OF MAGNETIC SUSCEPTIBILITY

Numerous previous studies have demonstrated a close parallelism between the ellipsoids of magnetic susceptibility and grain shape fabric, and measurement of anisotropy of magnetic susceptibility at low-field is now almost routinely used in granitoids for the analysis of both solid-state fabrics and the more subtle magmatic fabrics (see review by Bouchez, 1997, and references therein). AMS provides a rapid insight into the bulk internal structure of a pluton and facilitates the definition of fabric components, including especially the linear fabric component which is either difficult or impossible to recognize in the field. In the case of the Santa Rita Flat pluton, no

macroscopic grain-shape fabrics have been detected (apart from in cross-cutting shear zones), and therefore AMS analysis offers the only available research tool for documenting the presence of any subtle magmatic fabrics that may be present. However, the relationship between the grain shape fabric of a rock and its magnetic fabric depends on the nature of the magnetic (Fe bearing) minerals, and on the textural relationships between the mineral grains (Rochette, 1987; Jover et al., 1989; Borradaile, 1991; Rochette et al., 1992). If a sample contains more than one magnetic mineral, the magnetic fabric becomes a composite of two or more subfabrics. Therefore, interpreting AMS data requires careful identification and characterization of all the magnetic minerals contributing to the AMS signal.

The major rock forming minerals within granites (feldspar and quartz) are characterized by diamagnetic properties and give negative susceptibilities. Biotite, hornblende, and magnetite are the most important and common minerals that provides slightly positive susceptibilities. Biotite and hornblende are paramagnetic and have a magneto-crystalline anisotropy (Bouchez, 1997). Magnetite is ferromagnetic with a strongly positive susceptibility and, depending on the grain size, may exhibit a single-domain or a multi-domainal magnetic behavior. Magnetite in granites, due to its coarse grain size, has a multi-domainal nature (Benn et. al., 1993; Archanjo et. al., 1995). Therefore, within most granites magnetite grains have a magnetic anisotropy that is proportional to the grain shape ratio (Uyeda et. al., 1963), and the shape preferred orientation of the grains is likely to control the magnetic fabric (see review by Bouchez, 1997).

Methodology

Two oriented granite hand samples were collected at each of 64 stations located on a 1 km grid pattern (Fig. 6). AMS samples could not be collected in the northeast part of the pluton due to the extreme cliff-like nature of the exposures. The oriented samples were cored in the laboratory, and the 2.5 cm diameter cores were then oriented. The oriented cores were then cut into 2.6 cm length samples using a non-magnetic blade; an average of 7 samples being produced for each station. Anisotropy of magnetic susceptibility for the 461 oriented samples was measured at the Laboratoire de Pétrophysique et Tectonique, Université Paul-Sabatier,

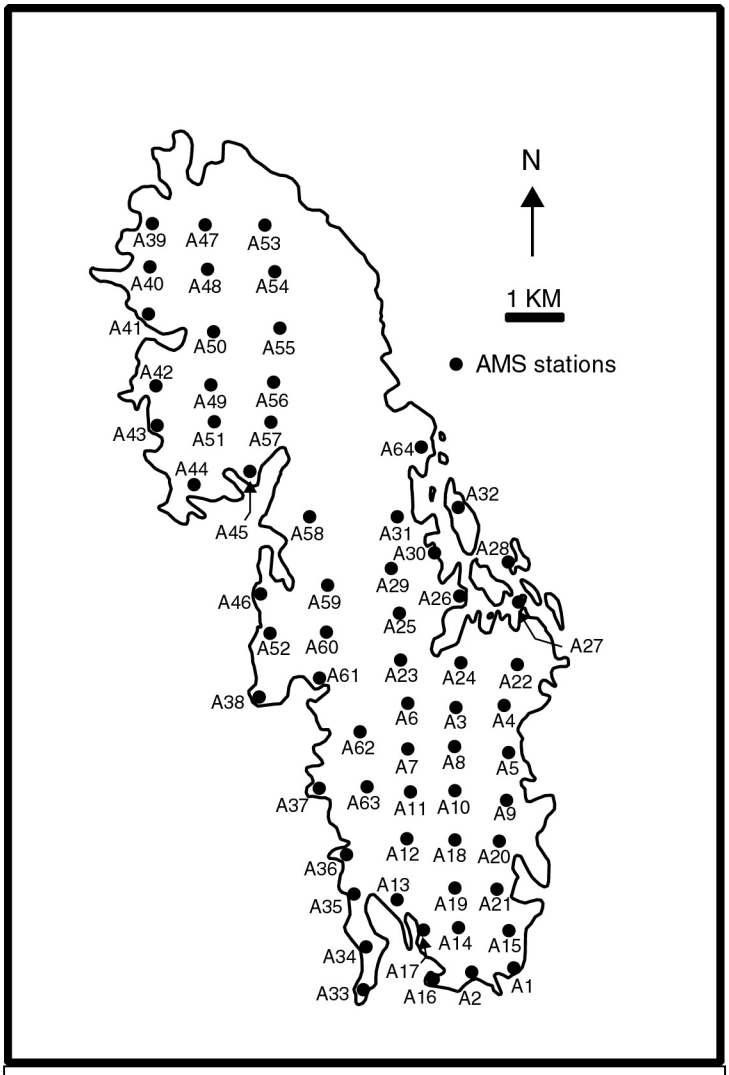

Figure 6: Location of sampling sites for AMS survey of the Santa Rita Flat pluton.

using a kappabridge KLY-2, manufactured by Agico (Brno, Czech Republic). Fifteen measurements from each sample were taken in different orientations, and the orientation and magnitude of the three principal axes of the AMS ellipsoid, $k_1 \geq k_2 \geq k_3$ for each sample were calculated from the bulk susceptibility data and the orientation of the sample using the ANISOFT package of Jelinek (1981). The working data for each site were computed from the tensor means of the sample data with the program EXAMS (Saint Blanquat, 1993) giving the bulk magnetic susceptibility magnitude of the site, the orientation and intensity of the three main susceptibility axes K_1, K_2, and K_3, and the usual intensity (P%, F%, L%) and shape (T) parameters. Directional data were automatically plotted on equal area stereonets using the EXAMS program, and contoured maps of the magnetic data were produced at Virginia Tech using the SURFER software package.

AMS data

Magnetic susceptibility. Typically, in ferromagnetic rocks susceptibility (K) is a measure of how much magnetite is present (see reviews by Tarling and Hrouda, 1993; Bouchez, 1997). The susceptibility values for the Santa Rita Flat pluton vary from 11 x 10^{-5} to 49 x 10^{-5} SI, averaging 23 x 10^{-5} SI (Fig. 7). The lower susceptibilities are generally observed around the outer edges of the pluton. Two traverses from north to south (A-B; B-C) in Figure 7 document the increase in susceptibility (and magnetite content) towards the central to southern part of the pluton. This agrees with the hornblende/biotite ratio map (Fig. 5), and the petrographic correlation of magnetite with hornblende (Fig. 4). As hornblende increases towards the south so does magnetite, and thus the susceptibility is typically higher in the southern portion of the pluton.

Magnetic anisotropy. The degree of magnetic anisotropy of an individual sample, expressed as a percentage ($P\% = 100[(k_1/k_3) - 1]$) refers to the degree of fabric development. Figure 8 is a contoured map of anisotropy values within the Santa Rita Flat pluton. Anisotropy values range from 0.5% to 9.7% (k_1/k_3=1.005; k_1/k_3=1.097), and have an average of 5.6%. 93% of the total anisotropy values lie between 3% and 8%.

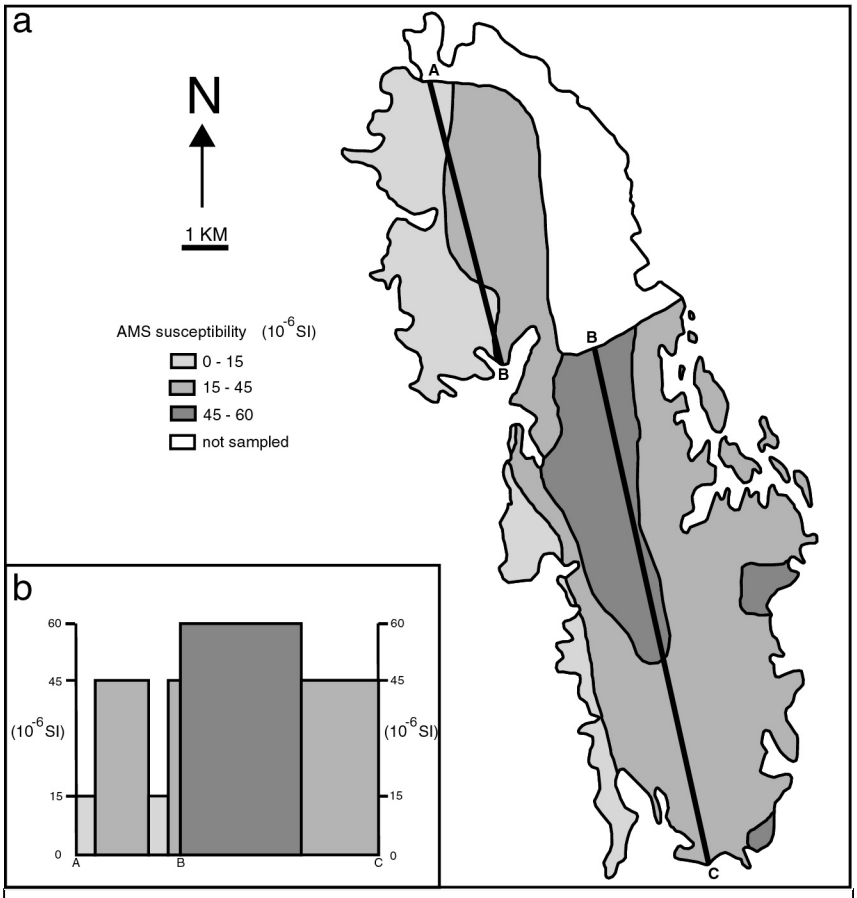

Figure 7: (a) Magnetic susceptibility contour map, and (b) A-B-C cross sectional histogram of susceptibility values within the Santa Rita Flat pluton. Note: susceptibility increases towards central and southern parts of pluton.

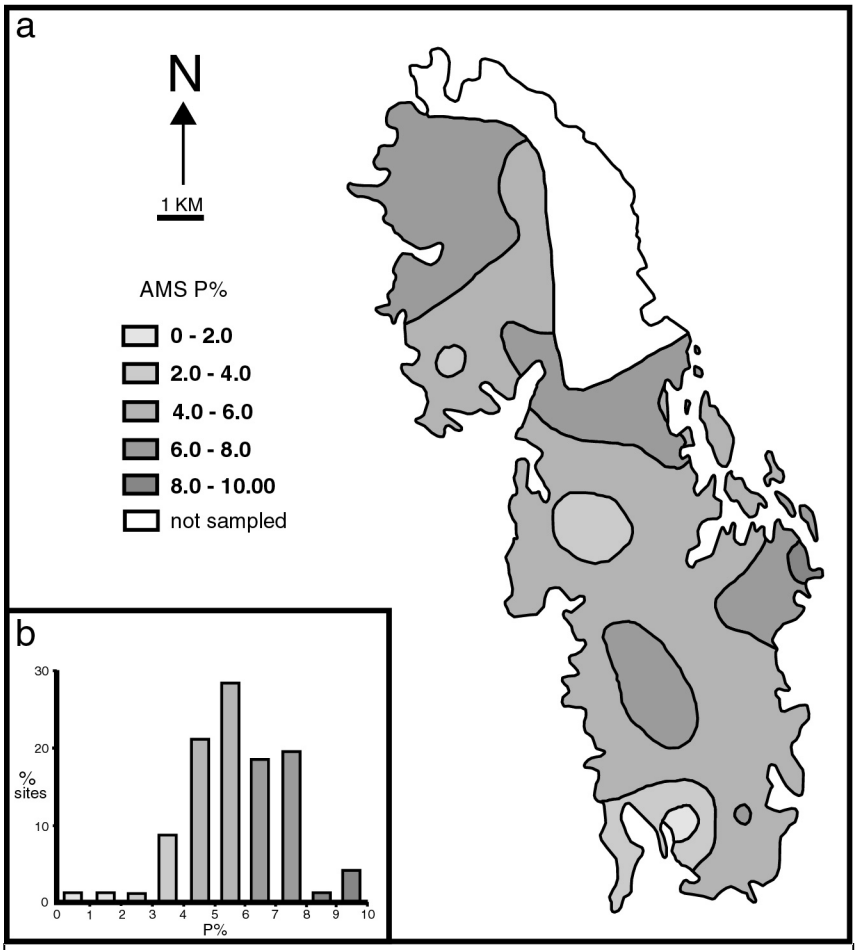

Figure 8: (a) Magnetic anisotropy contour map and, (b) frequency histogram of percent anisotropy within the Santa Rita Flat pluton.

The highest anisotropy values are recorded within the western flank of the Santa Rita Flat pluton.

Extremely wide ranges in anisotropy values, such as observed in the Santa Rita Flat pluton, cannot be entirely explained by the shape fabric intensity of magnetite (Archanjo et al., 1995). Plotting the values of total anisotropy against susceptibility may provide information on the shape fabric and homogeneity of distribution of the magnetite grains. Granites that contain both paramagnetic and ferromagnetic minerals are magnetically composite in nature and should show a positive correlation between total anisotropy and susceptibility (Rochette et. al., 1992). Figure 9 documents an abrupt positive correlation between the total anisotropy and susceptibility within the Santa Rita Flat pluton. An abrupt increase in total anisotropy with increasing susceptibility suggests that a distribution anisotropy exists among the magnetite grains (Bouchez, 1997; Saint Blanquat and Tikoff, 1997).

Shape parameter. Fabric symmetry may be described by using either the shape parameter T (Jelinek, 1981) or the Flinn shape parameter (Flinn, 1962) more commonly used in strain analysis. T was used for the Santa Rita Flat pluton. T values can range between –1 and +1, with prolate AMS ellipsoids having T values between –1 and 0, and oblate ellipsoids having T values between 0 and 1. 85% of the Santa Rita Flat pluton sample stations are characterized by oblate fabric ellipsoids (Fig. 10). Oblate fabrics are widely dispersed throughout the pluton and are recorded both in the pluton interior and at the pluton margins. In contrast, prolate fabrics are most frequently recorded at the pluton margins (Fig. 10). Oblate fabrics are commonly recorded in biotite/magnetite-rich granites, while prolate fabrics are expected in hornblende-rich granites (Bouchez, 1997). The Santa Rita Flat pluton is composed of both paramagnetic and ferromagnetic minerals and its AMS signature is therefore composite in nature. Plotting T against susceptibility values for individual sample sites (Fig. 11a) indicates that the oblate AMS ellipsoid within the Santa Rita Flat pluton is dominated by the magnetically stronger magnetite grains. As susceptibility increases within the pluton a more oblate fabric component is observed, suggesting a positive correlation between magnetite content and the degree of oblate fabric development. This may also be

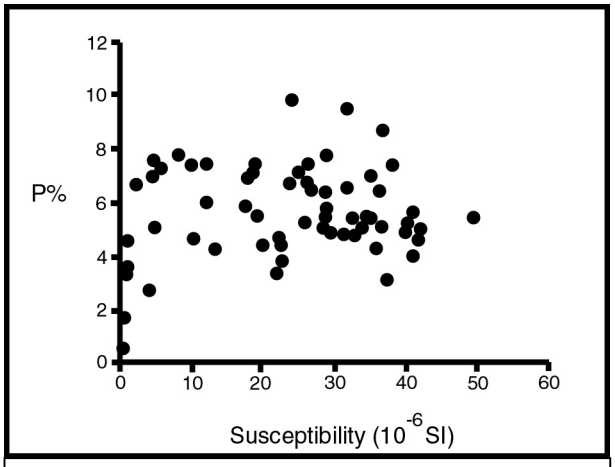

Figure 9: Magnetic susceptibility versus anisotropy (P%).

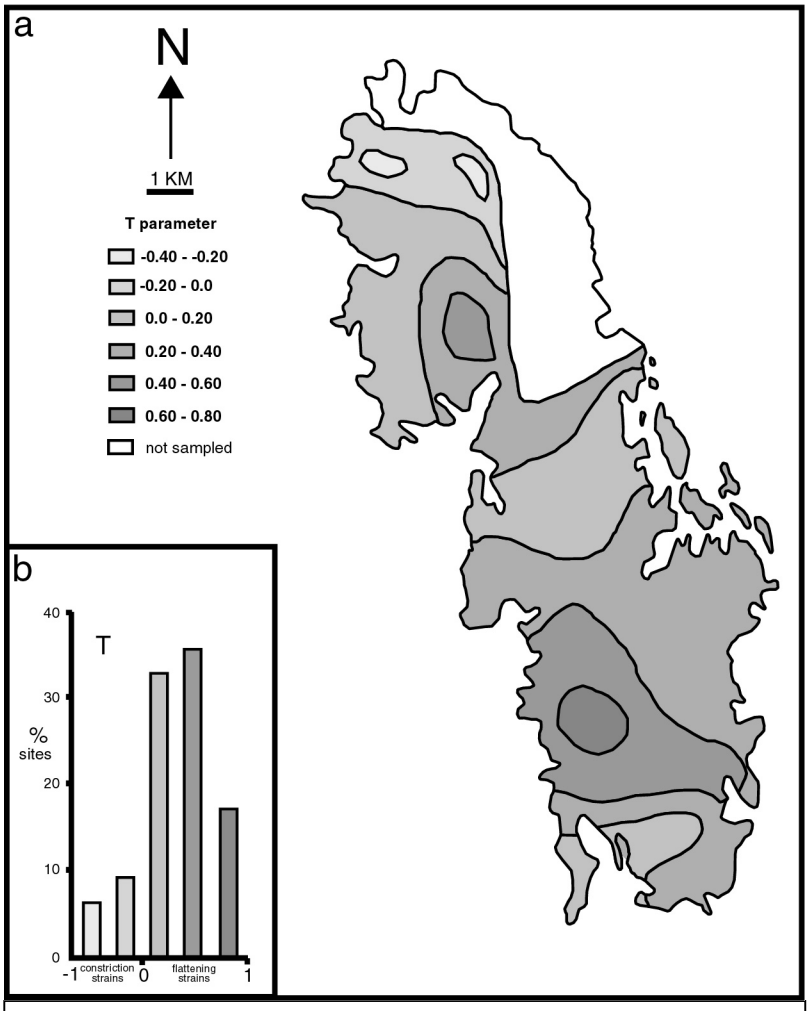

Figure 10: (a) Domainal distribution of shape parameter T, and (b) frequency histogram of constriction and flattening strains from the Santa Rita Flat pluton.

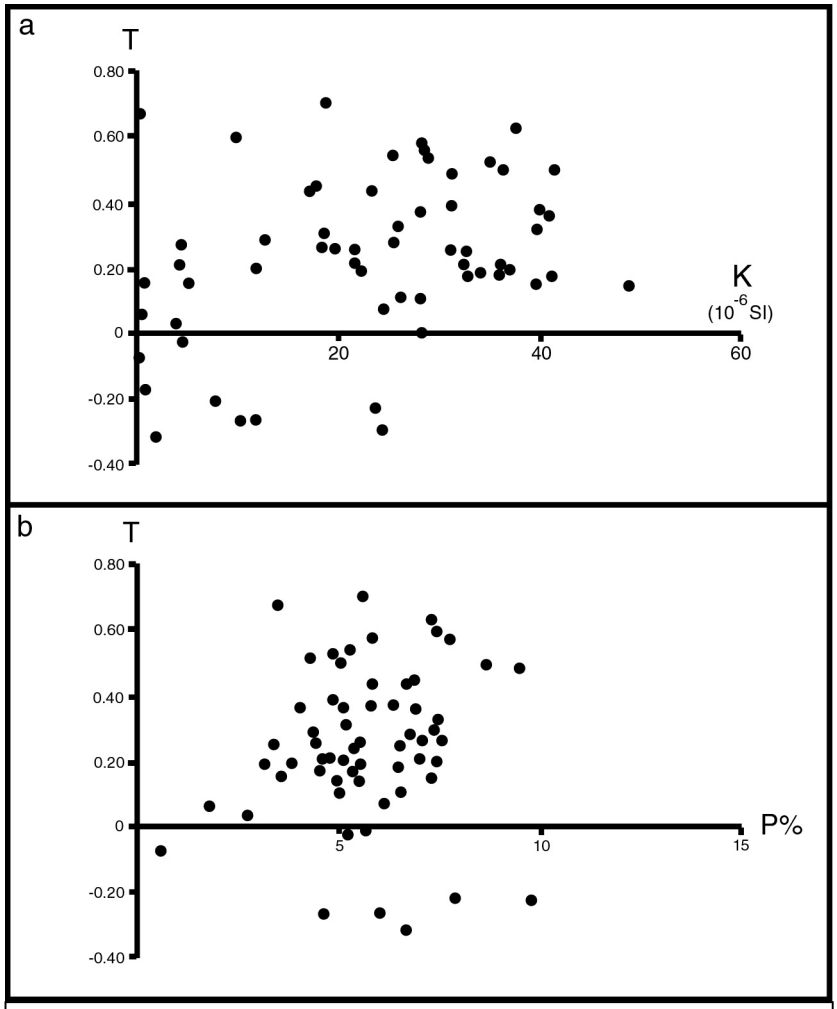

Figure 11: (a) Magnetic susceptibility versus shape parameter (T). (b) Magnetic anisotropy versus shape parameter (T).

indicated in Figure 11b where plotting of shape parameter T against anisotropy (P%) suggests a weak positive correlation between anisotropy and the degree of oblate fabric development.

Magnetic foliation and lineation. Maps of magnetic foliation and lineation within the Santa Rita Flat pluton are presented in Figures 12 and 13. The most notable features on the foliation map are the moderate dips of foliation towards the south and east, and the southward-plunging antiformal structure defined by foliation in the central and southern parts of the pluton (Fig. 12a). Poles to foliation (Fig. 12b) indicate that this antiformal structure plunges at 33° towards 162°. Lineation is generally gently-moderately plunging and trends NNW-SSE (Fig. 13a). The vector mean of lineation orientations plunges at 40° towards 153° (Fig. 13b). The close parallelism between the calculated axis of the antiform defined by foliation, and the vector mean of the lineations, indicates that the two structures are genetically linked and may have formed at the same time.

Within individual sites, the magnetic fabric orientation is remarkably stable from one core sample to the other, conferring a high degree of confidence to the magnetic foliation and lineation maps. Five fabric types, based on angular variation in orientation between the three principal susceptibility axes in different samples from the same station, have been distinguished for the Santa Rita Flat pluton (Fig. 14a). The relative frequency of each fabric set is indicated in Fig. 14b. Type 1) each set of principal axes are strongly clustered (27%); 2) each set of principal axes are moderately clustered (17%); 3) K3 is well defined and occupies a pole position to plane containing K1 and K2 (31%); 4) K1 is well defined and occupies a pole position to plane containing K2 and K3 (9%); and 5) axes are dispersed (16%). Only type 5 fabrics are difficult to quantitatively interpret in terms of their directional properties. The dominant occurrence of type 3 fabric types (K3 well defined) agrees well with the dominance of oblate magnetic fabric symmetries within the pluton. A frequency histogram of the within-site angular variability for k1 and k3 indicates that 62% of sites have less than a 30° angular range in orientation of k1, and 79% of sites have less than a 30° angular range in orientation of k3 (Fig. 14c).

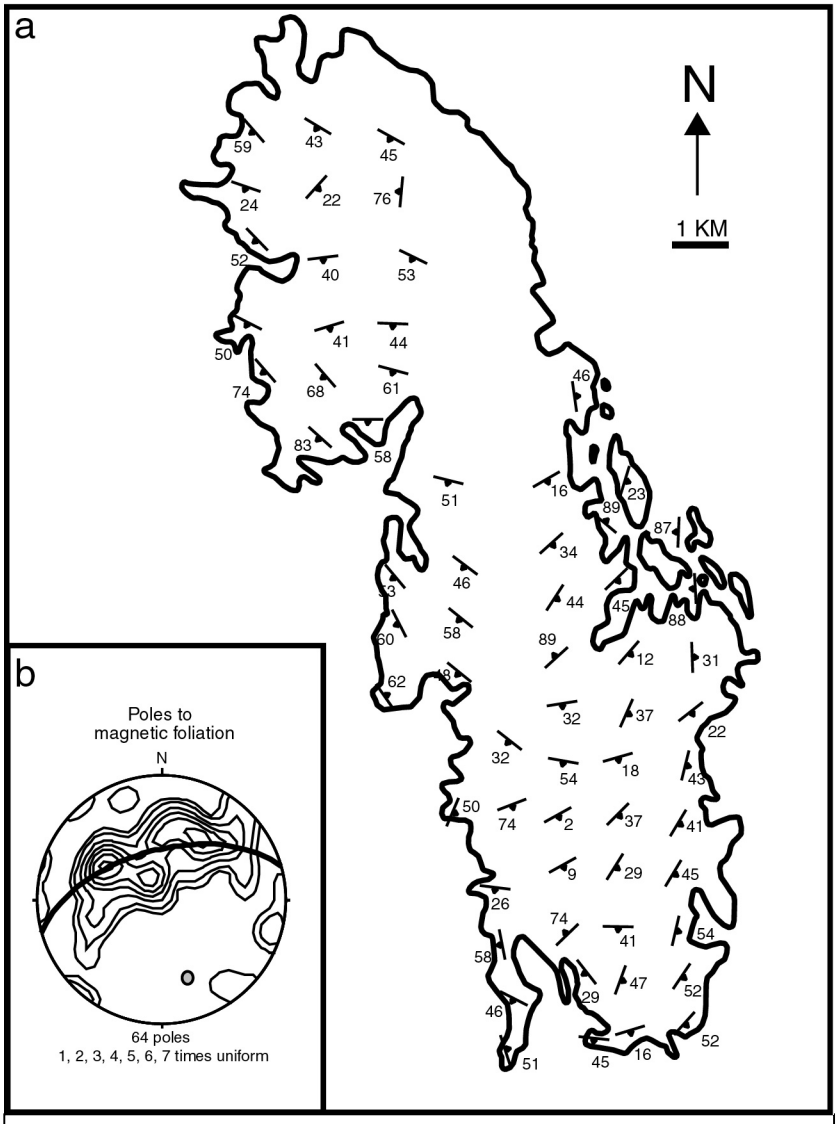

Figure 12: (a) Magnetic foliation map and, (b) stereoplot of poles to foliation. Note: foliation in southern part of pluton defines a south-plunging anitform; poles to foliation indicate antiform plunges at 33° towards 162°.

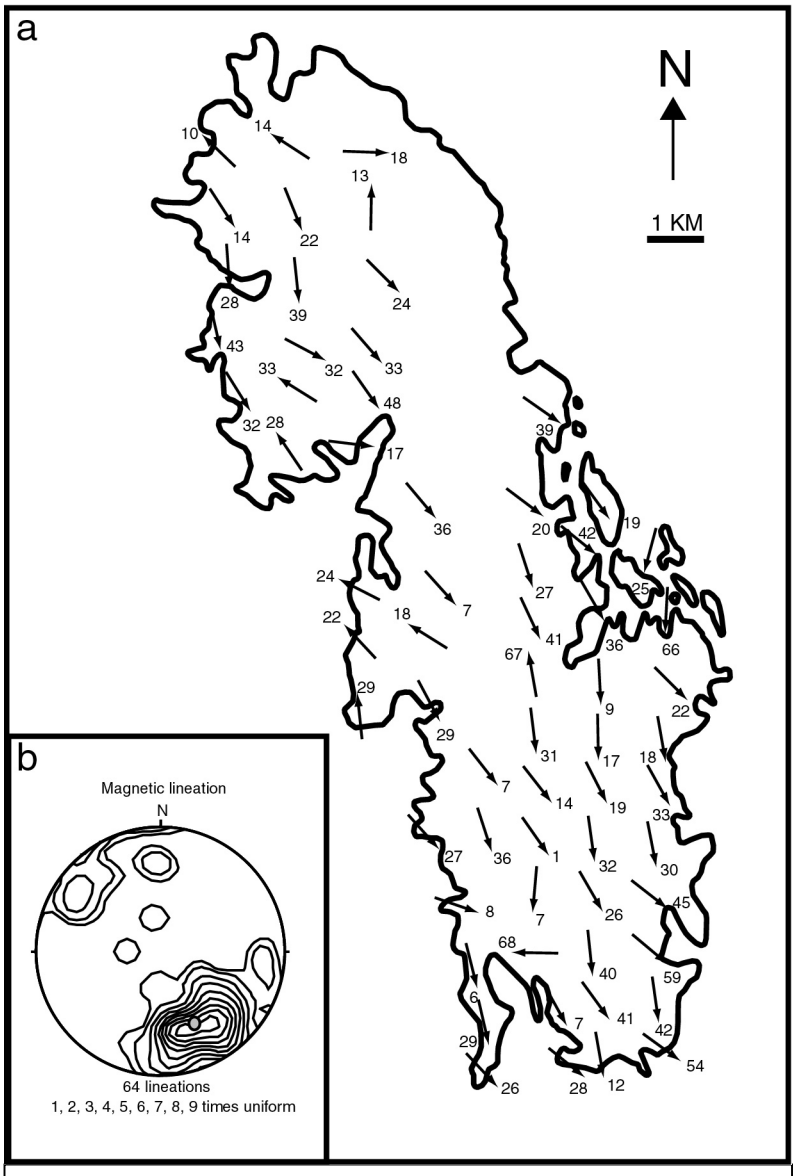

Figure 13: (a) Magnetic lineation map, and (b) stereoplot of lineations. Vector mean of magnetic lineations (orientation indicated on stereoplot) within the Santa Rita Flat pluton plunges at 40° towards 153°.

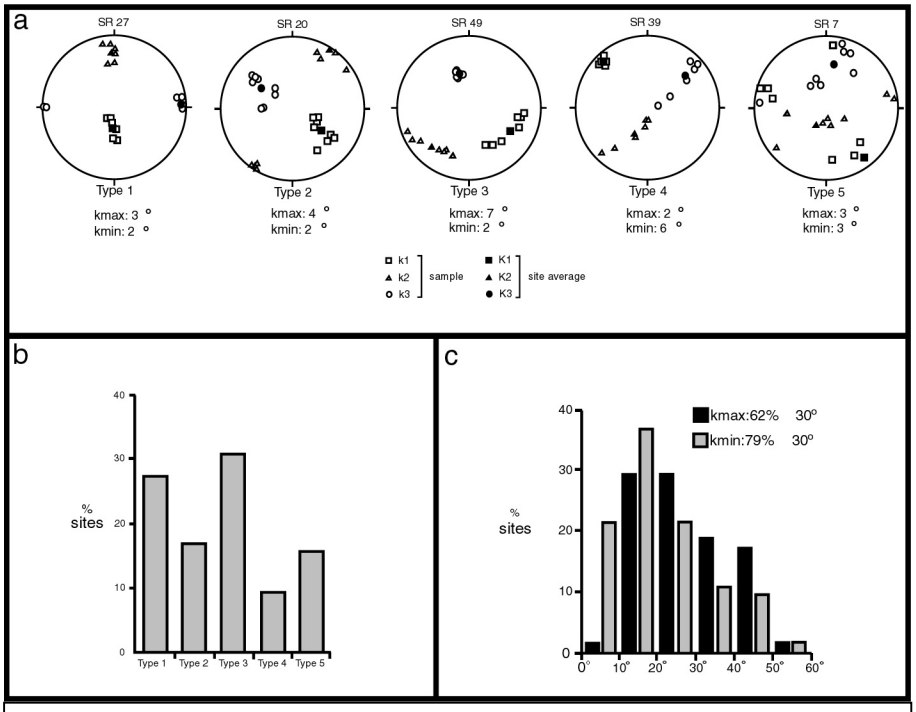

Figure 14: (a) Examples of the five distinct magnetic fabric types distinguished within the Santa Rita Flat pluton, based on unique angular relationship between the susceptibillity axes. (b) Frequency histogram of the five fabric types. (c) Frequency histogram of within-site angular variability between maximum and minimum principal magnetic susceptibility directions k1 and k3.

DISCUSSION

In recent years there has been widespread debate over the mechanisms of pluton emplacement, and the relative importance of tectonic versus magmatic processes in controlling pluton emplacement. Traditionally emplacement mechanisms have been divided into permitted and forcible categories and the rate of cavity opening relative to magma influx has commonly been regarded (e.g. Hutton, 1988) as being one of the prime factors in controlling the style of emplacement. Syntectonic emplacement of plutons within shear zones has become a favored model for overcoming space problems associated with pluton emplacement, and many recent studies have documented how development of fabrics within such plutons may be controlled by tectonic processes (e.g. Tikoff and Teyssier, 1992; Bouchez and Gleizes, 1995; Archanjo et. al., 1995; Aranguren et. al., 1997; Saint Blanquat and Tikoff, 1997). These basically fault-controlled plutons are usually elongate in map view, and display magnetic foliation patterns with characteristic sigmoidal traces reflecting the regional shear sense (e.g. Bouchez and Gleizes, 1995; Saint Blanquat and Tikoff, 1997). However, although regional-scale shear zones may commonly provide pathways for the mechanically efficient transport and emplacement of magma, it remains likely that magma may also take advantage of other mechanical anisotropies in the surrounding and overlying crust.

The Santa Rita Flat pluton displays a tabular shape in map view, and the lack of high-strain penetrative deformation fabrics within the pluton margins and surrounding wall rocks suggests a permitted rather than forcible emplacement mechanism. The pluton is located within a belt of north-northwest trending folds related to the East Sierran Thrust System (ESTS) that was active from ~185 - ~148 Ma (Dunne, 1986; Stevens et. al., 1997). Northwest trending folds are pervasive along the western flank of the Inyo and White Mountains, and may have accommodated strains at the lateral tips of thrust faults which crop out in the southern Inyo Mountains. Although the western part of the Santa Rita Flat pluton is obscured by Quaternary alluvial deposits, regional mapping (Ross, 1965) indicates that the metasedimentary rocks surrounding the eastern margin of the pluton young towards and may locally dip beneath the pluton (Fig. 2). Based upon the field mapping of Ross (1962, 1965) we propose that the pluton is located in the hinge zone of a southeast plunging synform

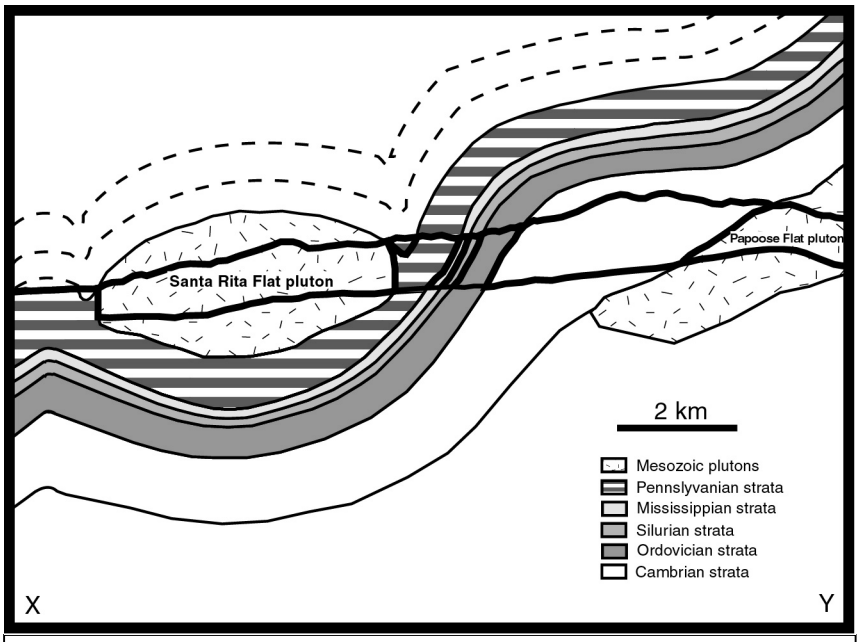

Figure 15: Inferred structure of metasedimentary rocks surrounding the Santa Rita Flat pluton. Line of section indicated in Figure 2. Bold lines are from geologic cross section of Ross (1965). Note: stratigraphic units and dips define an inferred asymmetric minor fold. The Santa Rita Flat pluton is located in the hinge zone of the synformal part of this inferred minor fold on the western limb of the Inyo Anticlinorium.

belonging to this suite of folds (Fig. 15). The pluton's U-Pb zircon age of 164 Ma overlaps in time with formation of the ESTS to the south, and we speculate that space for initial emplacement of the Santa Rita Flat pluton may have been produced by dilation due to layer-parallel slip between adjacent competent layers in the hinge zone of this km-scale thrust-related synform. We acknowledge, however, that direct evidence for the presence of this synform is lacking, because the country rocks flanking the western margin of the pluton are covered by Quaternary sediments (Fig. 1). This proposed synform could mark the southeastward extension of a northwest trending synform which has been mapped to the north of the pluton (Fig. 1), now off-set by intrusion of the Cretaceous Papoose Flat pluton (Fig. 1). The synform presumably forms part of a northeast-vergent asymmetric minor fold pair located on the southwest-dipping limb of the regional scale White-Inyo anticline (Fig. 1). Alternatively, if as suggested by Ross (1962, 1969) the Santa Rita Flat pluton can be correlated with the Tinemaha granodiorite in the eastern Sierra (Fig. 1), then the proposed synform (now offset by faulting in Owens Valley) may extend into the eastern Sierra due west of Big Pine (Fig. 1). There Bateman (1965) has mapped Paleozoic marble units surrounding eastern and northern margins of the granodiorite. Foliation in the marble dips inwards towards the pluton suggesting a southward plunging synformal structure. However, confirmation of the synformal structure cannot be made, because the western margin of the granodiorite is cut by younger plutonic rocks, and the southern margin is covered by alluvium and Quaternary basaltic lava flows.

Saddle reefs are cavity infilling structures located along the hinge zones of folds in which appreciable interlayer slip has occurred between adjacent competent layers, and have long been associated with important economic deposits (e.g. Mendelsohn, 1959; Ramsay, 1967). The characteristic three dimensional shape of saddle reef deposits includes: i) saddle like geometries in cross-section and, ii) pipelike geometries in plan view with the long axis of the pipe oriented parallel to the local fold hinge. The long axis of the Santa Rita Flat pluton in map view trends at ~155°, and is subparallel to the averaged magnetic lineation within the pluton (Fig. 13). At the regional scale, ESTS fold hinges along the western margin of the White-Inyo Range trend between ~140° and ~176°, and have an average orientation of ~151° (Dunne et. al., 1978; Dunne, 1986; Stevens et. al., 1997). Further, NW-trending ESTS fold hinges in the White-Inyo Range

have been correlated with similar trending minor folds along the Nevadan Synclinorium in the Sierra Nevada roof pendants located to the west (Schweickert, 1981). This parallelism between the pluton and surrounding regional-scale fold structures, coupled with their similar ages of formation, suggest that the Santa Rita Flat pluton may have been initially emplaced as a saddle reef during folding. Specifically, the pluton is inferred to have been emplaced along a minor NW trending fold that is located on the western limb of the Inyo Anticlinorium. Microstructures within the pluton appear to be of purely magmatic origin (Metz, 1978), and therefore the gently-moderately plunging south-southeast trending magnetic lineation (vector mean trend of 153°) is interpreted to reflect the stretching direction of the pluton along the axis of the saddle reef at the time of emplacement.

Although compatible with the structure of the surrounding and underlying metasedimentary rocks, this speculative model cannot in its simplest form, however, explain the south-southeast plunging antiformal structure defined by both the overlying metasedimentary rocks and the magnetic foliation within the pluton itself (Fig. 12). To account for this apparent paradox we propose a two stage model for evolution of the pluton (Fig. 16a). Initial formation of the pluton involved intrusion as a sill-like or "saddle reef" structure along a dilating stratigraphically controlled mechanical discontinuity in the hinge zone of the enveloping synform. Subsequent vertical inflation of this sill, however, resulted in local upward doming of the overlying pluton roof and formation of the antiformal structure now observed at the current erosion level in the central-southern part of the pluton and overlying locally preserved roof rocks (Fig. 16a). In agreement with this model, no corresponding fold structure is indicated by AMS analysis in the northern part of the pluton which, from previous work by Ross (1969) and Metz (1978), is exposed at a deeper level, and represents a section closer to the pluton core (Figs 16b and c). The increase in magmatic pressure necessary to produce upward doming of the pluton margin and overlying country rocks could have been due to locking of the regional-scale fold and a resultant increase in the rate of magma influx relative to the rate of cavity opening. This model offers a mechanism for explaining the small-scale southward plunging synforms mapped by Ross (1965) in the Mississippian strata immediately adjacent to the eastern flank of the pluton (Figs. 2 and 15). The feeder for

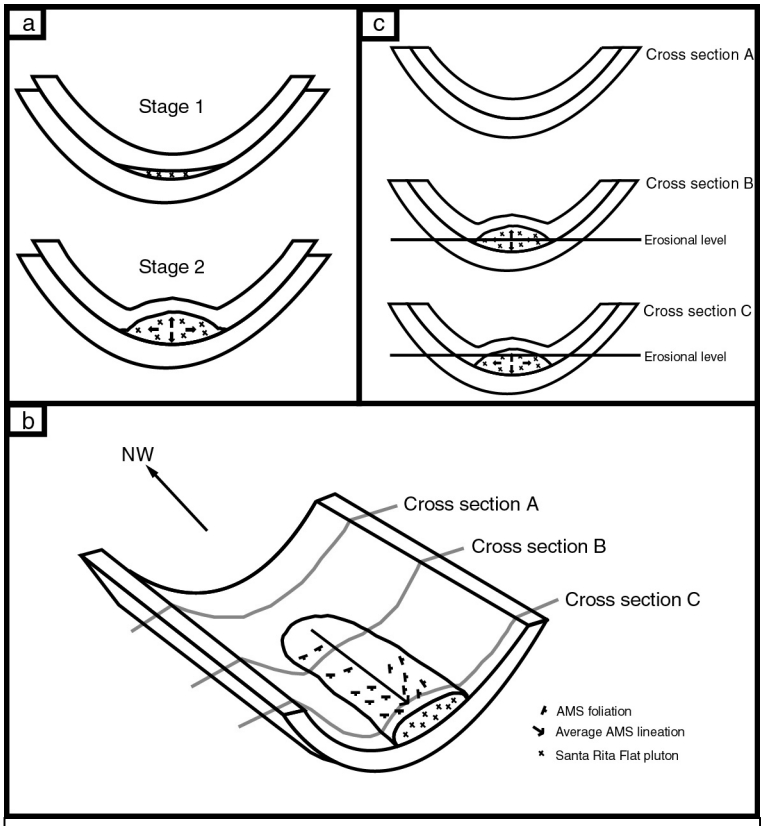

Figure 16: (a) Two-stage emplacement model for the Santa Rita Flat pluton. Stage 1 – tectonic induced folding of adjacent competent layers produces a pluton-scale saddle reef structure. Stage 2 – inflation of pluton within the saddle reef causes doming to occur near roof of the pluton (see text). (b) Three dimensional sketch illustrating location of the Santa Rita Flat pluton along hinge of a synform (see text). (c) Three serial cross sections taken across the inferred synform and indicating how present erosional surface relates to exposed structural level of pluton (see text).

the pluton is not exposed, however, and we have no information on its likely geometry (e. g. a cylindrical or planar conduit).

It remains to be determined whether other Middle-Late Jurassic plutons in the White Inyo Range could have been emplaced by a similar mechanism. We note, however, that both the Eureka Valley-Joshua Flat-Beer Creek (EJB) composite pluton (Morgan et al., 1998b) and the Sage Hen Flat pluton (Saint Blanquat and Law, unpublished data) located in the central White-Inyo Range (Fig. 1) are characterized by magnetic lineations which trend sub-parallel to those in the Santa Rita Flat pluton. In addition, the EJB pluton has previously been demonstrated to be situated within the hinge zone of a regional scale north-south trending synform (Morgan et al., 1998b), leading us to speculate that there may indeed be a similar emplacement mechanism for these plutons.

REFERENCES

Aranguren, A., Larrea, F. J., Carracedo, M., Cuevas, J., Tubia, J. M., 1997. The Los Pedroches Batholith (southern Spain): Polyphase interplay between shear zones in transtension and setting of granites. In: Bouchez, J. L., Hutton, D. H. W., Stephens, W. E. (eds), Granite: from segregation of melt to emplacement of fabrics, Kluwer Academic Publishers, Dordrecht, 215-229.

Archanjo, C. J., Launeau, P., and Bouchez, J. L., 1995. Magnetic fabric versus magnetite and biotite shape fabrics of the magnetite-bearing granite pluton of Gameleiras (Northeast Brasil). Physics of Earth and Planet Interiors 89, 63-75.

Bateman, P. C., 1965. Geology and Tungsten Mineralization of the Bishop District California. U. S. Geological Survey Professional Paper 470, 208 pp.

Bateman, P.C., 1992. Plutonism in the central part of the Sierra Nevada Batholith, California: U.S. Geological Survey Professional Paper 1483, 186 pp.

Bateman, P.C., Clark, L.C., Huber, N.K., Moore, J.G., and Rinehart, C.D., 1963. The Sierra Nevada batholith: a synthesis of recent work across the central part: U.S. Geological Survey Professional Paper 414-D, 46 pp.

Benn, K., Rochette, P., Bouchez, J. L., and Hattori, K., 1993. Magnetic susceptibility, magnetic mineralogy and magnetic fabric in a late Archean granitoid-gneiss belt. Precambrian Research 63, 59-81.

Borradaile, G. J., 1991. Correlation of strain with anisotropy of magnetic susceptibility. Pure and Applied Geophysics 135, 15-29.

Bouchez, J. L., 1997. Granite is never isotropic: an introduction to AMS studies of granitic rocks. In: Bouchez, J. L., Hutton, D. H. W., Stephens, W. E. (eds), Granite: from segregation of melt to emplacement of fabrics, Kluwer Academic Publishers, Dordrecht, 95-112.

Bouchez, J. L. and Gleizes, G., 1995. Two-stage deformation of the Mont-Louis-Andorra granite pluton (Variscan Pyrenees) inferred from magnetic susceptibility anisotropy. Journal of Geological Society of London 152, 669-679.

Chen, J. H-Y, 1977, Uranium-lead isotopic ages from the southern Sierra Nevada batholith and adjacent areas, California: Santa Barbara, University of California, Ph.D. thesis, 183 pp.

Clemens, J. D., 1998. Observations on the origins and ascent mechanisms of granitic rocks. Journal of Geological Society of London 155, 843-851.

Crowder, D. F., and Sheridan, M. F., 1972. Geologic map of the White Mountain peak quadrangle, Mono County, California. U. S. Geological Survey Map GQ-1012.

Cruden, A. R., 1998. On the emplacement of tabular granites. Journal of Geological Society of London 155, 853-862.

Dunne, G. C., 1986. Geologic evolution of the southern Inyo Range, Darwin Plateau, and Argus and Slate Ranges, east-central California – An overview. In: Dunne, G. C. (ed), Mesozoic and Cenozoic structural evolution of selected areas, east-central California, Geological Society of America Annual Meeting, Cordilleran Section, Los Angeles, California, 1986, Guidebook and Volume, Field Trips 2 and 14, 3-21.

Dunne, G. C., Gulliver, R. M., and Sylvester, A. G., 1978. Mesozoic evolution of rocks of the White, Inyo, Argus and Slate Ranges, eastern California. In: Howell, D. G. and McDougall, K. A. (eds), Mesozoic paleogeography of the western United States, Society of Economic and Paleontologic Mineralogists, Pacific Section, Book 8, 189-207.

Ernst, W. G., and Hall, C. A., 1987. Geology of the Mount Barcroft-Blanco Mountain area, eastern California. Geological Society of America Map and Chart Series. Map MCH066.

Flinn, D., 1962, On folding during three dimensional progressive deformation. Quarterly Journal Geological Society of London 118, 385-428.

Hanson, R. B., 1986. Geology of Mesozoic metavolcanic and metasedimentary rocks, northern White Mountains, California. Ph.D. dissertation, University of California, Los Angeles.

Hutton, D. H. W., 1988. Granite emplacement mechanisms and tectonic controls: Inferences from deformation studies: Royal Society of Edinburgh Transactions, Earth Sciences, v. 79, p. 245-255.

Jelinek, V., 1981. Characterization of the magnetic fabric of rocks. Tectonophysics 79, 63-67.

Jover, O., Rochette, P., Lorand, J. P., Maeder, M., and Bouchez, J. L., 1989. Magnetic mineralogy of some granites from the French Massif Central: origin of their low-field susceptibility. Physics of Earth and Planet Interiors 55, 79-92.

Krauskopf, K. B., 1971. Geologic map of the Mt. Barcroft Quadrangle, California-Nevada. U. S. Geological Survey Map GQ-960.

Law, R. D., Morgan, S. M., Casey, M., Sylvester, A. G., and Nyman, M., 1992. The Papoose Flat pluton of eastern California: A reassessment of its emplacement history in the light of new microstructural and crystallographic fabric observations. Transactions, Royal Society of Edinburgh, Earth Sciences 83, 361-375.

LeMaitre, R.W., 1989. A classification of igneous rocks and glossary of terms: Recommendations of the International Union of Geological Sciences Subcommision on the Systematics of Igneous Rocks: Oxford, Blackwell, 193p.

McKee, E. H., and Nelson, C. A., 1967. Geologic map of Soldier Pass quandrangle, California and Nevada. U. S. Geological Survey Map GQ-654.

Mendelsohn, F., 1959. Structure of the Roan Antelope Deposit. Transactions of the Institution of Mining and Metallurgy 68, 229-263.

Metz, J., 1978. Petrology of the Santa Rita Flat Pluton Inyo Mountains, California. Unpublished MS thesis, San Jose State University, 95 pp.

Morgan, S. S., Law, R. D., and Nyman, M. W., 1998a. Laccolith-like emplacement model for the Papoose Flat pluton based on porphyroblast-matrix analysis. Geological Society of America Bulletin 110, 96-110.

Morgan, S.S., Law, R.D., and St Blanquat, M., 1998b. Aureole deformation associated with inflation of the concordant Eureka Valley-Joshua Flat-Beer Creek composite pluton, central White-Inyo Range, eastern California. In: Behl, R. (ed.) Geological Society of America, Cordilleran Section 1998 Field Guidebook, p. 5.1 - 5.30.

Nelson, C. A., 1962. Lower Cambrian-Precambrian succession, White-Inyo Mountains California. Geological Society of America Bulletin 73, 139-144.

Nelson, C. A., 1966a. Geologic map of the Waucoba Mtn. Quadrangle, Inyo County, California. U. S. Geological Survey Map GQ-528.

Nelson, C. A., 1966b. Geologic map of the Blanco Mtn. Quadrangle, Inyo and Mono Counties, California. U. S. Geological Survey Map GQ-529.

Nelson, C. A., 1971. Geologic map of the Waucoba Spring Quadrangle, Inyo County, California. U. S. Geological Survey Map GQ-921.

Nelson, C.A., and Sylvester, A.G., 1971. Wall rock decarbonation and forcible emplacement of Birch Creek pluton, southern White Mountains, California: Geological Society of America Bulletin, v. 82, p. 2891-2904.

Paterson, S. R., 1991. Aureole Tectonics. In: Kerrick, D. M. (ed.), Contact metamorphism, Mineralogical Society America, Reviews in Mineralogy 25, 673-722.

Paterson, S. R., and Fowler, T. K., 1993. Re-examining pluton emplacement processes; Journal of Structural Geology, v. 15, p. 191-206.

Ramsay, J. G., 1967. Folding and fracturing of rocks. McGraw Hill, New York, 568 pages.

Ribbe, P. H., 1975. The chemistry, structure and nomenclature of feldspars. In: Ribbe, P. H. (ed), Feldspar mineralogy, Blacksburg, Virginia, Mineralogical Society of America Short Course Notes 2, R1-R72.

Rochette, P., 1987. Magnetic susceptibility of the rock matrix related to magnetic fabric studies. Journal of Structural Geology 9, 1015-1020.

Rochette, P., Jackson, M., and Aubourg, C., 1992. Rock magnetism and the interpretation of anisotropy of magnetic susceptibility. Reviews in Geophysics 30, 209-226.

Ross, D. C., 1962. Correlation of granitic plutons across faulted Owens Valley, California. U. S. Geological Survey Professional Paper 501-D, D86-D88.

Ross, D. C., 1965. Geology of the Independence quadrangle, Inyo County, California. U. S. Geological Survey Bulletin 1181-0, 64 pp.

Ross, D.C., 1967. Generalized geologic map of the Inyo Mountains region, California: U.S. Geological Survey Miscellaneous Geological Investigations Map I-506, scale 1:125,000.

Ross, D. C., 1969. Descriptive petrography of three large granitic bodies in the Inyo Mountains, California. U. S. Geological Survey Professional Paper 601, 47 pages.

Saint Blanquat, M., 1993, EXAMS; an Excel macro for automatic computing of AMS data. Unpublished program, University of Toulouse.

Saint Blanquat, M., Law, R.D., Bouchez, J.L., and Morgan, S.S., in review, Internal structure and emplacement of the Papoose Flat pluton: an integrated structural, petrographic and magnetic susceptibility study. Geological Society of America Bulletin

Saint Blanquat, M., and Tikoff, B., 1997. Development of magmatic to solid-state fabrics during syntectonic emplacement of the Mono Creek granite, Sierra Nevada batholith. In: Bouchez, J. L., Hutton, D. H. W., Stephens, W. E. (eds), Granite: from segregation of melt to emplacement of fabrics, Kluwer Academic Publishers, Dordrecht, 231-252.

Schweickert, R. A., 1981. Tectonic evolution of the Sierra Nevada Range. In: Ernst, W. G. (ed), The Geotectonic Development of California (Rubey Vol. I): Englewood Cliffs, N. J., Prentice-Hall, 87-131.

Stevens, C. H., Stone, P., Dunne, G. C., Greene, D. C., Walker, J. D., and Swanson, B. J., 1997. Paleozoic and Mesozoic evolution of east-central California. International Geology Review 39, 788-829.

Sylvester, A.G., Oertel, G., Nelson, C.A. and Christie, J.M., 1978. Papoose Flat pluton: a granitic blister in the Inyo Mountains, California: Geological Society of America Bulletin, v. 89, p. 1205-1219

Tarling, D. H. and Hrouda, F., 1993. The magnetic anisotropy of rocks. Chapman and Hall, London, 217 pages.

Tikoff, B., and Teyssier, C., 1992. Crustal scale, en-echelon ‘P-shear’ tensional bridges: a possible solution to the batholithic room problem. Geology 20, 927-930.

Tobisch, O. T. and Cruden, A. R., 1995. Fracture-controlled magma conduits in an obliquely convergent continental magmatic arc. Geology 23, 941-944.

Uyeda, S., Fuller, M. D., Belshe, J. C., and Girdler, R. W., 1963. Anisotropy of magnetic susceptibility of rocks and minerals. Journal of Geophysical Research 68, 279-291.

CHAPTER 2

Deformation mechanisms and strain paths within the Santa Rita shear system, eastern California: kinematic implications for shear zone evolution

ABSTRACT

The Santa Rita shear system (SRSS) is composed of a series of discrete NW-SE striking steeply dipping shear zones that cut and plastically deform granitic rocks of the Jurassic age Santa Rita Flat pluton, exposed in the Inyo Range of eastern California. The shear zones exhibit a domainal distribution of gently and steeply plunging stretching lineations, and are located at planar mechanical discontinuities between the granite and a series of felsic/mafic dikes which intrude the pluton. Mylonitized dikes within the shear zones contain syntectonic mineral assemblages not observed outside the shear zones, indicating that the dikes were intruded prior to shear zone development. Correlation with geometrically similar shear zones in the Sierra Nevada batholith to the west, indicates that the SRSS probably nucleated from a regional stress field in Cretaceous times (~90-78 Ma).

Strain is heterogeneous within the shear zones, with local development of protomylonite, mylonite, ultramylonite and phyllonite. Strain heterogeneity within the granite is attributed to fluid infiltration and chemical reaction and alteration of feldspar to fine-grained mica. These deformation-induced mineral changes would have resulted in progressive mechanical weakening over time of rocks within the SRSS. The phyllonites occur predominantly within steeply lineated shear zones and contain mylonitized foliation-parallel quartz veins. The pattern of c-axis preferred orientation in these quartz veins indicates that deformation within the shear zones occurred under plane strain conditions. Locally, quartz veins also cut the foliation planes, reflecting high pore fluid pressures during evolution of the SRSS. These cross-cutting quartz veins are also plastically deformed, and their c-axis patterns indicate weak constrictional strains. The orientation of the shear zones, together with their strain paths, are used to develop a transpressional kinematic model for development of the SRSS within a progressively rotating stress field.

INTRODUCTION

Strains are rarely homogeneously distributed in the earth's crust, but are most commonly localized into narrow, subparallel sided domains loosely referred to as shear zones (see review by Ramsay, 1980). Such shear zones commonly develop in mechanically isotropic rocks where the lack of a planar anisotropy results in the rocks being unable to buckle or fold in response to an applied stress field. In such situations, the localized development of shear zones (either brittle or plastic) may be the only mechanism by which isotropic rocks are able to deform. The nucleation of shear zones in otherwise homogeneous plutonic rocks is often attributed to the presence of pre-existing meso-scale or micro-scale heterogenities such as fractures (Segall and Pollard, 1983; Segall and Simpson, 1986; Goodwin and Wenk, 1995), although nucleation may also locally be influenced by subtle original grain-shape fabrics in polymineralic rocks (Ingles et. al., 1999). Within evolving shear zones (including fault zones) rocks frequently undergo strain softening promoted by processes such as hydrolytic weakening and reaction-enhanced softening, with the mechanically stronger minerals controlling shear zone development (White et. al., 1980; O'Hara, 1988). Determination of strain softening mechanisms in natural shear zones has traditionally involved microstructural analysis, and assessment of the dominant deformation mechanisms (brittle fracture, crystal plasticity and diffusive mass transfer), based on the presence or absence of characteristic microstructures associated with these deformation mechanisms. However, microstructures and grain-shape fabrics that develop as a result of these deformation mechanisms may be progressively overprinted at high strains in evolving shear zones. Therefore, in order to quantify the deformation history of a shear zone, including its microstructural development and strain path (e.g. simple shear, pure shear etc.), it may be critically important to identify domains of progressively varying finite strain (e.g. undeformed host rock - high strain zones).

Shear zones that developed within the brittle-plastic transition zone have provided some of the most important opportunities to study shear zone nucleation and development (e.g. Simpson, 1985; Segall and Simpson, 1986; Sibson et. al, 1988; Burgmann and Pollard, 1992, 1994; Christiansen and Pollard, 1997; Tourigny and Tremblay, 1997; Guermani and Pennacchioni, 1998). Shear zones that developed within the brittle-plastic transition zone exhibit evidence for the operation of more than one deformation mechanism, and commonly contain varying meso- and micro-scale grain shape fabrics (see review by Snoke et al., 1998). Whether or not an individual shear zone develops by dominantly brittle or plastic grain-scale processes is controlled primarily by a range of intrinsic and extrinsic variables including: temperature, effective confining pressure, strain rate, grain size, mineralogy, and chemical environment. Shear zones that nucleate

in the brittle-plastic transition zone may also experience a massive amount of fluid infiltration, leading to veining and formation of economically important mineral deposits (Kerrich, 1986; Sibson et. al., 1988).

The Santa Rita shear system (SRSS) of eastern California (Fig. 1) is composed of a series of discrete steeply dipping shear zones that cut and plastically deform granitic rocks of the Jurassic Santa Rita Flat pluton (Fig. 2). The SRSS is composed of two sets of shear zones: i) N to NW striking shear zones with shallowly plunging lineations, and ii) NW to WNW striking shear zones with steeply plunging lineations. The dominant deformation mechanism within the shear zones is crystal plasticity (quartz grains), although the presence of both mylonitic and non-mylonitic quartz veins within the shear zones indicates the simultaneous operation of brittle fracture mechanisms. Quartz veins are not recorded outside the shear zones. The presence of mutually overprinting brittle and plastic structures suggests that the SRSS nucleated within the brittle-plastic transition zone (Segall and Simpson, 1986). The cyclical nature of the brittle and plastic structures suggests that fluctuations in pore fluid pressures within the SRSS may have been the primary cause for observed overprinting relationships between brittle and plastic structures (Kerrich, 1986; Sibson et. al., 1988; Sibson, 1990, 1992; Sibson and Scott, 1998).

An analysis of the deformation mechanisms and local strain paths associated with evolution of the SRSS has been made by integrating field mapping with microstructural, isotopic dating, and petrofabric analyses. Key outcrops indicating the cyclical nature between brittle and plastic deformation were documented in the field, and oriented samples from these outcrops were used for microstructural and petrofabric analysis. The orientation of the shear zones, together with their strain paths, were used to develop a transpressional kinematic model for development of the SRSS within a progressively rotating stress field.

GEOLOGIC BACKGROUND

The Santa Rita Flat pluton (164 Ma; Chen, 1977) is one of many Jurassic plutons in the White-Inyo Range (Fig. 1) that intrude metasedimentary rocks ranging from Neoproterozoic to late Paleozoic in age (Nelson, 1962; Ross, 1965, 1967). Although the Santa Rita Flat pluton lies within the Inyo Range, the pluton is considered part of the Sierra Nevada batholith, and has been correlated (Ross, 1962, 1969) with the Tinemaha granodiorite, located 20 km to the NW in the eastern Sierra Nevada (Fig. 1). The Santa Rita Flat pluton ranges in composition from granite to quartz monzonite, and is exposed

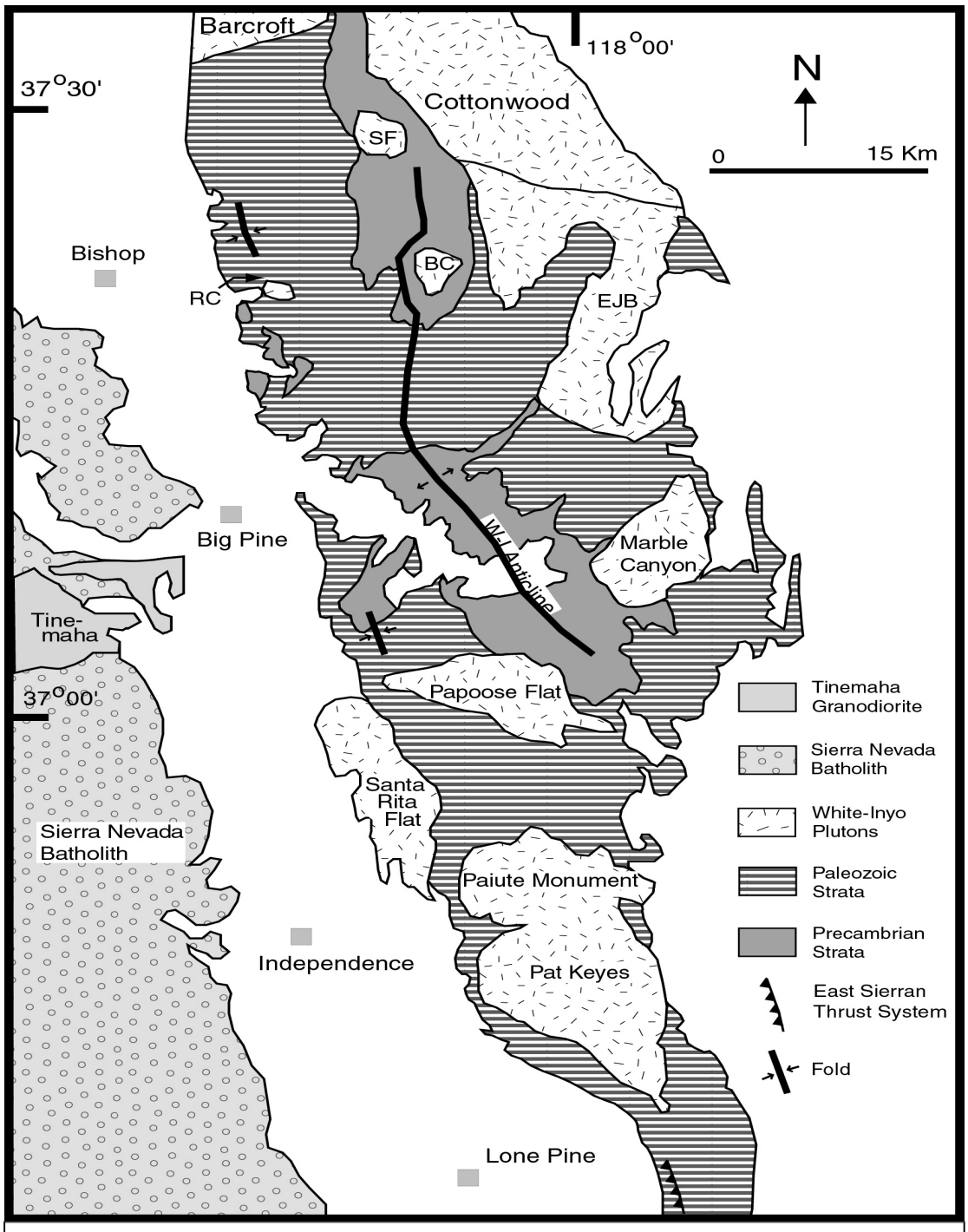

Figure 1: Simplified regional geologic map of the southern part of the White Mountains, northern part of the Inyo Range and adjoining easternmost part of the Sierra Nevada Batholith. Jurassic plutons include from north-south: Barcroft, Sage Hen Flat (SF), Cottonwood, Eureka Valley-Joshua Flat-Beer Creek (EJB), Redding Canyon ? (RC), Marble Canyon, Tinemaha, Santa Rita Flat, Pauite Monument and Pat Keyes plutons. Cretaceous plutons include the Birch Creek (BC) and Papoose Flat plutons.

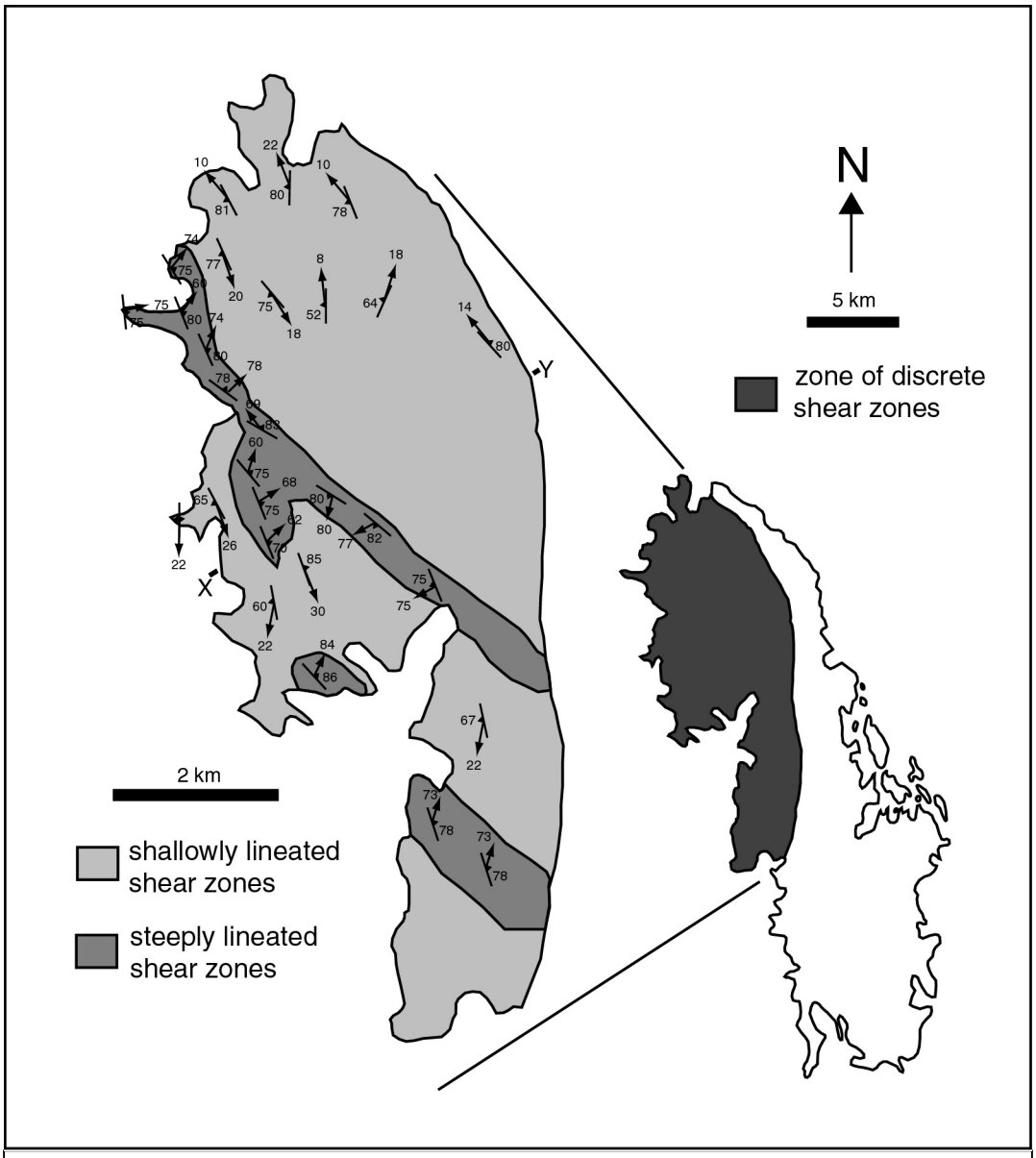

Figure 2: Enlarged map (left) of western flank of the Santa Rita Flat pluton (right). Western flank of pluton is deformed by discrete shear zones collectively referred to as the Santa Rita Shear System. Note: foliation symbols represent individual shear zones, and between shear zones the Santa Rita Flat granite is undeformed. X-Y indicates line of cross section in Figure 15.

over an area measuring approximately 6 by 17.5 km (Ross, 1962; Metz, 1978). In terms of map distribution, the most common rock type is a biotite granite with megacrysts of hornblende.

The SRSS cuts the western flank of the Santa Rita Flat pluton (Fig. 2), and individual shear zones making up the SRSS are located along the margins of felsic and mafic dikes which also cut the pluton. These mafic and felsic dikes were first mapped within the Santa Rita Flat pluton by Ross (1965), and were later noted by Metz (1978). The dikes were correlated with the Independence Dike Swarm (IDS), which crops out from the Sierra Nevada and White Mountains southwards to the Mojave Desert. Both the age of individual dikes which cut the Santa Rita Flat pluton, and the age of the IDS as a whole, has proved problematic. Following the work by Moore and Hopson (1961) and Smith (1962) on the IDS, the Santa Rita Flat dikes were interpreted to be of Cretaceous age (Ross, 1965; Metz, 1978). However, subsequent dating by Chen and Moore (1979) and James (1989) of felsic dikes from the IDS yielded a now generally accepted Late Jurassic age of ~148 Ma for the swarm. More recently, mafic dikes of similar orientation, which also appear to belong to the IDS, have been dated by Coleman et al. (1994) at 90-94 Ma (Late Cretaceous). Although accepting that some "Independence-like" dikes may be of Cretaceous age, Glazner et al. (1999) have argued that the main regional dike swarm is of Jurassic age (~ 148-150 Ma) and developed within a bulk sinistral transpressional shear system. Two dikes from the Santa Rita Flat pluton have so far been dated; zircons from only one size fraction yielded a U-Pb age of 164 ± 2 Ma (see Chapter 3 of this thesis).

Due to the close association between shear zones and "Independence" dikes within the Santa Rita Flat pluton, and the generally accepted Late Jurassic age for the IDS, Brudos and Paterson (1993) and Carl et al. (1998) have speculated that these dikes are of Jurassic age and were syntectonically emplaced along the shear zones. However, the dikes had not been isotopically dated, and no detailed analyses of the geometric and temporal relationships between the dikes and shear zones had been made.

FIELD RELATIONSHIPS

Individual shear zones within the SRSS anastomose both in plan view and in vertical down-dip cross section, and can be traced along strike for distances ranging from tens to hundreds of meters. The shear zones are discrete and range in width from the mm scale to 20-30 meters. Two dominant sets of shear zones, distinguised by the pitch of lineation on foliation, are observed within the SRSS (Figs. 2 and 3): i) a set of approximately 158-175° striking shear zones that dip moderately-steeply to the west and have stretching lineations that plunge shallowly to the northwest or southeast; ii) steeply lineated shear

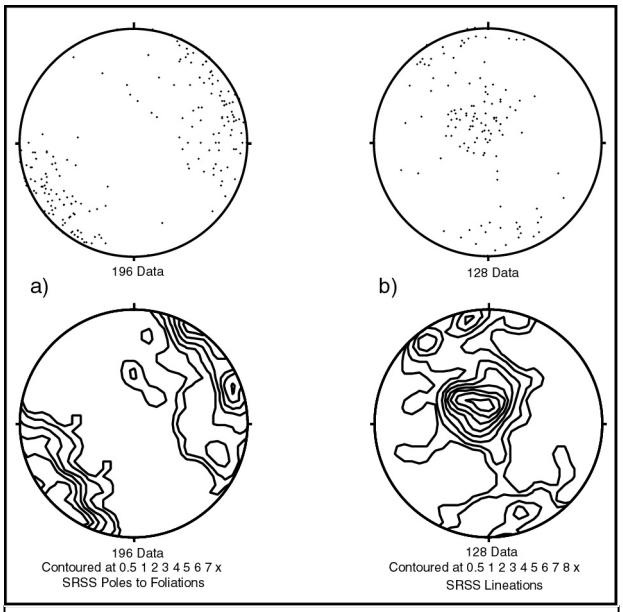

Figure 3: Equal area stereonet plots of poles to foliation (a) and stretching lineations (b) in the Santa Rita Shear System.

zones that dip steeply to the north or south, one group strikes approximately 158-175°, the second group strikes at approximately 120°. The widest and most laterally continuous shear zones are associated with steeply plunging lineations. Ductile (crystal plastic) grain shape fabrics are most easily observed at the outcrop scale in the widest shear zones.

Mutual cross-cutting relationships indicate that the shallowly and steeply lineated 158-175° striking shear zones formed at the same time. In contrast, the steeply lineated 158° striking shear zones appear to curve into subparallelism with adjacent steeply lineated 120° striking shear zones, and their lineations locally change from a northeast to a northwest plunge direction (Fig. 2). This suggests that the 120° striking shear zones may post-date the 158-175° striking shear zones. The shear zones within the SRSS are localized along pluton-dike contacts, and commonly contain quartz veins that may either occur along, or cut across the shear zones. The granite of the Santa Rita Flat pluton, and the felsic and mafic dikes within the shear zones, have dominantly been deformed in a ductile (plastic) manner, whereas the quartz veins within the shear zones were deformed by both brittle and ductile processes.

DEFORMATION MECHANISMS, SHEAR SENSES AND STRAIN PATHS

Santa Rita Flat granite and felsic/mafic dikes

Outside the shear zones the granite does not contain any macroscopic grain shape fabric, although anisotropy of magnetic susceptibility analysis has revealed that the pluton is characterized by a well organized pattern of magnetic foliation and lineation, reflecting subtle original magmatic fabrics (see Chapter 1). In contrast, within individual shear zones the granite has been variably strained to produce a spectrum of low to high strain fabrics (protomylonite to ultramylonite/phyllonite). The deformed granite is characterized by a strongly developed foliation and stretching lineation. The foliation is defined by the grain shape preferred orientation of micas, quartz ribbons and elongate quartz and feldspar porphyroclasts. Stretching lineations on the foliation planes are defined by the preferred grain shape alignment of quartz and mica grains.

Porphyritic felsic dikes commonly occur within the shear zones, and in high strain zones are frequently marked by porphyroclastic mylonite. Foliation within the mylonitic felsic dikes is defined by the strong preferred grain shape alignment of micas, whereas stretching lineations on the foliation plane are defined by a preferred grain shape alignment of micas, quartz, and locally, feldspar porphyroclasts. The mafic dikes within

shear zones are typically located close to, or at, the shear zone boundaries. The mafic dikes are strongly foliated, and have faint stretching lineations. The foliations and stretching lineations observed on the foliation planes are marked by the preferred grain shape alignment of chlorite and biotite grains.

A range of foliation types are observed within the shear zones, and locally both C and C' foliations are developed; see Passchier and Trouw (1996, p. 111) for a review of terminology used. There are two main orientations of C-foliations from mylonites within shallowly lineated shear zones: i) 158°, 85° NE, and ii) 175°, 85° SW. C'-foliations are locally observed in these shear zones and have a strike and dip of 015°, 64° NW. The strike of C-foliations from mylonites within steeply lineated shear zones ranges from 174° to 120° (Fig. 2). The dip of C-foliations along these steeply lineated shear zones varies from 80° to 85° NE, although locally the C-foliation may dip steeply (80°) to the SW (Fig. 2). Dip of S-foliations in these shear zones varies from 55° SW to 90°. S-C foliations from mylonites within the shallowly lineated shear zones document a dominant oblique dextral sense of shear, whereas shear sense indicators from steeply lineated NE-dipping shear zones document a northeast over southwest sense of movement (steeply dipping reverse-sense shear zones) (Fig. 4). Shear zones that are steeply lineated and dip to the SW indicate a southwest side down and northeast side up sense of motion (steeply dipping normal-sense shear zones) (Fig. 5).

Shear senses could not always be directly inferred from macroscopic grain shape fabrics in shear zones with intensely developed mylonites. Therefore, microstructural analyses were made using oriented samples. Microstructural shear sense indicators observed included: displaced broken feldspar porphyroclasts (Fig. 6a), sigma-type porphyroclasts (Figs. 6b), oblique S-C fabrics (Fig. 6c), mica fish (Fig. 6d), asymmetric pressure shadows (Fig. 6e), delta-type porphyroclasts and asymmetric folded quartz/feldspar micro-veinlets. In all cases where both macroscopic and microscopic shear sense indicators were present, both sets gave the same shear sense.

Quartz grains within both the sheared granite (protomylonite – phyllonite) and felsic dikes have dominantly been deformed by crystal plastic processes. The quartz grains exhibit ubiquitous undulose extinction, and some have been deformed into highly elongate or ribbon-like shapes (type 2 quartz ribbons of Boullier and Bouchez, 1978). These quartz ribbons are locally folded (Fig. 7a) and the limbs of the folded ribbons are characterized by pinch and swell structures. Microstructural evidence for diffusive mass transfer of quartz was observed in the finer grained mylonites (ultramylonite) derived from both the granite and felsic dikes. Microstructures associated with crystal plastic

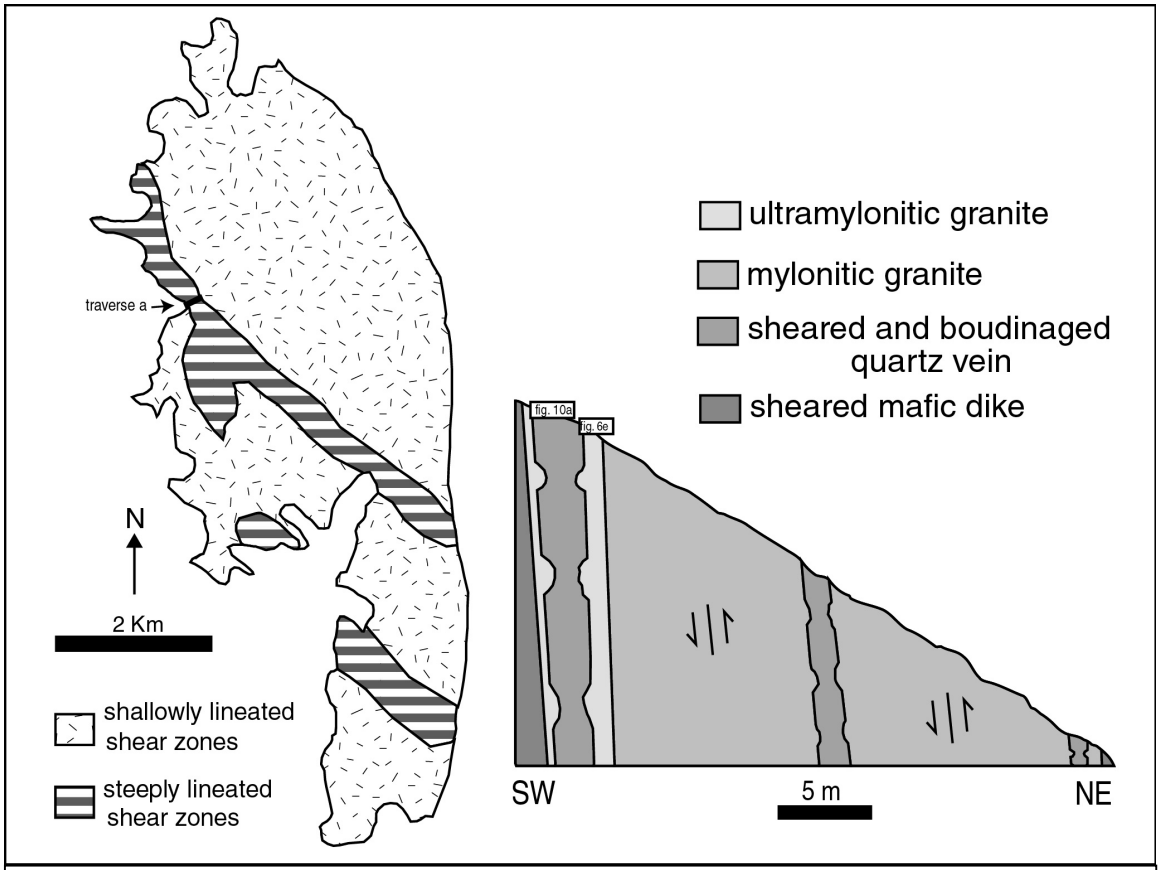

Figure 4: Cross section through steeply lineated shear zone at Traverse A. The cross section is viewed towards the NW. Note: Photomicrographs taken from collected samples along traverse A are illustrated in Figures 6e and 10a.

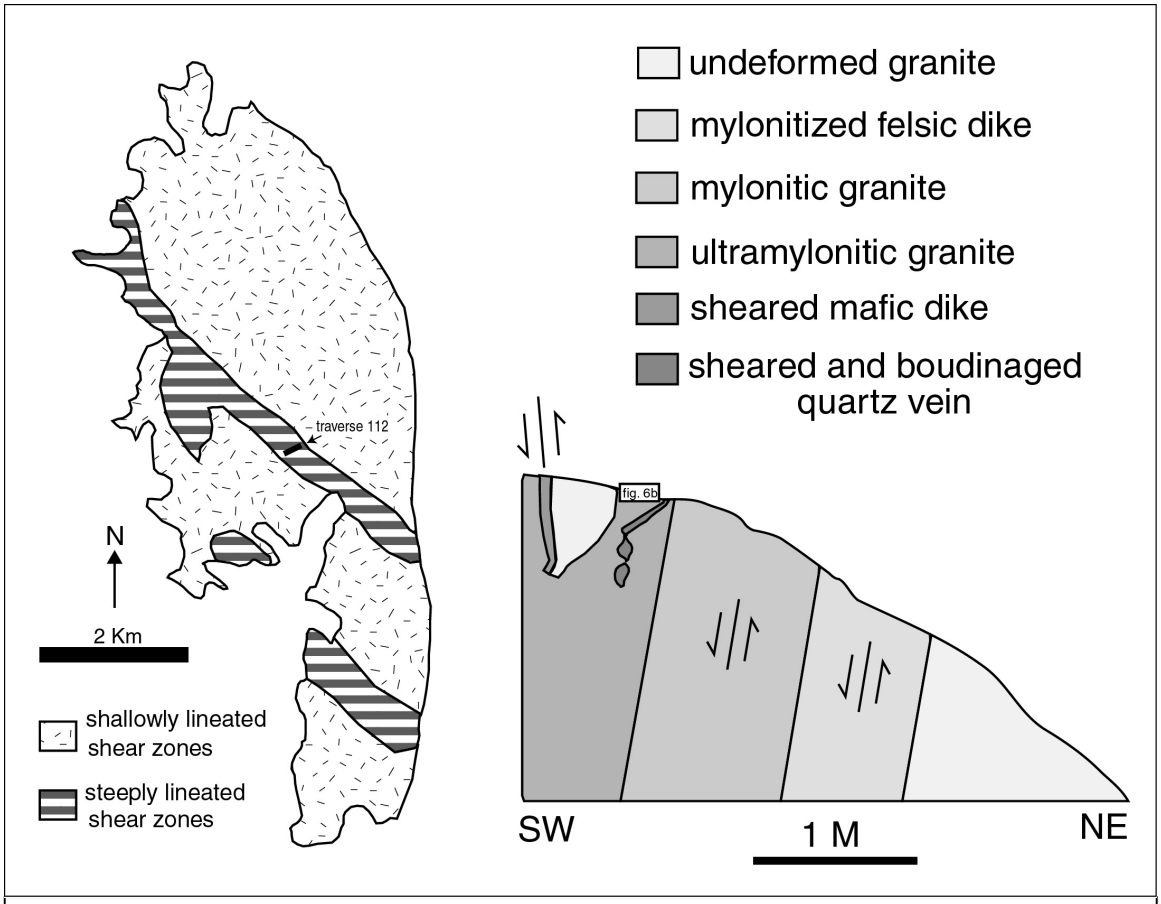

Figure 5: Cross section, viewed towards the NW, through steeply lineated shear zone at location 112. Foliation in shear zone dips steeply to SW, except in sheared mafic dike adjacent to large boudin (right) where it is deflected into a NE dip. Location of boudinaged quartz vein illustrated in Figure 8c is indicated. Note: Photomicrographs taken from a sample collected along traverse 112 is illustrated in Figure 6b.

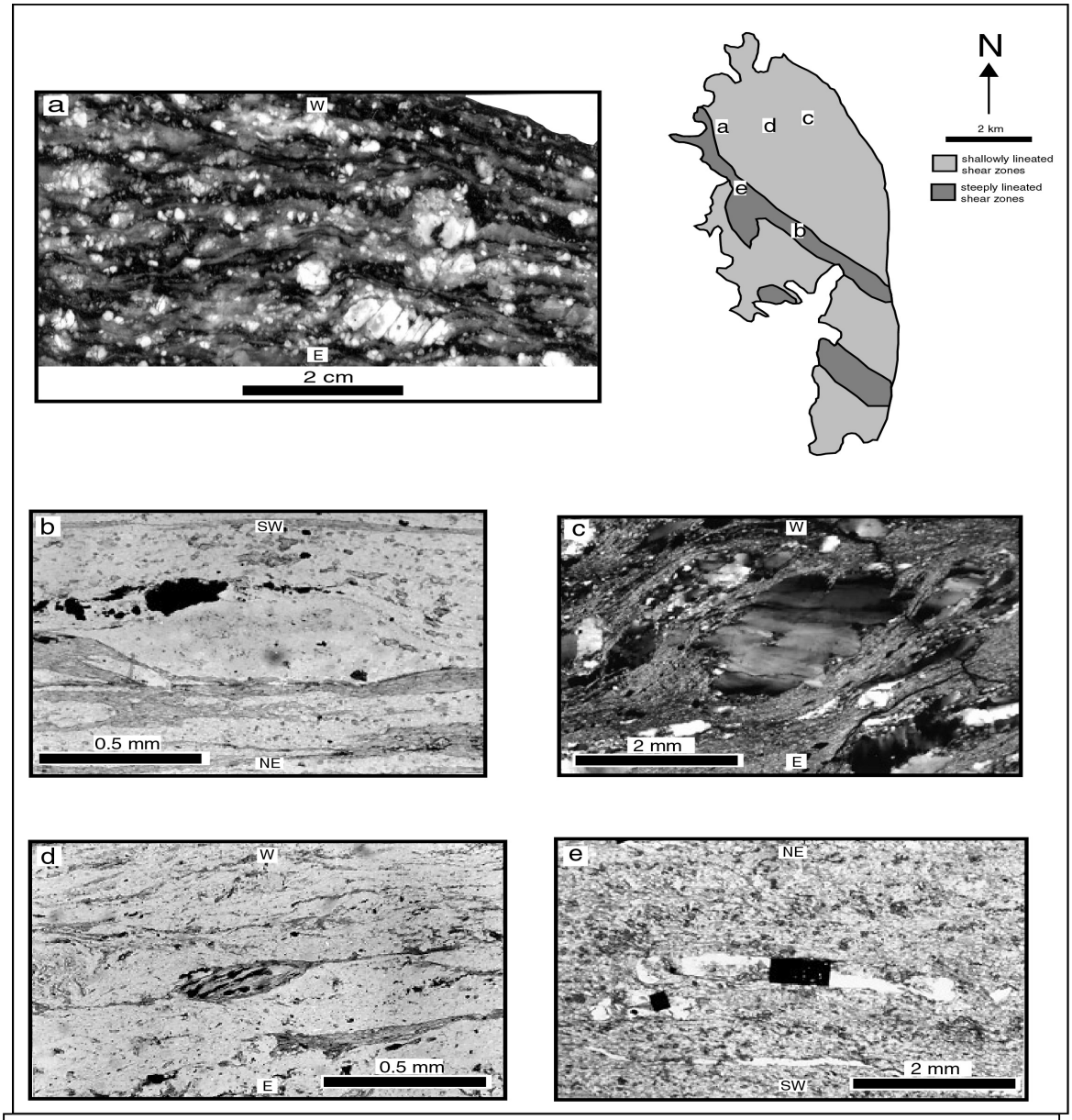

Figure 6: Microstructures from penetratively deformed Santa Rita Flat granite and felsic/mafic dikes; all sections cut perpendicular to macroscopic foliation and parallel to stretching lineation. (a) Polished slab of sheared granite from shallowly lineated shear zone; view downwards. Displacement of fractured feldspar porphyroclast indicates a dextral shear sense. Quartz ribbons anastomose around feldspar porphyroclast; biotite grains clustered in layers which define macroscopic foliation. (b) Sigma-type porphyroclast from steeply lineated ultramylonite viewed towards NW indicating a NE over SW shear sense. (c) S-C fabric from shallowly lineated phyllonite indicating a dextral shear sense, view downwards. (d) Mica fish from shallowly lineated sheared felsic dike indicating a dextral shear sense, view downwards. (e) Rigid grains of cubic opaque oxide from sheared steeply lineated mafic dike viewed towards NW; asymmetric pressure shadows indicate a NE over SW shear sense. Locations for samples in a-e are indicated.

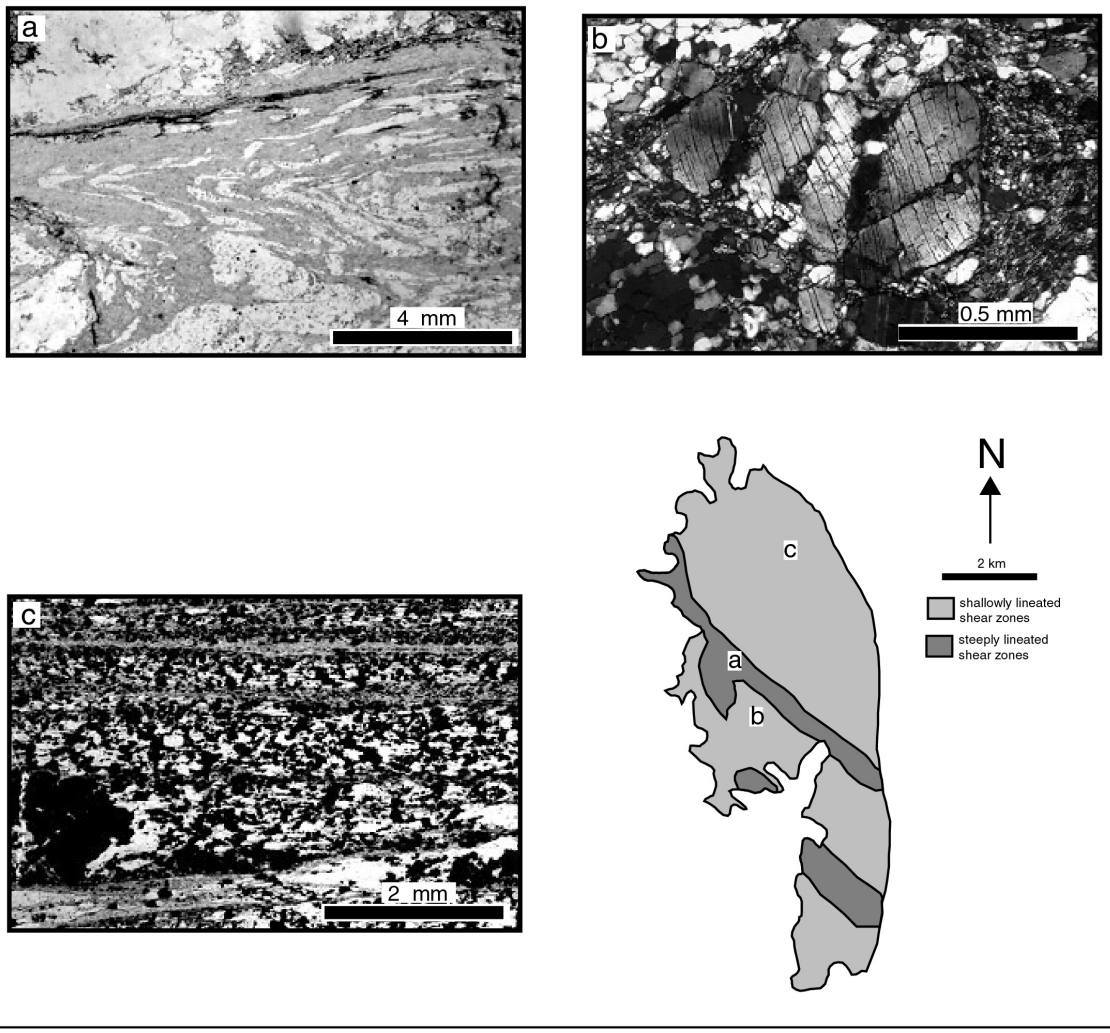

Figure 7: Microstructures from penetratively deformed Santa Rita Flat granite; all sections cut perpendicular to macroscopic foliation and parallel to stretching lineation. (a) Narrow folded quartz ribbons; limbs of the folded ribbons are characterized by pinch and swell structures. (b) Fractured plagioclase feldspar grain; note kinking and slight undulatory extinction within feldspar. (c) Opaque oxide grains defining foliation-parallel banding in granite ultramylonite. Locations for samples in a-c are indicated.

deformation of quartz grains in ultramylonites and phyllonites derived from the granite are frequently overprinted by brittle fractures.

Porphyroclasts in the sheared granite and felsic/mafic dikes are predominantly composed of plagioclase feldspar. The plagioclase porphyroclasts are well preserved in the sheared felsic dikes, but are moderately altered to epidote in the sheared granite, and strongly altered to epidote in the sheared mafic dikes. The mafic dikes have been intensely sheared and contain less than 1% plagioclase. Small amounts of fine-grained muscovite (sericite) have replaced the plagioclase feldspar in all these rocks. K-feldspar porphyroclasts occur only in the sheared granite and felsic dikes, and make up 31% of the matrix composition. The K-feldspar porphyroclasts display well developed reaction textures with fine-grained muscovite (sericite) grains, indicating that the fine-grained muscovite formed from the breakdown of the K-feldspar porphyroclasts during shearing (O'Hara, 1988). Both the plagioclase and K-feldspar porphyroclasts are fractured, and display weak kinking and undulatory extinction (Fig. 7b), indicating that deformation of the porphyroclasts involved both dislocation glide mechanisms and limited cataclasis. Feldspar porphyroclasts in the sheared felsic dikes are typically fractured when they are significantly larger than the surrounding matrix grains, but are less highly fractured and have their long axes aligned parallel to the enveloping foliation, when they are of a similar size to the matrix grains. This suggests that while the larger feldspar porphyroclasts deformed by brittle processes, the smaller porphyroclasts underwent rigid-body rotation.

Muscovite grains formed as K-feldspar, and to a lesser extent plagioclase, broke down during shearing of the granite and felsic dikes. In contrast, biotite altered to chlorite as strain increased in the sheared granite and felsic/mafic dikes. Granite protomylonites and porphyroclastic felsic dike mylonites contain K-feldspar and muscovite grains, whereas granite ultramylonites and phyllonites contain only muscovite and quartz porphyroclasts and ribbons.

Chlorite and to a lesser extent biotite grains are uncommon in the mafic dikes, and presumably formed from alteration of the more abundant mafic mineral phases. Biotite typically forms from the breakdown of amphibole, and is itself altered to chlorite. The sheared mafic dikes within the SRSS, however, show no direct alteration textures to confirm that the biotite grains were derived from alteration of hornblende, although locally biotite grains are replaced by chlorite.

Muscovite, biotite, and chlorite grains define the prominent foliation in all the sheared rocks of the SRSS and are oriented parallel to the stretching lineations. This prominent foliation is interpreted as a C-foliation along which significant shear strains accumulated.

Muscovite, biotite, and chlorite grains also define a grain shape fabric, oriented oblique to the C-foliation, across which significant shortening strains accumulated (S-foliation). Along the C-foliation, muscovite grains form mica-fish microstructures (Fig. 6d), indicating that ductile processes accommodated deformation (Lister and Snoke, 1984). Biotite and chlorite occur as grains clustered into layers, stacked grains in the pressure shadow regions of more rigid grains, and in the neck regions of boudinaged porphyroclasts. The grains are usually kinked and exhibit a sweeping undulatory extinction. These microstructural relationships indicate that formation of the biotite and chlorite grain shape fabrics involved kinking and pressure solution processes (Passchier and Trouw, 1996).

Quartz and K-feldspar veinlets cut the mylonitic foliation in the sheared granite in an orthogonal fashion, and contain small actinolite needles that occur as inclusions within the veinlets. The actinolite inclusions display a grain shape preferred orientation that is parallel to the mylonitic foliation present in the surrounding sheared granite. In contrast, quartz and K-feldspar veinlets within the sheared mafic dikes contain only small actinolite needles with random orientations. These veinlets are commonly oriented subparallel to the prominent foliation (C-surface), although locally they are folded. Quartz grains within the veinlets are plastically deformed, whereas K-feldspar grains are undeformed.

Calcite is commonly observed in the sheared granite and felsic/mafic dikes. Calcite grains are found in the neck regions of feldspar and quartz porphyroclast microboudins, and as fracture infillings within cracked feldspar porphyroclasts in the sheared granite and felsic dikes. Calcite layers occur along foliation planes in the sheared mafic dikes, and make up 10-20% of the rock matrix. The calcite grains within these layers are strongly flattened and stretched into ribbons. These microstructures indicate that the calcite is syntectonic with respect to shearing of the granite and the felsic/mafic dikes. Opaque cubic oxide grains occur along and within the foliation planes of the sheared granite and felsic/mafic dikes. These opaque grains define a distinct foliation-parallel banding in the granite ultramylonites (Fig. 7c). Pressure shadow fringes are always observed around these rigid oxide grains. The pressure shadows are symmetrically developed with respect to foliation in the sheared granite and felsic dikes, but are strongly asymmetric in the sheared mafic dikes (Fig. 6e). The syntectonic nature of calcite and oxide mineralization suggests that CO_2 and FeO rich hydrothermal fluids circulated within the shear zones during deformation (Conti et. al., 1998).

Quartz veins - shape fabrics

Quartz veins predominantly occur along the foliation planes (Fig. 8d) within the SRSS shear zones, although some veins locally cross-cut foliation within the NW striking steeply lineated shear zones. Both types of quartz vein may be strongly foliated and lineated (crystal plastic deformation), and display pinch and swell structures both in XZ and YZ sections (Figs. 8b and c). This boudin geometry indicates that the quartz veins underwent flattening strains and were slightly more competent than the surrounding mylonites. Stretching lineations within the mylonites are deflected around the boudins. N22°E striking quartz veins cut both shallowly and steeply lineated NW striking shear zones; the veins have a gentle-moderate (<45°) dip to the WNW in the shallowly lineated shear zones, and a very gentle (<5°) dip to either the WNW or ESE in the steeply lineated shear zones. These cross-cutting veins are unfoliated, although the vein margins have well-developed slickenside lineations (Fig. 8a). These observations indicate that the quartz veins developed after the main mylonitization within the shear zones, and that the earlier generations of veins were plastically deformed during the later stages of shear zone development, whereas the unfoliated quartz veins record the waning stages of motion on the shear zones.

Three distinct microstructural types of quartz veins are distinguished within the SRSS. Type 1 veins are characterized by dynamically recrystallized quartz grains; no original grain shapes associated with original vein formation are preserved. Type 2 veins are characterized by intense penetrative plastic deformation in which individual quartz grains are ribbon-like in cross section. Type 3 veins are characterized by large quartz grains with no shape preferred orientation; these veins have slickensided surfaces (diffusive mass transfer), and cut both steeply and shallowly lineated shear zones. Type 1 and 3 are the most common quartz veins within the SRSS; Type 2 veins are only rarely observed.

Type 1 veins. Type 1 veins are composed of dynamically recrystallized quartz veins in which the more elongate grains display a preferred grain shape alignment (Sb) which is oblique to a spaced foliation (Sa) defined by thin zones of mica located between larger original quartz grains (Fig. 9a). This spaced foliation is oriented subparallel to the local

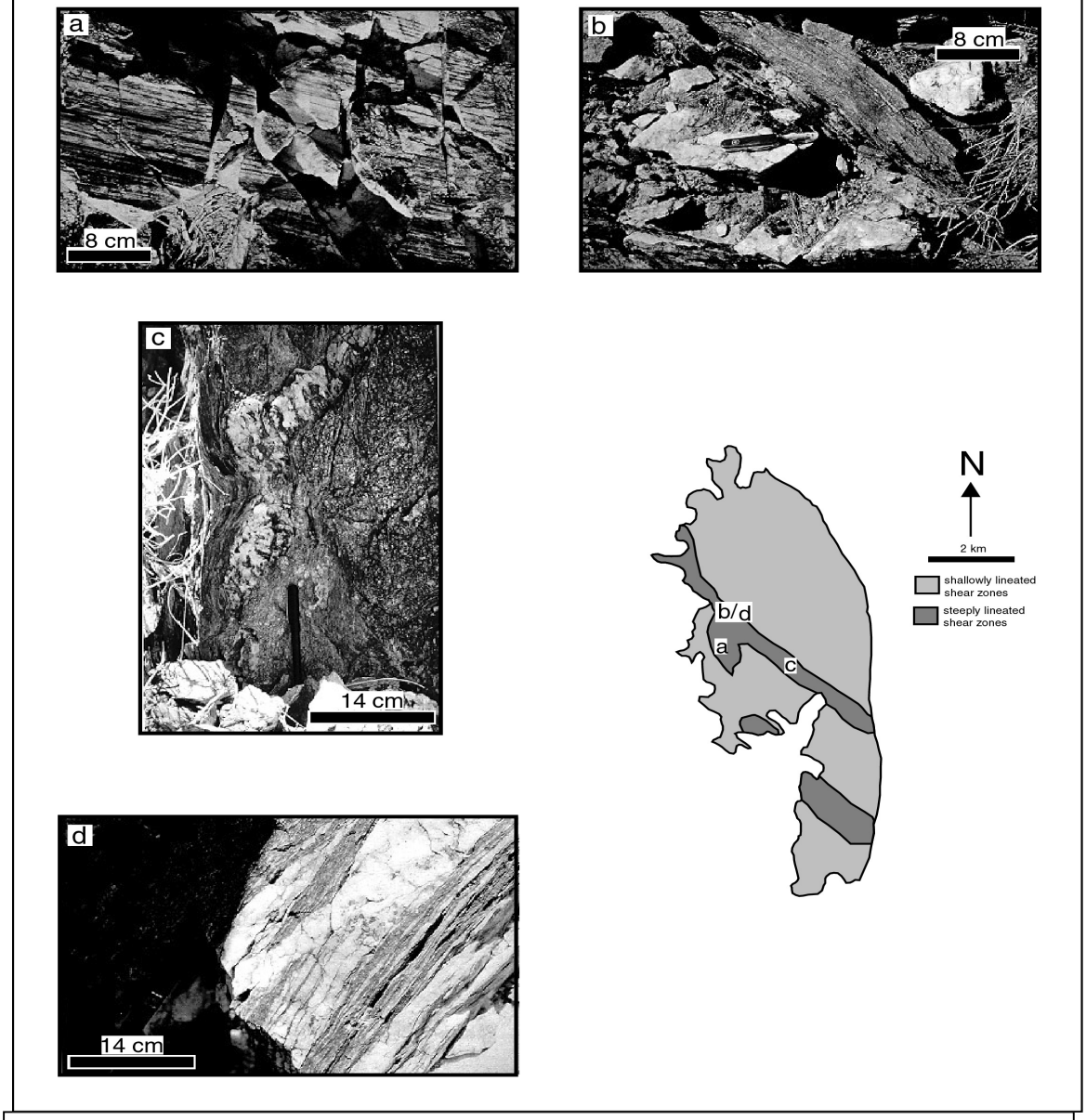

Figure 8: Outcrops of deformed quartz veins. (a) Lineated surface of gently dipping, 022° striking, quartz vein which cross-cuts mylonitic foliation. (b) Boudinaged quartz vein from steeply lineated northwest-striking shear zone; section is perpendicular to stretching lineation. (c) Boudinaged quartz vein from steeply lineated northwest-striking shear zone; section is perpendicular to foliation and parallel to stretching lineation. Note: at base of exposure vein is parallel to vertical foliation in surrounding mylonitic granite; traced upwards vein cuts across foliation; see text for details. (d) Branching quartz veins locally oriented either parallel or oblique to foliation in surrounding mylonitic granite. Locations for samples in a-d are indicated.

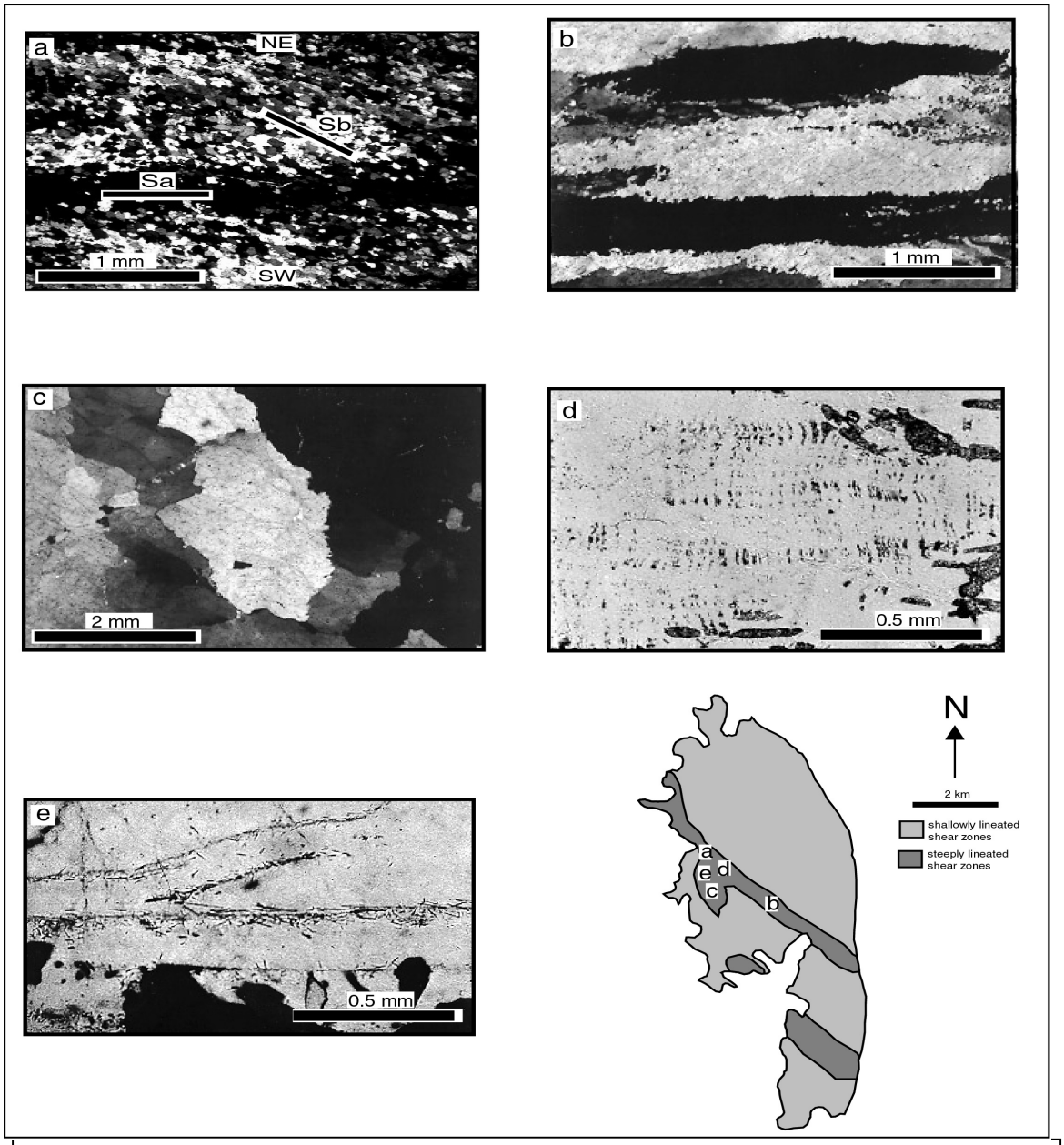

Figure 9: Quartz vein microstructures. (a) Totally recrystallized Type 1 quartz vein, microstructures indicate recrystallization by subgrain rotation (regime 2 recrystallization of Hirth and Tullis, 1992). Obliquity between elongate recrystallized grains (Sb) and macroscopic foliation (Sa, horizontal in micrograph) indicates sinistral shear sense; terminology after Law et al., (1984). (b) Partially recrystallized Type 2 quartz vein containing quartz ribbons with core and mantle microstructures (regime 2 recrystallization of Hirth and Tullis, 1992). (c) Type 3 quartz vein with lobate grain boundaries indicating strain induced grain-boundary-migration (regime 1 recrystallization of Hirth and Tullis, 1992). (d) Type 3 quartz vein with inclusion trails oriented perpendicular to vein margins. Orthogonal inclusion pattern indicates vein opened at right angles to margins (Cox, 1987). (e) Preferred alignment of elongate actinolite crystals within healed microfracture from Type 3 quartz vein.

vein margins. The obliquity between Sa and Sb (terminology after Law et al., 1984) indicates that the Type 1 veins have undergone a non-coaxial strain history, and the sense of obliquity in XZ sections (i.e. cut perpendicular to foliation and parallel to the macroscopic stretching lineation) has been used as a shear sense criterion (see reviews by Means, 1981; Lister and Snoke, 1984; Hanmer and Passchier, 1991; Passchier and Trouw, 1996). The microstructures of the quartz grains within these Type 1 veins indicate that they developed by subgrain rotation recrystallization, and are similar to microstructures produced by Hirth and Tullis (1992) at moderate temperatures in experimentally deformed and recrystallized quartzite (their Regime II recrystallization).

Type 2 veins. The recrystallized grain shapes in Type 2 veins are very similar to those in Type 2 veins, but recrystallization is less extensive and ribbon-like remnants of the original quartz grains are preserved (Fig. 9b). These remnant grains are several orders of magnitude larger in size than the dynamically recrystallized grains, the long axes of the ribbon grains defining the macroscopic foliation. Although the recrystallization mechanism is the same in Type 1 and 2 quartz veins, c-axis fabrics from the remnant ribbon-like grains in Type 2 veins are symmetric with respect to foliation (see below), indicating that these veins have undergone an approximately coaxial strain history

Type 3 veins. Quartz grains in Type 3 veins display strong undulatory extinction that varies from sweeping to patchy in appearance. Boundaries between adjacent quartz grains are frequently lobate (Fig. 9c), suggesting at least limited grain boundary migration driven by differences in dislocation density between adjacent grains (White, 1976). These microstructures are similar to those produced by Hirth and Tullis (1992) at low temperatures and relatively fast strain rates in experimentally deformed and recrystallized quartzite (their Regime I recrystallization). In some Type 3 veins, crack-seal inclusion trails are preserved within individual quartz grains (Fig. 9d); their orientations indicate that the veins opened approximately at right angles to the vein margins (Ramsay, 1980; Cox, 1987; Petit et. al., 1999). Brittle fractures with localized zones of cataclastic grain size reduction are common in Type 3 veins. Minute actinolite needles displaying a preferred grain shape alignment are present along some of the healed microfractures (Fig. 9e).

Quartz veins - crystallographic fabrics

Each type of vein described above is characterized by a distinct pattern, or group of patterns, of quartz c-axis preferred orientation, indicating that each vein type developed along a unique strain path.

Type 1 quartz veins. The quartz c-axis fabrics from Type 1 veins are characterized by symmetric small-circle girdles with moderate opening angles (38°) centered about Z, that are connected by a planar distribution of c-axes passing through Y and contain point maxima at Y (Fig. 10; samples A2, A3, AT22, AT32). These fabrics are transitional between Type I and Type II cross-girdles as defined by Lister (1977). All the observed fabrics are, with the exception of sample AT32, symmetric with respect to foliation (XY) and lineation (X), indicating approximately coaxial strain path conditions. Sample AT32 is characterized by a greater concentration of c-axes along a single girdle that is inclined with respect to X and Z (Fig. 10c), and is very similar to simulated asymmetric Type I cross girdles described by Lister and Williams (1979). The sense of fabric asymmetry in sample AT32 (Fig. 10c) is consistent with the NE over SW shear sense indicated by the obliquity between Sa and Sb (Fig. 9a).

Type 2 quartz veins. Only one Type 2 vein was found, and this displays a diffuse c-axis fabric which is transitional between a small circle girdle fabric with a small opening angle (28°) centered about Z, and a cross-girdle fabric intersecting in Y (Fig. 10; sample SR112). This diffuse composite fabric is similar to Type I cross-girdle fabrics as defined by Lister (1977), and is thought to indicate approximate plane strain deformation under low temperature conditions (Lister and Dornsiepen, 1982).

Type 3 quartz veins. Type 3 quartz veins have two distinctive but diffuse c-axis patterns (Fig. 11): i) symmetric small-circle girdle fabrics of large opening angle (67°) centered about the stretching lineation (X), and ii) cross-girdle fabrics containing a point maximum at Y (Type II cross-girdle of Lister, 1977) and connected to symmetric small circles with wide opening angles (48°) centered around Z. Symmetric small circles centered about X are generally regarded as being indicative of constrictional strains (see reviews by Schmid and Casey, 1986; Law, 1990). Interpretation of Type II cross-girdles is more complex as they may develop both under strain path conditions intermediate between plane strain and constriction at moderate temperatures (greenschist facies), and under plane strain deformation at higher (amphibolite-granulite facies) temperatures

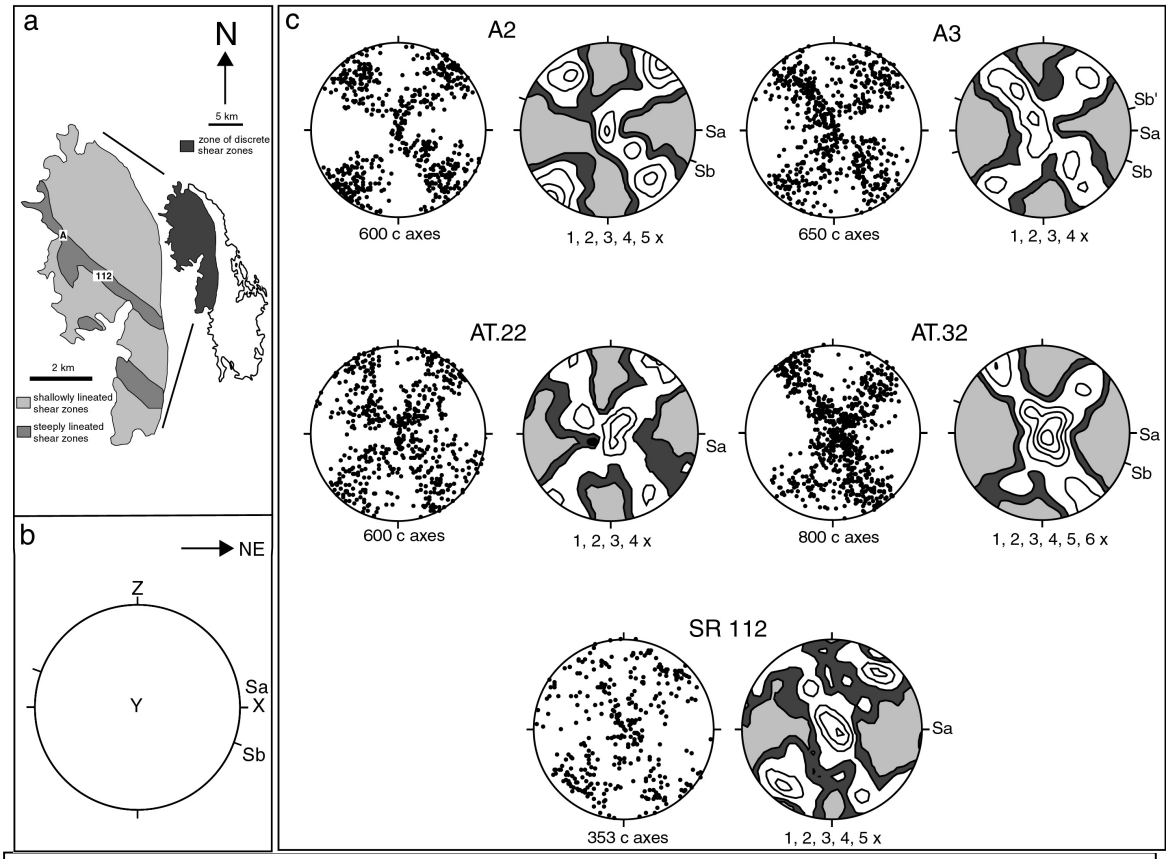

Figure 10: Crystal preferred orientation in Type 1 and Type 2 quartz veins. (a) Sample location map. (b) Grain shape fabric reference frame; X = stretching lineation, XY = macroscopic foliation, Z = pole to foliation, Sa = macroscopic foliation, Sb = preferred alignment of elongate recrystallized grains. (c) Quartz c-axis fabrics from veins in steeply lineated shear zones (viewed towards NW). Note: Obliquity between Sa and Sb in steeply lineated shear zones indicates a sinistral (NE side up) shear sense. All lower hemisphere equal area projections.

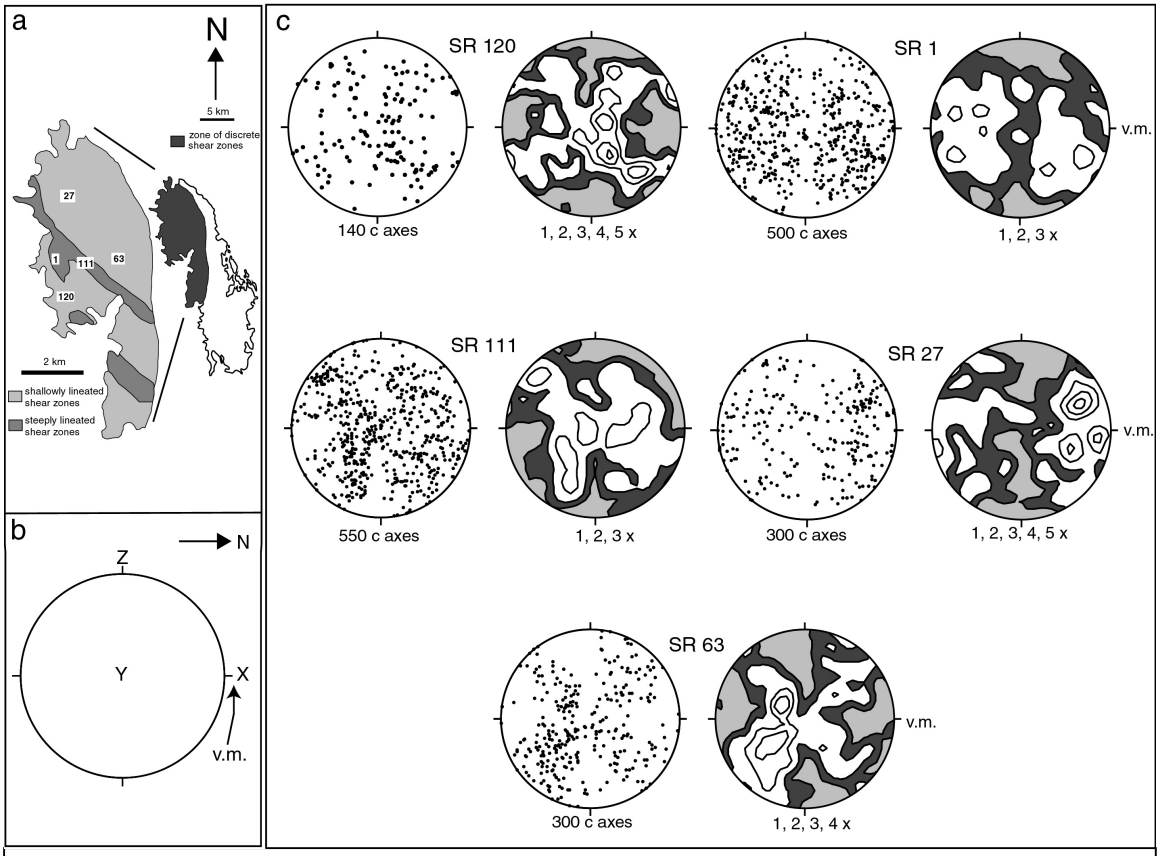

Figure 11: Crystal preferred orientation in Type 3 quartz veins. (a) Sample location map. (b) Grain shape fabric reference frame; X = stretching lineation, XY = macroscopic foliation, Z = pole to foliation, vm = vein margin. (c) Quartz c-axis fabrics from Type 3 quartz veins; fabrics viewed downwards. All lower hemisphere equal area projections.

(Lister and Dornsiepen, 1982; Schmid and Casey, 1986). Type II cross girdles that develop under transitional constriction strains usually have large opening angles about X (Schmid and Casey, 1986). In contrast, the Type II girdles observed in the SRSS quartz veins have large opening angles about Z, suggesting that they developed under a strain path close to plane strain. However, the microstructures and syn-tectonic minerals in these veins (Fig. 9) indicate low temperature (greenschist facies) conditions of deformation. We therefore tentatively interpret the Type II cross girdle fabrics as diffuse small circle girdles centered about X that extend towards Y, as indicating weak constrictional strains.

DEFORMATION CONDITIONS WITHIN THE SANTA RITA SHEAR SYSTEM

In the following discussion, the mineral assemblages, microstructures and crystal fabric described above, are used to interpret the deformation conditions within the evolving SRSS. Particular emphasis is placed on the chemical and mechanical roles that fluid infiltration may have had on influencing shear zone evolution.

Metamorphism, fluid activity and strain heterogeneity

The presence of syntectonic chlorite, sericite, actinolite, and epidote within the shear zones indicates that deformation occurred under subgreenschist to greenschist facies conditions, and at temperatures of approximately 250-400°C (Tourigny and Tremblay, 1997). Similarly, the plastic behavior of quartz, and synchronous brittle behavior of feldspar, suggest that deformation occurred under mid to upper-greenschist conditions and at temperatures of approximately 300-500°C (see reviews by Simpson, 1985; O'Hara, 1988; Snoke et al., 1998).

Strain is heterogeneously distributed within the SRSS, and this strain heterogeneity provides important information on fault rock rheology during shearing. Strain is most heterogeneous within the granite, and individual shear zones may locally contain protomylonite, mylonite, ultramylonite, or phyllonite derived from the granite (Fig.12). The alteration of feldspar to mica (O'Hara, 1988; Janecke and Evans, 1998), and the presence of calcite and opaque oxide layers along the mylonitic/phyllonitic foliation (Fig. 7c), indicate that these shear zones were zones of high fluid activity. Open pit mines are scattered along the western flank of the Santa Rita Flat pluton, and are usually positioned in shear zones where granite has been deformed into ultramylonite or phyllonite. Exploration targets for these pit mines include gold, as well as copper and tungsten minerals, concentrated by hydrothermal processes. High fluid presures would undoubtedly have had an important mechanical influence on development of the shear

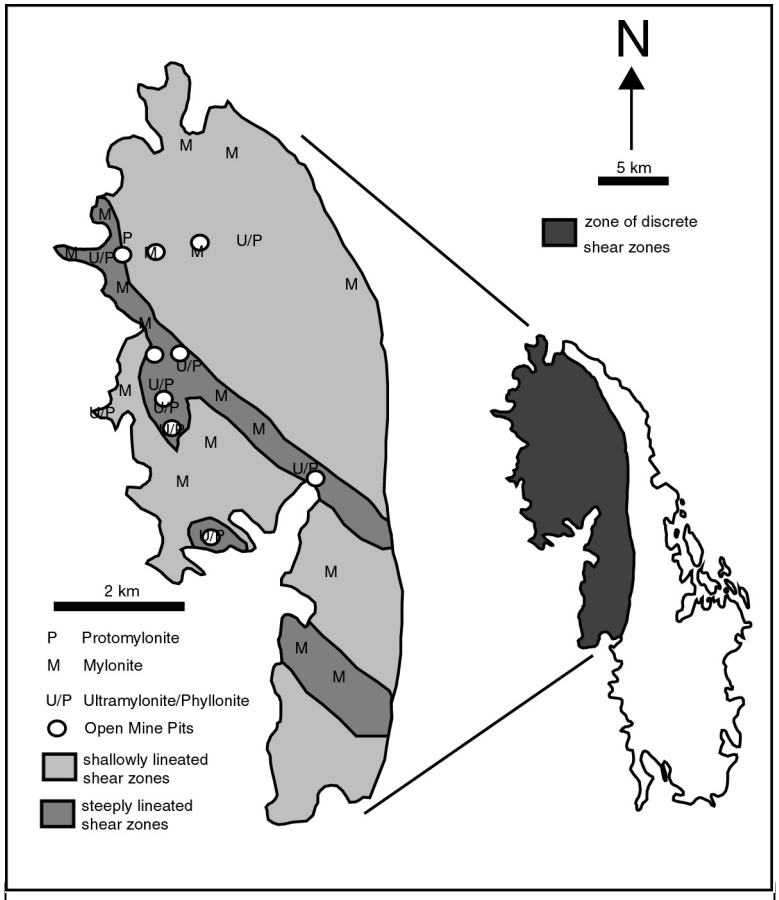

Figure 12: Strain heterogeneity within the Santa Rita Shear System and location of open pit mines. Majority of mines are along steeply lineated ultramylonite and phyllonite shear zones.

zones. Ultramylonite and phyllonite within the SRSS occurs in steeply dipping shear zones with steeply plunging lineations; kinematic analyses (described above) indicate an oblique reverse sense of motion on these shear zones. Assuming Andersonian faulting (i.e. with the principal stresses horizontal and vertical), reverse motion on such steeply dipping shear zones would only be mechanically feasible at low differential stresses and high pore fluid pressures (e.g. Sibson, 1985; Sibson et al., 1988). In addition, the chemical alteration of feldspar (the mechanically strongest mineral phase in the granite protolith) to mica would have dramatically lowered the mechanical strength of the rocks within the shear zones, allowing penetrative deformation and slip to occur at lower resolved shear stresses (White et. al., 1980; Janecke and Evans, 1988; O'Hara, 1988). The undeformed granite protolith outside the shear zones contains up to 50-60% feldspar. In contrast, within the shear zones the phyllonites contain no feldspar, and the ultramylonites contain less than 5% feldspar; both the phyllonites and mylonites are dominantly composed of quartz porphyroclasts/ribbons and fine-grained muscovite, these mechanically relatively weak phases making up >70% of the rock.

Variation in strain intensity may be a direct reflection of the local infiltration of chemically active fluids within the evolving shear zones. However, the distribution and migration paths of these fluids may not have been the same in the mylonites and ultramylonites/phyllonites. Pervasive veining is observed within the mylonitic shear zones, but has not been recorded in the ultramylonites and phyllonites. This may indicate that while within the phyllonite zones, fluids were either pervasively expelled or used up in mineral reactions, within the mylonite zones they were channeled into localized high fluid pressure domains, resulting in brittle fracture and mineralization. This ultimately suggests that different shear zones were probably weakened by different mechanisms. Phyllonitic shear zones were weakened over time by the chemical breakdown of feldspar to mica, whereas the mylonitic shear zones were dominantly weakened by repeated cycles of localized high fluid pressure.

Linkage between quartz deformation and feldspar dissolution within ultramylonites and phyllonites

As outlined above, chemical breakdown of feldspar led to mica enrichment within the deformed granite of the SRSS, and ultimately to formation of phyllonitic shear zones. These mineral reactions might be expected to lead to a change in dominant deformation mechanisms. For example, Hippertt and Hongn (1998) have argued that deformation mechanisms in quartz should progressively change with mica enrichment during progressive strain. They documented crystal plastic microstructures from quartz grains in

low-strain mylonites, whereas quartz grains with pressure solution microstructures were observed within high strain ultramylonites/phyllonites, suggesting that crystal plastic microstructures have been progressively overprinted by pressure solution microstructures with increasing strain. However, within the SRSS ultramylonites and phyllonites, crystal plastic quartz microstructures are still observed at the highest strains, indicating that a switch from dominant crystal plasticity to diffusive mass transfer in the quartz grains did not occur with increasing bulk strain magnitude.

The absence of pressure solution microstructures in quartz grains from the SRSS high strain zones may indicate that either the imposed bulk strain rates were too high for significant pressure solution of individual quartz grains, or that the quartz grains were above a critical minimum size for grain-scale pressure solution (see review by White, 1976). The absence of pressure solution may also be a reflection of the relative dissolution rates of quartz and feldspar in the shear zones. Within the high strain zones feldspar content is either extremely low, or all feldspar has been altered to mica, indicating that feldspar dissolved at a faster rate than any other mineral in the sheared granite. Fracturing of the rigid feldspar grains would have increased the surface area of feldspar fragments exposed to chemical attack, thereby enhancing the rate of feldspar breakdown. While the feldspar grains were undergoing fracture and incipient alteration to mica, the mechanically weaker adjacent quartz grains would have simultaneously deformed by crystal plastic processes. However, as breakdown of feldspar to mica progressed, quartz would have become the strongest mineral phase, and deformation would have been partitioned between the quartz porphyroclasts and the fine-grained mica. The fine-grained mica would now accommodate the majority of the imposed strain by a combination of grain boundary sliding, kinking and crystal plasticity, possibly resulting in an increase in bulk strain rate within the shear zone. This increase in strain rate might locally be reflected in fracturing of the now relatively more rigid quartz porphyroclasts, the fractures overprinting the crystal plastic microstructures that developed during earlier dissolution of the original feldspar grains.

Strain within Type 1 quartz veins

Type 1 quartz veins occur primarily along, but also locally cut, foliation in the steeply lineated northwest striking shear zones, indicating that they formed at a relatively late stage in the transformation of granite into mylonite. The mylonites are characterized by a lack of feldspar and an increase in white mica relative to the granite protolith, ultramylonites and phyllonites being recorded in the highest strain shear zones. Similarly developed pinch-and-swell structures on vein cross sections oriented both parallel (XZ)

and perpendicular (YZ) to the macroscopic stretching lineation (Fig. 8b=YZ plane and 8c=XZ plane) suggest flattening strains. However, quartz c-axis fabrics from these veins (Fig. 10c) indicate that they have been deformed under plane strain conditions. This difference in inferred strain symmetry suggests some form of spatial or temporal strain path partitioning.

One possibility is that the difference in strain symmetry indicated by the oblate boudin shapes and crystal fabrics might reflect a spatial variation in strain path, with plane strain accumulated in the vein interiors, and flattening strain simultaneously accumulated at the vein margins. Ramsay and Wood (1974) have demonstrated that strain markers indicating apparent flattening deformation may develop under plane strain conditions when volume loss by pressure solution is important. However, whether oblate boudin shapes could develop by this mechanism under plane strain conditions remains unclear. In addition, the fact that the mylonites and ultramylonites (which might be expected to have undergone the greatest volume loss) surrounding the veins display both a strongly developed foliation and stretching lineation, suggests that they have accumulated significant strain magnitudes under approximate plane strain conditions.

If spatial strain path partitioning can be discounted, then the difference in inferred strain symmetry must be related to temporal strain path partitioning. Fabric simulation studies by Lister and co-workers indicate that in quartzites 40% shortening is sufficient to result in gross changes to an already existing fabric (Hobbs 1985, p. 477). Therefore it is unlikely that the flattening strain indicated by the boudin shapes was superimposed on an older plane strain fabric, as the crystallographic fabrics should have been overprinted and replaced by flattening strain fabrics. Assuming a temporal variation in strain path, it seems most probable that a plane strain deformation has been superimposed upon an older flattening fabric.

A schematic rheologic model for development of the quartz vein - matrix system within the evolving shear zones is illustrated in Figure 13. Field data clearly indicate that the quartz veins developed after initial formation of the mylonitic foliation, and the observed alteration of the rheologically strong feldspar porphyroclasts to fine grained mica implies that the granite matrix surrounding the quartz veins would have become progressively weaker with increasing finite strain. At a critical ratio of mica to feldspar, a point in time would be reached at which the quartz veins would become mechanically stronger than the surrounding (now mica-rich) matrix. Once this critical ratio was exceeded, than the competence contrast between the veins and their matrix would facilitate boudinage of the quartz veins (see review by Ramsay, 1983). The observed pinch and swell structures and crystal fabrics suggest that this boudinage occurred under

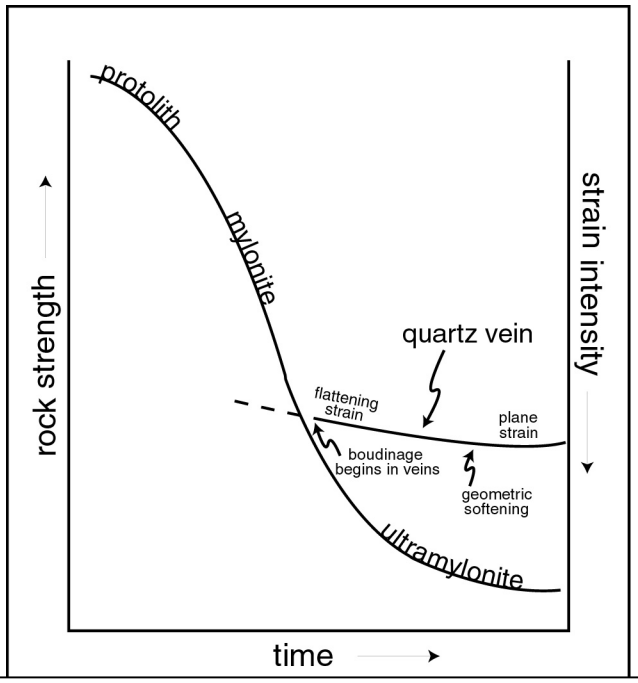

Figure 13: Schematic model for progressive mechanical evolution of granite protolith and Type 2 quartz veins within the Santa Rita Shear System. With shearing feldspar in granite is altered to fine-grained mica causing reaction-enhanced strain softening; granite protolith progressively altered to protomylonite, mylonite, ultramylonite and finally phyllonite at highest shear strains. Quartz veins form by hydraulic opening of mylonitic foliation (see Fig. 14b) at relatively late stage in deformation history. If quartz veins form while a significant percentage of feldspar is still present in granite protolith, then protolith will be mechanically stronger than veins. However, with progressive alteration of feldspar to mica, a critical mica percentage will be reached at which veins become mechanical stronger than surrounding granite mylonite (cross-over point of granite and quartz vein curves) and veins may then begin to boudinage within less competent granitic matrix. Development of crystallographic fabric leads to geometric softening of quartz veins. Potential influence of cyclical changes in pore fluid pressure on rock strength are not included in this diagram.

flattening strain conditions, but was then overprinted at the grain scale by plane strain fabrics. This interpretation is consistent with the observed parallelism between the stretching direction within the quartz veins (inferred from the c-axis fabrics) and the macroscopic stretching lineations on the vein margins and in the surrounding mica-rich matrix. Local curving of matrix stretching lineations around the boudinaged veins is most simply interpreted as reflecting local flow and accommodation of the weaker matrix material (under approximate plane strain conditions) adjacent to the pre-existing more rigid boudin shapes.

The inferred switch from flattening to plane strain conditions with increasing strain presumably reflects a change of kinematics at the shear zone scale. However, the question of why pinch and swell structures reflecting the inferred later plain strain conditions did not develop remains to be answered. Several possible explanations can be proposed, the most obvious of which is that the magnitudes of plane strain deformation were simply not high enough to modify the pre-existing boudin shapes. However, it is also possible that crystallographic fabric development within the plastically deforming quartz veins may have led to geometric softening of the veins (see reviews by White et al., 1980, Lister and Williams, 1983, Takeshita and Wenk 1988) and reduction of the competence contrast between the veins and their matrix to a critical value beneath that required for continued boudin formation. Numerical simulations of quartz fabric development indicate that at low temperatures (similar to those under which the SRSS was operative), flattening strains are energetically favored over constrictional strains (see review by Wenk, 1994), and quartzites become softer in flattening with increasing strain (Takeshita and Wenk, 1988).

Pore fluid pressure

In recent years analyses of vein systems, particularly in fault-controlled quartz-gold vein systems, has led to considerable advances in our understanding of how the mechanical evolution of fault zones may be influenced by fluctuations in pore fluid pressure (e.g. Sibson et. al., 1988; Miller et. al., 1992, 1994). At shallow crustal levels tensile fractures may be formed, but at greater depths the increase of confining pressure (at least in dry rocks) induces formation of shear fractures. Under high fluid pressures, however, tensile failure by hydraulic fracturing may occur at depths in excess of 30 km (see review by Fyfe et al., 1978). Models for progressive vein formation in both isotropic and anisotropic materials have been developed, and these models have been used to infer the orientation of externally applied principal stress directions from observed vein orientations (Allison and Kerrich, 1979; Kerrich, 1986; Sibson and Scott, 1998). An

important common assumption in these models is that the externally applied principal stresses are either horizontal or vertical (i.e. an Andersonian stress field).

Kerrich (1986) has suggested that a planar anisotropy, such as foliation, within a shear zone will cause refraction of the local stresses and hydraulic fractures will tend to form either parallel or normal to this anisotropy. The steeply lineated NW striking shear zones of the SRSS contain numerous quartz veins that have developed along the foliation, but also locally cut the foliation (Figs. 8c and d). A model for the progressive development of these veins is proposed in Figure 14. This model is based on an earlier model originally proposed by Allison and Kerrich (1979) and Kerrich (1986), and attempts to explain formation of variably oriented veins in a foliated reverse-slip shear zone subjected to an externally applied stress field of constant orientation, with σ_1 horizontal and σ_3 vertical. The maximum externally applied principal stress is assumed to be approximately perpendicular to foliation within the steeply dipping reverse-sense shear zones. Initiation of the veins is assumed to be by tensile failure rather than by opening of dilational jogs on shear surfaces. This assumption of orthogonal vein opening is strongly supported in the Type 3 quartz veins by the presence of minute crack-seal mineral inclusions and calcite layers (Figs. 9d and e) that are oriented orthogonal to the vein margins (cf. Ramsay, 1980; Cox, 1987; Petit et. al., 1999).

On a Mohr diagram the envelope for failure parallel to a pre-existing planar anisotropy will plot at lower stresses than the envelope for failure normal to the anisotropy (Fig. 14). As pore fluid pressure increases the effective stresses will be progressively reduced, and tensile failure will occur when σ_3 intersects the foliation-parallel envelope if there are any pre-existing sub-horizontal planes of weakness oriented perpendicular to σ_3 (Fig. 14a). Tensile failure and vein formation along the steeply dipping foliation, however, requires greater pore fluid pressures and will occur when σ_1 intersects the foliation-parallel envelope, as long as σ_3 is less than the tensile strength of the rock measured parallel to foliation (Fig. 14b). Tensile failure normal to foliation (to produce sub-horizontal veins) in addition to requiring high pore fluid pressures, also requires larger differential stresses (Fig.14c) than those needed for foliation-parallel vein formation (Fig. 14b). Regardless of the initial mode of formation, however, fluids would have to move into the cracks at either a similar or faster rate than crack dilation in order to maintain high pore fluid pressure fluids within the dilating cracks (Brace et al., 1966; Brace and Martin, 1968; Barquins and Petit, 1992; Petit et. al., 1999).

Within the SRSS, many individual quartz veins appear to have formed both along, and locally across, foliation. An example of a quartz vein from Traverse 112 (Fig. 2), that locally formed in a tension crack oriented parallel to foliation, but traced upwards along

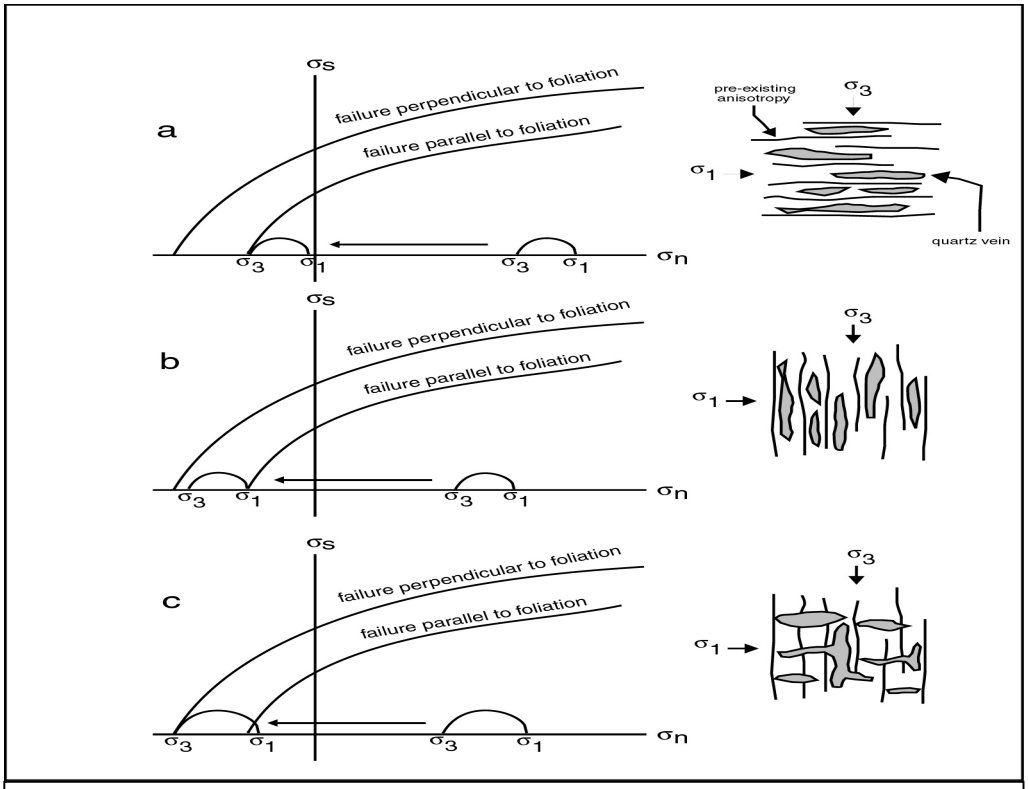

Figure 14: Schematic Mohr diagrams illustrating inferred effective stress conditions for quartz vein formation within the Santa Rita Shear System by hydraulic fracturing parallel and perpendicular to foliation (adapted from Allison and Kerrich, 1979; Kerrich, 1986). Maximum externally applied principal stress (σ1) is horizontal in a-c. (a) Horizontal vein formation by tensile failure of pre-existing planar anisotropy occurs when effective minimum principal stress (σ3-Pf) magnitude equals tensile strength of rock measured perpendicular to planar anisotropy. (b) Tensile failure and vein formation along steeply dipping foliation occurs when effective maximum principal stress (σ1-Pf) equals tensile strength of rock measured perpendicular to foliation, and effective minimum principal stress (σ3-Pf) is less than tensile strength of rock measured parallel to foliation. (c) Tensile failure perpendicular to steeply dipping foliation and formation of horizontal cross-cutting veins occurs when effective maximum principal stress (σ1-Pf) magnitude is greater than tensile strength of rock measured perpendicular to foliation and effective minimum principal stress (σ3-Pf) magnitude is equal to tensile strength of rock measured parallel to foliation. Note: greater differential stress in (c) compared with (b).

its length cuts across foliation, is shown in Figure 8c. Whether this variation in vein geometry indicates a spatial or temporal variation in effective stress conditions remains uncertain. However, noting that across-foliation tensile failure requires higher differential stresses (Fig. 14c) than along foliation tensile failure (Fig. 14b), it seems unlikely that contemporaneous differential stresses would vary significantly over such a short distance as suggested by the vein in Figure 8c. If this assumption is justified, this would indicate that across-foliation fracturing may be associated with discrete episodes of higher externally applied differential stress.

TECTONIC INTERPRETATION OF THE SANTA RITA SHEAR SYSTEM

Most analyses of shear zones rely heavily on several fundamental assumptions including: i) that the shear zones are "Andersonian", and ii) that all the features in a set of shear zones can be attributed to a single progressive deformation, rather than reactivation of pre-existing structures. The essence of the Anderson (1951) assumption is that the principal stresses are either vertical or horizontal, and that there is a simple relationship between slip on shear zones and their orientation relative to external axes of shortening and extension. The analysis then becomes one of plane strain conjugate simple shear development using Mohr-Coulomb failure criteria. Although some counter examples have been recorded (see review by Poulson and Robert, 1989), particularly where pre-existing anisotropies are involved, the internal consistency between theory and observations in many natural examples suggests that these assumptions are generally valid, at least to a practical first order approximation. In recent years, however, attention has focused on the concepts of transpression and transtension across shear zones, in which the externally applied principal stresses are not oriented at the angles assumed in the Andersonian model. In the case of transpression, for example, the principal compressive stress is oriented at a higher angle to the shear zone than predicted by Andersonian principles, leading to shortening across the shear zone during slip along the shear zone.

Principal stress directions inferred from dip-slip shear zones

Within the SRSS two groups of steeply lineated shear zones, striking at 120° and 158-175°, are recognized; both groups dip steeply (70-90°) towards either the NE or SW (Fig. 2). Field relations (see above) suggest that 120° striking shear zones are younger than the 158-175° striking shear zones. Microstructural analysis of both sets of shear zones indicates a NE side up, and SW side down, relative sense of dip-slip motion. In map view, these steeply lineated shear zones are clustered into two well-defined

approximately NW-SE trending domains which intersect near the western margin of the Santa Rita Flat pluton (Fig. 2). The NNE dipping shear zones are dominant, and the SSW dipping shear zones are only recorded in one domain (Fig. 2).

The observed reverse sense of dip motion on the NNE dipping shear zones (120° strike) would indicate that σ_1 should be horizontal and oriented at 030° if Andersonian principles apply. The presence of subhorizontal quartz veins cutting across the foliation in these shear zones supports the suggestion that σ_1 was horizontal. Within the northern domain of steeply lineated shear zones, the dip direction changes from NNE to SSW traced towards the SE along the domain axis (Fig. 2). The observed normal sense of motion on the SSW dipping shear zones would indicate that σ_1 should be vertical if Andersonian principles apply; i.e. the maximum horizontal stress was less than the lithostatic load. In other words, the maximum horizontal principal stress is less than the lithostatic load. This is supported by the absence of flat-lying veins within these shear zones; the majority of veins in these shear zones are oriented parallel to the SSW dipping foliation. However, care must be exercised in using the absence of flat-lying veins to infer that σ_1 was vertical. Study of Figure 14 indicates that steeply dipping veins could have formed with σ_1 horizontal if pore fluid pressures were of sufficient magnitude (Fig. 14b), but flat-lying veins would only have formed at larger differential stresses (Fig. 14c).

In the absence of clear cross-cutting relationships between the NNE and SSW dipping steeply lineated shear zones, it is assumed that they are of broadly the same age. However, the consistent NNE side up, and SSW side down, shear sense in both sets of shear zones rules out the possibility of them being a conjugate pair. The change from a NNE to SSW dip direction occurs around an undeformed approximately 2 km wide block of granite separating the two dip domains (Fig. 2). This block may have acted as a stress guide across which the stresses were refracted. A schematic cross section drawn across this block (Fig. 15) illustrates how the two sets of shear zones may join at depth to form part of a braided network. Kinematic interpretation of the two sets of shear zones remains problematic, however, assuming that they were active at the same time. The observed shear senses are not compatible with either upward or downward relative motion of the central undeformed block between the two sets of shear zones. If rotation of the central block has occurred, however, then the observed shear senses would be compatible with a clockwise rotation of the central block about a horizontal axis viewed towards the NW.

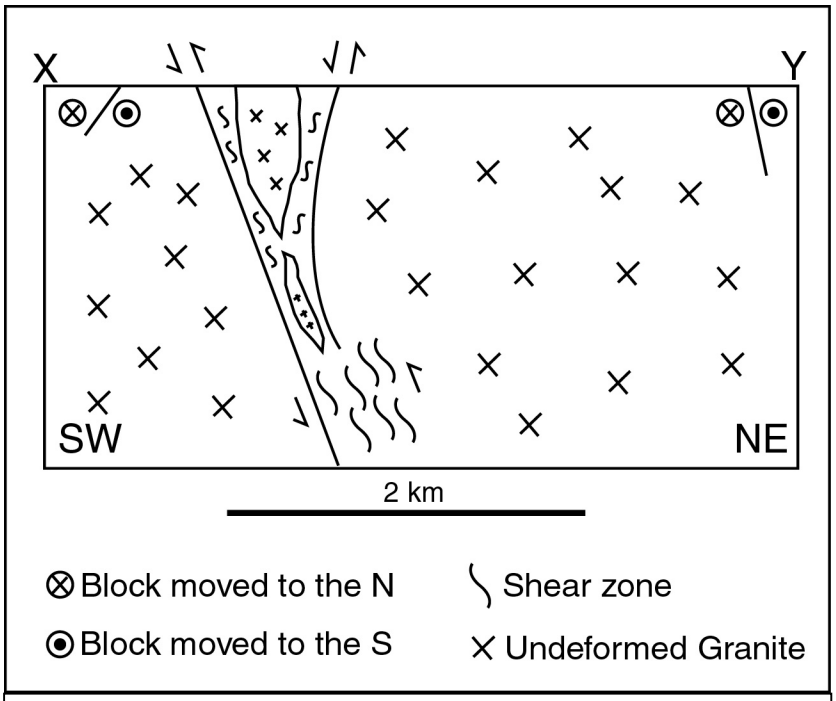

Figure 15: Cross-section oriented at right angles to steeply lineated shear zones. Note: Opposite dip-slip shear senses on either side of ~2 km wide undeformed granite block. Line of section indicated in Figure 2, section is viewed towards the NW.

Principal stress directions inferred from strike-slip shear zones

In an idealized Andersonian strike-slip fault zone, σ_1 should be horizontal and σ_2 vertical; tension fractures in the fault zone should be vertical and strike parallel to σ_1. Within the SRSS, gently pitching stretching lineations are only recorded in 158-175° striking dextral shear zones that dip moderately-steeply to the west, lineation plunging shallowly (0-20°) to the NNW or SSE. Strict Andersonian theory predicts that σ_1 for steeply dipping 158-175° striking dextral strike slip shear zones should be horizontal and oriented at 008-025°, assuming an angle of internal friction of 30°. However, if there is a component of shortening (i.e. transpression) across these shear zones, then σ_1 will be oriented at a higher angle to the shear zone boundaries.

Quartz-feldspar veins striking 068° and dipping steeply (>80°) to the NNW, locally cross cut the foliation in shear zones with lineation plunging gently to the SSE, but are themselves penetratively deformed, indicating that they developed during on-going mylonitization. The quartz-feldspar veins are oriented perpendicular to the stretching lineation in the surrounding mylonites, and indicate that σ_1 was oriented at a high angle to the shear zone margins. In contrast, unfoliated quartz veins are oriented oblique to the local stretching lineation, striking at 022° with gentle-moderate (<45°) dips to the WNW. These unfoliated quartz veins cut right across the shallowly lineated shear zones, and appear to have formed at a late stage in shear zone development.

Andersonian theory predicts that formation of the shallowly lineated strike-slip shear zones, and the steeply dipping reverse dip-slip shear zones (120° strike) belonging to the SRSS, should be associated with horizontal maximum principal compressive stresses trending 008-025° and 030° respectively. Field relations (see above) suggest that the shallowly lineated shear zones are older than the steeply lineated 120° striking shear zones, but are broadly contemporaneous with the 158-175° striking reverse dip-slip shear zones. Formation of the 158-175° striking reverse dip-slip shear zones suggests a horizontal maximum principal compressive stresses trending 068-085°, i.e. orthogonal to the margins of the 158-175° striking dextral strike-slip shear zones. If both sets of shear zones are contemporaneous, this suggests that there was an important component of shortening (transpression) across the strike-slip shear zones. This is strongly supported by the 068° striking quartz-feldspar veins that are oriented perpendicular to the stretching lineation in the strike-slip shear zones and formed during mylonitization. We conclude that during evolution of the SRSS, the horizontal maximum principal compressive stress rotated counterclockwise from an initial ENE-WSW trend to a later NNE-SSW trend.

Initiation and timing of shear zones within the Santa Rita Flat pluton

Mylonitic shear zones within the Santa Rita Flat pluton have only been recorded along contacts between the granite and cross-cutting felsic and mafic dikes, suggesting that the shear zones have nucleated along preexisting planes of weakness. Shear zones often nucleate within homogeneous granites along pre-existing structures such as cooling and expansion joints, and plastic deformation is frequently preceded by a phase of brittle deformation (Segall and Simpson, 1983). The Santa Rita Flat pluton has been dated at 164 Ma (U-Pb zircon age) (Ross, 1969; Chen, 1977; Chen and Moore 1982), and felsic and mafic dikes which cut the pluton have generally been assumed to belong to the Independence dike swarm (Ross, 1962; Metz, 1978; Brudos and Paterson, 1993; Carl et. al., 1998). The Independence dike swarm is generally accepted to be of Late Jurassic age (~148 Ma), although recent isotopic dating has demonstrated that some "Independence" dikes are of Late Cretaceous age (83-90 Ma) (see review by Carl et al., 1998). Two dikes from the Santa Rita Flat pluton have so far been dated; zircons from only one size fraction yielded a U-Pb age of 164 ± 2 Ma (see Chapter 3 of this thesis).

The dikes of the Independence dike swarm are often observed to be spatially closely associated with shear zones, and locally have been documented to either cut, or be cut by, these shear zones (e.g. Carl et. al., 1998; Glazner et al., 1999). These field relationships have been taken to indicate that the dikes and shear zones are broadly contemporaneous, and that isotopic dating of the dikes will therefore also give the age of shear zone formation. However, microstructural and petrographic data for the Santa Rita Flat pluton (see above) suggests that dikes belonging to the SRSS were emplaced prior to shear zone nucleation. Therefore, all that can be deduced using this line of reasoning is that the SRSS shear zones are younger than 163 Ma (provisional U-Pb zircon age of the felsic dikes).

Two major periods of Mesozoic age shear zone formation have been documented in the Sierra Nevada batholith and adjacent sectors of Owens Valley and the Mojave Desert. Late Jurassic intrusion of the NW-SE striking Independence dike swarm (~148 Ma) overlapped in time with shear zone formation within the dikes and adjacent wall rocks, the mylonitic shear zones accommodating sinistral strike-slip and east side-up dip-slip displacement (Glazner et al., 1999). Although these Late Jurassic shear zones are of similar orientation to the SRSS shear zones, we argue that they are of a different age because, unlike the SRSS shear zones, they appear to be broadly synchronous with dike emplacement, and are associated with sinistral (rather than dextral) strike-slip motion.

Two distinctly different types of steeply dipping Cretaceous age shear zones have been documented along the eastern crest of the Sierra Nevada batholith. The first type of

shear zones generally strike NE, and are characterized by gently plunging stretching lineations and slickensides on steeply dipping foliation. The shear zones may locally be either brittle or ductile in nature; they are very narrow (cm-scale) in plan view, with apparent sinistral off sets on the order of millimeters to tens of meters (Segall and Pollard, 1983; Segall and Simpson, 1986). Hydrothermal micas from these shear zones have yielded $^{40}Ar/^{39}Ar$ plateau ages of ~79 Ma (Segall et. al., 1990). The second type of Cretaceous age shear zones strike between N and NW; these are much larger (km-scale) shear zones and are associated with the transpressional Sierra Crest shear system (Greene and Schweickert, 1995; Tikoff and Saint Blanquat, 1997). Shear zones within the northern part of the Sierra Crest shear system have steeply plunging lineations lying within the mylonitic foliation, whereas shear zones from the southern part of the Sierra Crest shear system have shallowly plunging lineations (Tikoff and Greene, 1997). Both the steeply and shallowly lineated shear zones give dextral apparent off sets in plan view. The Sierra Crest shear system is intruded by a series of syntectonic granites; dating of these intrusions indicates that the shear system was active from approximately 88 to 79 Ma (Tikoff and Saint Blanquat, 1997).

In terms of size and deformation mechanisms, the SRSS is similar to the NE striking Cretaceous age shear zones. However in terms of orientation and kinematics the SRSS is very similar to the larger scale NW striking Cretaceous age shear zones. If the SRSS was active at the same time as the two sets of Cretaceous age shear zones in the Sierra Nevada batholith to the west, then strike-slip motion on the SRSS could only be in the observed dextral sense. If this structural and temporal correlation is correct, then the SRSS would be the first documented Cretaceous age transpressional shear system in the White-Inyo mountains. This correlation will be tested by Ar-Ar analysis of white mica from the SRSS. White mica separates suitable for Ar-Ar analysis (Phil Gans, personal communication 1999) have been hand picked from microstructural sites in which it can be demonstrated that the micas grew during penetrative shearing, and are currently awaiting analysis at UC Santa Barbara.

Transpression and a model for the Santa Rita shear system

As outlined above, field relationships indicate that reverse dip-slip and dextral strike-slip motion on the steeply dipping 158-175° striking shear zones belonging to the SRSS were contemporaneous, suggesting that there was an important component of shortening (transpression) across the strike-slip shear zones. Field relationships also indicate that dip-slip and strike-slip motion on the steeply dipping 158-175° shear zones predates reverse dip-slip motion on steeply dipping 120° striking shear zones. We therefore

concluded that during evolution of the SRSS, the horizontal maximum principal compressive stress rotated counterclockwise from an initial ENE-WSW trend to a later NNE-SSW trend.

The older sets of dip-slip and strike-slip shear zones contain foliation-parallel Type 1 and 2 quartz veins whose crystallographic fabrics indicate approximate plane strain deformation (Fig. 10c). These shear zones are themselves cut by 022° striking Type 3 quartz veins whose crystallographic fabrics indicate weak constrictional strains (Fig. 11c). Modeling of transpressional shear zones indicates that such zones should record flattening strains, whereas constrictional strains should predominate in transtensional shear zones (Sanderson and Marchini, 1984; Dewey et al., 1998). However, constrictional strains may occur in transpressional zones when the crust is extended laterally along the shear zone boundaries (Dias and Ribeiro, 1994; Dewey et al., 1998). Supporting evidence for late extension along the SRSS shear zones may be provided by the presence of steeply dipping C′ foliations which strike at 015°. Although the formation of C′ foliations is not well understood, they are generally thought to develop at a late stage during mylonitization (Platt and Vissers, 1980; Platt, 1984; Dennis and Secor, 1987; Passchier, 1991), and indicate synchronous across shear zone shortening and along shear zone stretching (see reviews by Passchier, 1991; Passchier and Trouw 1996, p. 113).

A model for evolution of the SRSS, involving both across shear zone shortening (transpression), and along shear zone stretching, is summarized in Figure 16. In stage one of this model, transpressional dextral shearing on widely distributed NW trending strike-slip shear zones is accompanied by localized reverse dip-slip motion on similarly oriented shear zones. By stage two a counterclockwise rotation of the externally applied maximum principal compressive stress has occurred, leading to formation of more westerly striking reverse dip-slip shear zones which cross-cut the earlier NW shear zones. This rotation of the externally applied stress field is presumably associated with a change in motion at the plate scale. Along shear zone stretching may have occurred throughout the evolution of the SRSS. However, the alignment of C’ foliations at a low angle to the Type 3 quartz veins which cross-cut the early shear zones and contain weakly developed constrictional c-axis fabrics, suggests that along-strike extension may have occurred at a relatively late stage. We refer to this late stage along strike extension as stage 3 in Figure 16.

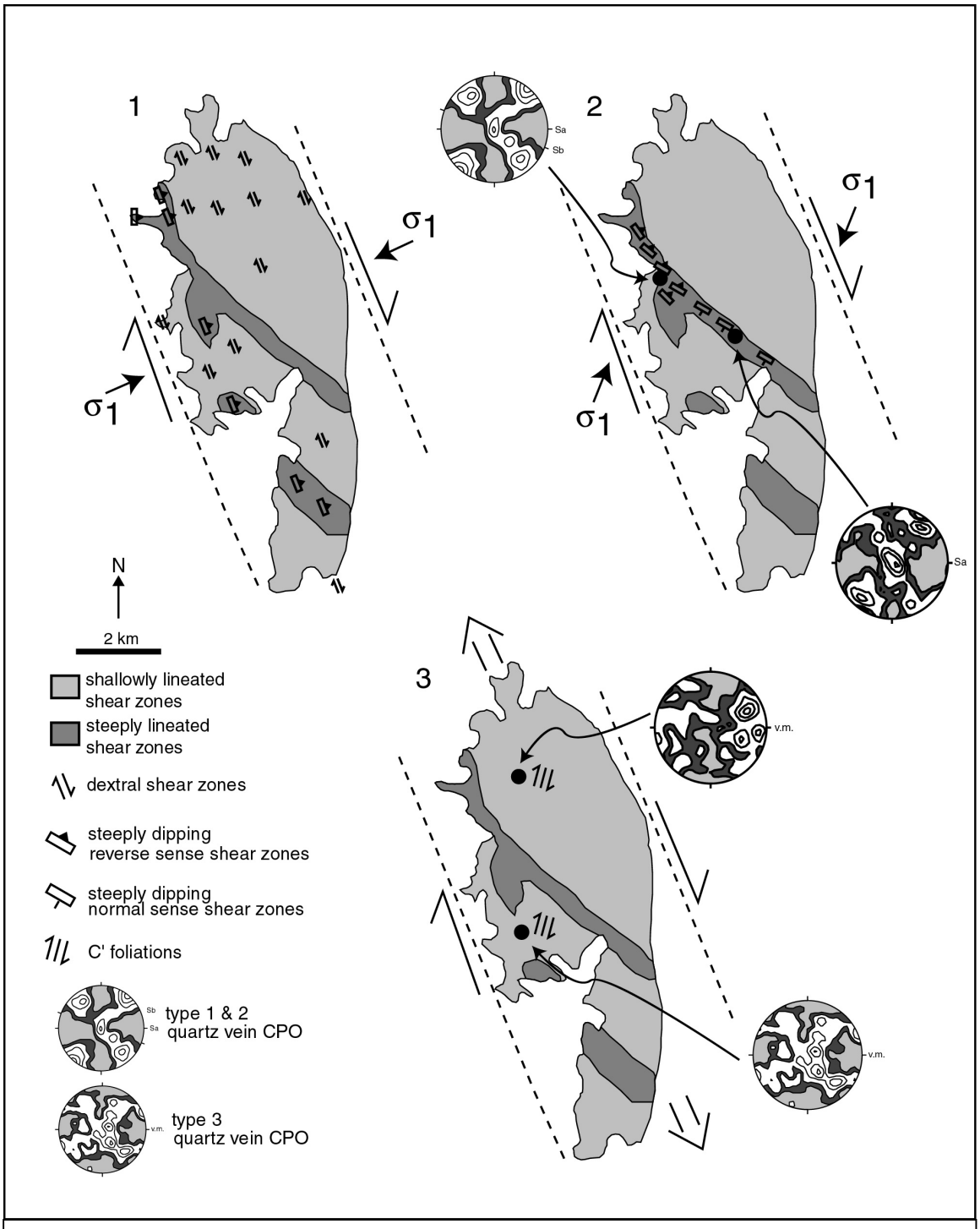

Figure 16: Model for progressive evolution of the Santa Rita Shear System. STAGE 1: Transpressional dextral shearing on widely distributed NW trending strike-slip shear zones accompanied by localized reverse dip-slip motion on shear zones of similar orientation. STAGE 2: Counterclockwise rotation of externally applied maximum compressive stress leads to formation of more westerly striking reverse dip-slip shear zones which cross-cut earlier NW dip-slip shear zones. NW trending strike-slip shear zones may still be active at this stage. STAGE 3: Along-strike extension of shear zones, see text for details.

CONCLUSIONS

Integration of field mapping with microstructural and petrographic analysis of the Santa Rita shear system leads to the following conclusions:

1. Strain was localized within the Santa Rita Flat granite along steeply dipping mafic and felsic dikes that were emplaced prior to shear zone nucleation.

2. Elevated pore fluid pressures within the shear zones are indicated by the occurrence of quartz veins that cut along and across mylonitic foliation. Elevated pore fluid pressures mechanically weakened the Santa Rita shear system (SRSS) over time. Fluid infiltration accompanying shearing also led to accelerated alteration of feldspar to fine-grained muscovite, resulting in the progressive weakening of the shear zone rocks.

3. All shallowly lineated NNW-striking shear zones are characterized by dextral strike-slip motion, whereas NNW-striking steeply lineated shear zones that dip steeply to the NE are characterized by NE over SW (reverse dip-slip) motion. These strike-slip and reverse dip-slip faults appear to be synchronous, indicating an important component of shortening (transpression) across the shear zones. Steeply lineated shear zones that locally dip steeply to the SW are characterized by a SW down and NE side up (normal-sense dip-slip) motion.

4. WNW-striking steeply lineated shear zones cross cut both the NNW striking strike-slip and dip-slip faults, indicating a counterclockwise rotation of the externally-applied stress field.

5. Foliation patterns in the strike-slip shear zones indicate that horizontal along-shear-zone extension occurred during late-stage development of the SRSS. Quartz crystallographic fabrics from veins associated with the evolving shear zones indicate that along-shear-zone extension was locally accompanied by a change in strain symmetry from plane strain to constriction.

REFERENCES

Allison, I. and Kerrich, R., 1979. History of deformation and fluid transport in shear zones at Yellowknife. In: Morton, R.D., (ed.), Proceedings of Gold Workshop, Yellowknife, Northwest Territories, p. 201-222.

Anderson, E. M., 1951, The Dynamics of Faulting. Oliver and Boyd, Edinburgh, 206 pp.

Barquins, M. and Petit, J. P., 1992, Kinetic instabilities during the propagation of a branch crack: effects of loading conditions and internal pressure. Journal of Structural Geology 14, 893-903.

Boullier, A. M. and Bouchez, J. L., 1978. Le quartz en rubans dans les mylonites. Bulletin de la Societe Geologique de France 7, 253-262.

Brace, W.F. and Martin, R.J., 1968. A test of the law of effective stress for crystalline rocks of low porosity. International Journal of Rock Mechanics and Mining Science 5, 415-426.

Brace, W.F., Paulding, B.W. and Scholz, C. 1966. Dilatency in the fracture of crystalline rocks. Journal of Geophysical Research 71, 3939-3953.

Brudos, T. C. and Paterson, S. R., 1993. The Santa Rita shear zone: major Mesozoic deformation along the western flank of the White-Inyo Range, California. Geological Society of America Abstracts with Programs 25, 15.

Burgmann, R. and Pollard, D. D., 1992. Influence of the state of stress on the brittle-ductile transition in granitic rock: evidence from fault steps in the Sierra Nevada, California. Geology 20, 645-648.

Burgmann, R. and Pollard, D. D., 1994. Strain accommodation about strike-slip fault discontinuities in granitic rock under brittle-to-ductile conditions. Journal of Structural Geology 16, 1655-1674.

Carl B. S., Glazner, A. F., Bartley, J. M., Dinter, D. A., and Coleman, D. S., 1998. Independence dikes and mafic rocks of the eastern Sierra. In: Behl, R. (ed.) Geological Society of America, 94th Annual Meeting of Cordilleran Section, 1998 Field Guidebook, p. 4.1 - 4.26.

Chen, J. H-Y, 1977, Uranium-lead isotopic ages from the southern Sierra Nevada batholith and adjacent areas, California: Santa Barbara, University of California, Ph.D. thesis, 183 pp.

Chen, J. H. and Moore, J. G., 1979. Late Jurassic Independence dike swarm in eastern California. Geology 7,. 129-133.

Chen, J. H. and Moore, J. G., 1982. Uranium-lead isotopic ages from the Sierra Nevada batholith, California. Journal of Geophysical Research 87, 4761-4784.

Christiansen, P. P. and Pollard, D. D., 1997. Nucleation, growth, and structural development of mylonitic shear zones in granitic rock. Journal of Structural Geology 19, 1159-1172.

Coleman, D. S., Bartley, J. M., Glazner, A. F., and Carl, B. S., 1994. Late Cretaceous dikes in the Independence swarm, California. EOS Transactions, American Geophysical Union 75, 686.

Conti, P., Funedda, A., and Cerbai, N., 1998. Mylonite development in the Hercynian basement of Sardinia (Italy). Journal of Structural Geology 20, 121-133.

Cox, S. F., 1987. Antitaxial crack-seal vein microstructures and their relationship to displacement paths. Journal of Structural Geology 9, 779-787.

Dennis, A. J. and Secor, D. T., 1987. A model for the development of crenulations in shear zones with applications from the southern Appalachian Piedmont. Journal of Structural Geology 9, 809-817.

Dewey, J. F., Holdsworth, R. E., and Strachan, R. A., 1998. Transpression and transtension zones. In: Holdsworth, R. E., Strachan, R. A., and Dewey, J. F. (eds), Continental Transpressional and Transtensional Tectonics. Geological Society London, Special Publications 135, 1-14.

Dias, R. and Ribeiro, A., 1994. Constriction in a transpressive regime: an example in the Iberian branch of the Ibero-Armorican arc. Journal of Structural Geology 16, 1543-1554.

Fyfe, W.S., Price, N.J. and Thompson, A.B. 1978. Fluids in the Earth's Crust. Elsevier, Amsterdam, 383 pp.

Glazner, A.F., Bartley, J.M. and Carl, B.S., 1999. Oblique opening and noncoaxial emplacement of the Jurassic Independence dike swarm, California. Journal of Structural Geology 21, 1275-1284.

Goodwin, L. and Wenk, H. R., 1995. Development of phyllonite from granodiorite: Mechanisms of grain-size reduction in the Santa Rosa mylonite zone, California. Journal of Structural Geology 17, 689-708.

Greene, D. C. and Schweickert, R. A., 1995. The Gem Lake shear zone: Cretaceous dextral transpression in the northern Ritter Range pendant, eastern Sierra Nevada, California. Tectonics 14, 945-961.

Guermani, A. and Pennacchioni, G., 1998. Brittle precursors of plastic deformation in a granite: an example from the Mont Blanc massif (Helvetic, western Alps). Journal of Structural Geology 20, 135-148.

Hanmer, S. and Passchier, C. W., 1991. Shear sense indicators: a review. Geological Survey Canadian Paper 90, 71 pp.

Hippertt, J. F. and Hongn, F.D. 1998. Deformation mechanisms in the mylonite/ultramylonite transition. Journal of Structural Geology 20, 1435-1448.

Hirth, G. and Tullis, J., 1992. Dislocation creep regimes in quartz aggregates. Journal of Structural Geology 14, 145-159.

Hobbs, B.E., 1985. The geological significance of microfabric analysis. In: Wenk, H-R. (ed.) Preferred Orientation in Deformed Metals and Rocks: an Introduction to Modern Texture Analysis, pp. 463 - 484. Academic Press, Orlando.

Ingles, J., Lamouroux, C., Soula, J-C., Guerrero, N., and Debat, P., 1999. Nucleation of ductile shear zones in a granodiorite under greenschist facies conditions, Neouvielle massif, Pyrenees, France. Journal of Structural Geology 21, 555-576.

James, E. W., 1989. Southern extension of the Independence dike swarm of eastern California. Geology 17, 587-590.

Janecke, S. U. and Evans, J. P., 1988, Feldspar-influenced rock rheologies. Geology 16, 1064-1067.

Kerrich, R., 1986. Fluid infiltration into fault zones: chemical, isotopic and mechanical effects. Pure and Applied Geophysics 124, 225-268.

Law, R. D., 1990. Crystallographic fabrics: a selective review of their applications to research in structural geology. In: Knipe, R. J. and Rutter, E. H. (eds.), Deformation Mechanisms, Rheology and Tectonics. Geological Society of London Special Publication 54, 335-352.

Law, R. D., Knipe, R. J., and Dayan, H., 1984. Strain path partitioning within thrust sheets: microstructural and petrofabric evidence from the Moine thrust zone at Loch Eriboll, North-West Scotland. Journal of Structural Geology 6, 477-497.

Lister, G. S., 1977. Discussion: Crossed girdle c-axis fabrics in quartzites plastically deformed by plane strain and progressive simple shear. Tectonophysics 39, 51-54.

Lister, G. S. and Dornsiepen, U. F., 1982. Fabric transitions in the Saxony granulite terrain. Journal of Structural Geology 4, 81-92.

Lister, G. S. and Snoke A. W., 1984. S-C Mylonites. Journal of Structural Geology 6, 617-638.

Lister, G. S. and Williams, P. F., 1979. Fabric development in shear zones: theoretical controls and observed phenomena. Journal of Structural Geology 1, 283-279.

Lister, G. S. and Williams, P. F., 1983. The partitioning of deformation in flowing rock masses. Tectonophysics 92, 1-33.

Means, W. D., 1981. The concept of steady-state foliation. Tectonophysics 78, 179-199.

Metz, J., 1978. Petrology of the Santa Rita Flat pluton Inyo Mountains, California. M. S. thesis, San Jose State University, 95 pp.

Miller, L. D., Barton, C. C., Fredericksen, R. S., and Bressler, J. R., 1992. Structural evolution of the Alaska Juneau gold deposit, southeastern Alaska. Canadian Journal of Earth Sciences 29, 865-878.

Miller, L. D., Goldfarb, R. J., Gehrels, G. E., and Snee, L. W., 1994. Genetic links among fluid cycling, vein formation, regional deformation and plutonism in the Juneau gold belt, southeastern Alaska. Geology 22, 203-206.

Moore, J. G. and Hopson, C. A., 1961. The Independence dike swarm in eastern California. American Journal of Science 259, 241-259.

Nelson, C. A., 1962. Lower Cambrian-Precambrian succession, White-Inyo Mountains, California. Geological Society of America Bulletin 73, 139-144.

O'Hara, K. D., 1988. Fluid flow and volume loss during mylonitization: an origin for phyllonite in an overthrust setting, North Carolina, USA. Tectonophysics 156, 21-36.

Passchier, C. W., 1991. Geometric constraints on the development of shear bands in rocks. Geologie en Mijnbouw 70, 203-211.

Passchier, C. W. and Trouw, R. A. J., 1996. Microtectonics. Springer, New York, 289 pp.

Petit, J. P., Wibberley, C.A.J., and Ruiz, G., 1999, 'Crack-seal', slip: a new fault valve mechanism? Journal of Structural Geology 21, 1199-1207.

Platt, J. P., 1984. Secondary cleavages in ductile shear zones. Journal of Structural Geology 6, 439-442.

Platt, J. P. and Vissers, R. L. M., 1980. Extensional structures in anisotropic rocks. Journal of Structural Geology 2, 397-410.

Poulson, K.K. and Robert, F., 1989. Shear zones and gold: practical examples from the southern Canadian Shield. In: Bursnall, J.T. (ed.), Mineralization and Shear Zones. Geological Association of Canada, Short Course Notes, Volume 6, p. 239-266.

Ramsay, J. G., 1980. Shear zone geometry: a review. Journal of Structural Geology 2, 83-99.

Ramsay, J. G., 1983. Rock ductility and its influence on the development of tectonic structures of mountain belts. In: Hsu, K. J. (ed.), Mountain Building Processes. Academic Press, London, 111-127.

Ramsay, J. G. and Wood, D.S., 1973. The geometric effects of volume change during deformation processes. Tectonophysics 13, 263-277.

Ross, D. C., 1962. Correlation of granitic plutons across faulted Owens Valley, California. U. S. Geological Survey Professional Paper 501-D, D86-D88.

Ross, D. C., 1965. Geology of the Independence quadrangle, Inyo County, California. U.S. Geological Survey Bulletin 1181-0, 64 pp.

Ross, D. C., 1967. Generalized geologic map of the Inyo Mountains Region, California. U. S. Geological Survey Miscellanceous Investigations Map I, 506, 1:125,000 scale.

Ross, D. C., 1969. Descriptive petrography of three large granitic bodies in the Inyo Mountains, California. U. S. Geological Survey Professional Paper 601, 47 pp.

Sanderson, D. J. and Marchini, W. R. D., 1984. Transpression. Journal of Structural Geology 6, 449-458.

Schmid, S. M. and Casey, M., 1986. Complete fabric analysis of some commonly observed quartz c-axis patterns. In: Hobbs, B. E. and Heard, H. C. (eds.), Mineral and Rock Deformation: Laboratory Studies - The Paterson Volume. American Geophysical Union, Geophysical Monograph 36, 263-286.

Segall, P., Mckee, E. H., Martel, S. J., and Turrin, B. D., 1990. Late Cretaceous age of fractures in the Sierra Nevada batholith, California. Geology 18, 1248-1251.

Segall, P. and Pollard, D. D., 1983. Nucleation and growth of strike-slip faults in granite. Journal of Geophysical Research 88, 555-568.

Segall, P. and Simpson, C., 1986. Nucleation of ductile shear zones on dilatant fractures. Geology 14, 56-69.

Sibson, R. H., 1985. A note on fault reactivation. Journal of Structural Geology 7, 751-754.

Sibson, R. H., 1990. Conditions for fault-valve behaviour. In: Knipe, R. J. and Rutter E. H. (eds.), Deformation Mechanisms, Rheology and Tectonics. Geological Society of London Special Publication 54, 15-28.

Sibson, R. H., 1992. Implications of fault valve behaviour for rupture nucleation and recurrence. Tectonophysics 211, 283-293.

Sibson, R. H., Robert, F., and Poulsen, K. H., 1988. High-angle reverse faults, fluid-pressure cycling, and mesothermal gold-quartz deposits. Geology 16, 551-555.

Sibson, R. H. and Scott, J., 1998. Stress/fault controls on the containment and release of overpressured fluids: Examples from gold-quartz vein systems in Juneau, Alaska; Victoria, Australia and Otago, New Zealand. Ore Geology Reviews 13, 293-306.

Simpson, C., 1985. Deformation of granitic rocks across the brittle-ductile transition. Journal of Structural Geology 7, 503-511.

Smith, G. I., 1962. Large left-lateral displacement on Garlock fault, California, as measured from offset dike swarms. American Association of Petroleum Geologists Bulletin 46, 85-104.

Snoke, A.W., Tullis, J. and Todd, V.R., 1998. Fault-Related Rocks: A Photographic Atlas. Princeton, New Jersey, Princeton University Press, 617pp.

Takeshita, T. and Wenk, H.-R. 1988. Plastic anisotropy and geometrical hardening in quartzites. Tectonophysics 149, 345 - 361.

Tikoff, B. and de Saint Blanquat, M., 1997. Transpressional shearing and strike-slip partitioning in the Late Cretaceous Sierra Nevada magmatic arc, California. Tectonics 16, 442-459.

Tikoff, B. and Greene, D. C., 1997. Stretching lineations in transpressional shear zones: an example from the Sierra Nevada batholith, California. Journal of Structural Geology 19, 29-39.

Tourigny, G. and Tremblay, A., 1997. Origin and incremental evolution of brittle/ductile shear zones in granitic rocks: natural examples from the southern Abitibi Belt, Canada. Journal of Structural Geology 19, 15-27.

Wenk, H.-R., 1994. Preferred orientation patterns in deformed quartzites. Reviews in Mineralogy 29, 177-208.

White, S. H., 1976. The effects of strain on the microstructures, fabrics, and deformation mechanisms in quartzites. Philosophical Transactions of the Royal Society of London 283, 69-86.

White, S. H., Burrows, S. E., Carreras, J., Shaw, N. D., and Humphreys, F. J., 1980. On mylonites in ductile shear zones. Journal of Structural Geology 2, 175-187.

CHAPTER 3

U/Pb dating of two felsic dikes from the Santa Rita shear system

INTRODUCTION

The Santa Rita Flat pluton is cut by a series of NW-trending felsic and mafic dikes, and shear zones have nucleated along the planar contacts between the pluton and the dikes. The pluton has been dated at 164 Ma (U-Pb zircon age) by Chen (1977) and is one of many middle to late Jurassic plutons in the White-Inyo Range (Fig. 1) that intruded metasedimentary rocks ranging from Neoproterozoic through late Paleozoic in age (Nelson, 1962; Bateman et al., 1963; Ross, 1965; Bateman, 1992). The felsic and mafic dikes which cut the Santa Rita Flat pluton have been correlated (Ross, 1965) with the Independence Dike Swarm (IDS), which can be traced over 600 km from the Sierra Nevada and White Mountains southwards to the Mojave Desert. The IDS has been dated at 148 Ma (Chen and Moore, 1979; James, 1989); however "Independence-like" mafic dikes have also been dated at 90-94 Ma (Coleman et al., 1994). Due to the close association between shear zones and "Independence" dikes within the Santa Rita Flat pluton, and the generally accepted Late Jurassic age for the IDS, Brudos and Paterson (1993) and Carl et al. (1998) have speculated that these dikes are also of Jurassic age and were syntectonically emplaced along shear zones. However, the dikes had not been isotopically dated, and no detailed analyses of the geometric and temporal relationships between the dikes and shear zones had been made (see Chapter 1). This chapter documents the dating of two felsic dikes from the Santa Rita Shear System (SRSS).

METHODS

Two felsic dike samples weighing 18.32 kg (SR 31) and 17.64 kg (SR112) were collected from the SRSS (Fig. 1). The samples were crushed and heavy minerals were initially separated using a Wilfley table. Final separation for zircon crystals involved magnetic separation, followed by three stages of heavy liquid separation (s-tetra-bromoethane – methylene iodide – thallium malonate-formate). 100 acicular, euhedral, clear, and inclusion-free zircon crystals were then hand picked in air, and grouped into four size fractions (143 μm – 114 μm – 70 μm – 41 μm) for each sample. The picked zircons were cleaned, weighed, dissolved, and prepared using standard column chemistry before loading onto rhenium filiaments. Due to technical difficulties, only the 41 μm, 70 μm, and 143 μm size fractions could be analyzed by mass spectrometry in Virginia Tech's Petrogenesis, Isotope Geology, and Tectonics Laboratory.

ANALYTICAL RESULTS

A U/Pb concordia diagram for zircon size fractions taken from two felsic dikes is presented as Figure 2. Confidence in a U-Pb age is determined by the concordancy and overlapping of different size fractions on a U/Pb concordia diagram. However, there is clearly no overlapping of the different size fractions from the two felsic dikes, and only one size fraction (sample SR.112, size fraction = 70μm) lies on the U/Pb concordia.

DISCUSSION AND CONCLUSIONS

Discordancy for the three size fractions indicated in Figure 2 could be related to either incomplete dissolution of the zircon crystals during analysis, or Pb loss in the zircons during deformation (see Chapter 1). The zircons from the three discordant size fractions were selected because of their clear and inclusion-free nature. Therefore, Pb loss probably did not occur, but instead incomplete dissolution of the zircon crystals during analysis likely contributed to their discordant nature and range of ages (Fig. 2). The one size fraction that lies on the U/Pb concordia represents complete dissolution of the zircon crystals with no Pb loss during mylonitization.

The microstructural and petrographic data for the Santa Rita Flat pluton suggests that dikes belonging to the SRSS were emplaced prior to shear zone nucleation (see Chapter 1). Therefore, the concordant 164 $\pm$ 2 Ma age from one of the SR112 size fractions may represent the crystallization age for the emplacement of the dikes within the Santa Rita Flat pluton. The crystallization age from felsic dike sample SR112 is within analytical error the same as the U-Pb zircon crystallization age (164 $\pm$ 1 Ma) obtained by Chen (1977) for the pluton itself. This suggests that the dikes may have been emplaced during the late stages of cooling within the Santa Rita Flat pluton, although it is emphasised that the U-Pb data from the dikes are not of good quality.

The age of mylonitization within the SRSS will be assessed by Ar-Ar analysis of syn-deformational white mica. White mica separates suitable for Ar-Ar analysis (Phil Gans, personal communication 1999) have been hand picked from microstructural sites in which it can be demonstrated that the micas grew during penetrative shearing, and are currently awaiting analysis at UC Santa Barbara.

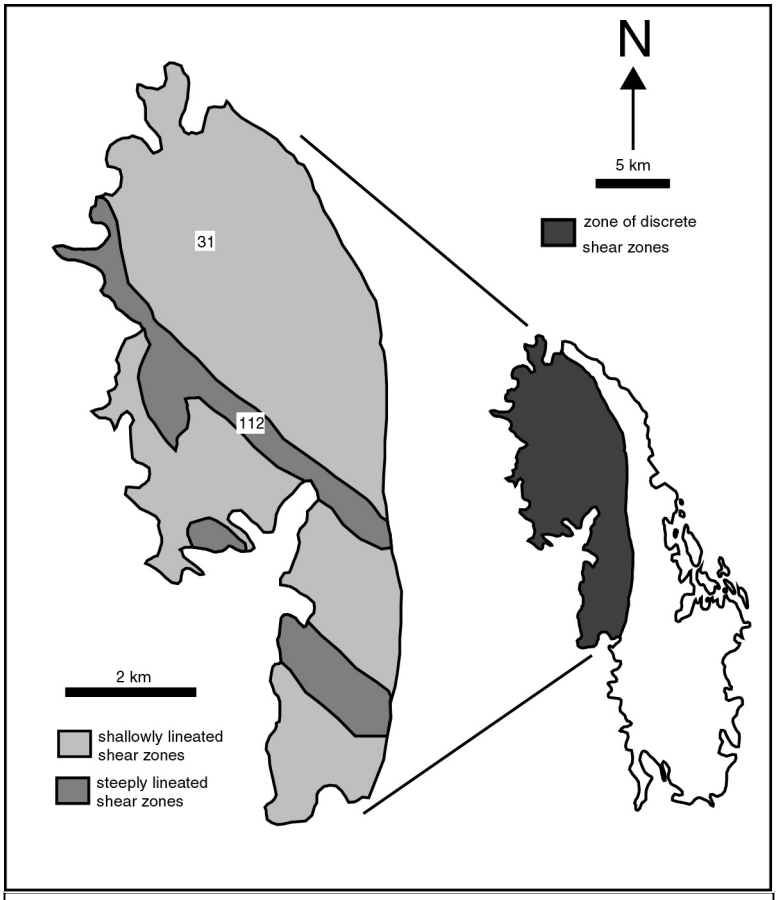

Figure 1: Location of felsic dike samples collected for U/Pb dating of zircons.

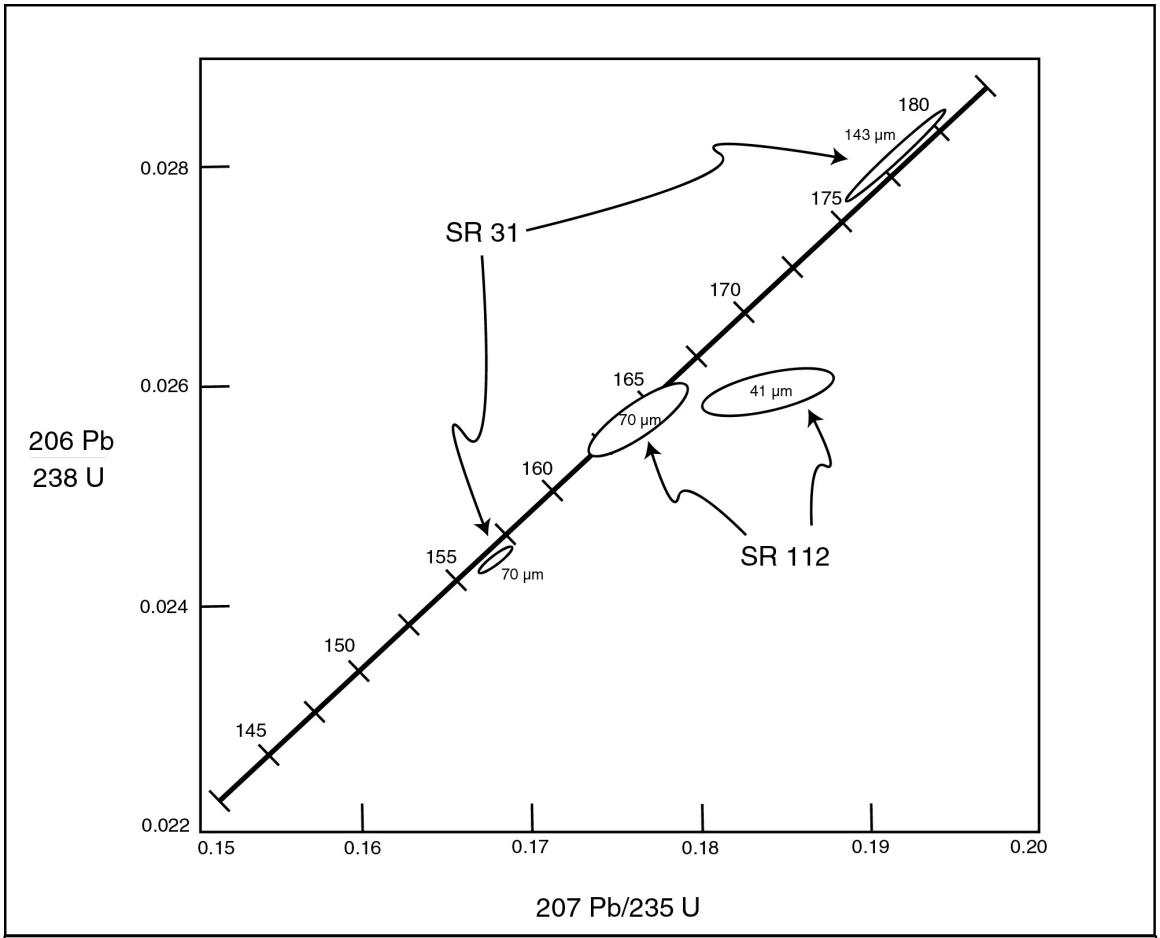

Figure 2: U/Pb concordia diagram for 207Pb/235U age of deformed felsic dikes from the Santa Rita shear system. Only the 70 µm size fraction from SR 112 lies on the concordia. The discordancy illustrated from the other size fractions from SR 31 and SR 112 are probably due to incomplete dissolution of the zircon crystals during analysis.

REFERENCES

Bateman, P. C., 1992, Plutonism in the central part of the Sierra Nevada Batholith, California, U.S. Geological Survey Professional Paper 1483, 186 pp.

Bateman, P. C., Clark, L. D., Huber, N. K., Moore, J. G., and Rinehart, C. D., 1963, The Sierra Nevada batholith – A synthesis of recent work across the central part: U. S. Geological Survey Professional Paper 414-D, 46 pp.

Brudos, T. C. and Paterson, S. R., 1993. The Santa Rita shear zone: major Mesozoic deformation along the western flank of the White-Inyo Range, California. Geological Society of America Abstracts with Programs 25, 15.

Carl B. S., Glazner, A. F., Bartley, J. M., Dinter, D. A., and Coleman, D. S., 1998. Independence dikes and mafic rocks of the eastern Sierra. In: Behl, R. (ed.) Geological Society of America, 94th Annual Meeting of Cordilleran Section, 1998 Field Guidebook, p. 4.1 - 4.26.

Chen, J. H-Y, 1977, Uranium-lead isotopic ages from the southern Sierra Nevada batholith and adjacent areas, California: Santa Barbara, University of California, Ph.D. thesis, 183 pp.

Chen, J. H. and Moore, J. G., 1979. Late Jurassic Independence dike swarm in eastern California. Geology 7. 129-133.

Coleman, D. S., Bartley, J. M., Glazner, A. F., and Carl, B. S., 1994. Late Cretaceous dikes in the Independence swarm, California. EOS Transactions, American Geophysical Union 75, 686.

James, E. W., 1989. Southern extension of the Independence dike swarm of eastern California. Geology 17, 587-590.

Nelson, C. A., 1962. Lower Cambrian-Precambrian succession, White-Inyo Mountains, California. Geological Society of America Bulletin 73, 139-144.

Ross, D. C., 1965. Geology of the Independence quadrangle, Inyo County, California. U.S. Geological Survey Bulletin 1181-0, 64 pp.

VITA

John Vines received his B. A. degree in geology from North Carolina State University in Raleigh, NC. Following the completion of his Master's degree at Virginia Tech, John Vines will start an internship with Marathon Oil Company. After the internship he will return to Virginia Tech in fall of 2000 to begin a Ph.D. in geology.